MODELING ULTRAVIOLET (UV) LIGHT EMITTING DIODE (LED) ENERGY PROPAGATION IN REACTOR VESSELS

THESIS

John P. Richwine, Captain, USAF

AFIT-ENV-14-M-55

DEPARTMENT OF THE AIR FORCE
AIR UNIVERSITY

AIR FORCE INSTITUTE OF TECHNOLOGY

Wright-Patterson Air Force Base, Ohio

AFIT-ENV-14-M-55

MODELING ULTRAVIOLET (UV) LIGHT EMITTING DIODE (LED) ENERGY PROPAGATION IN REACTOR VESSELS

THESIS

Presented to the Faculty

Department of Systems Engineering and Management

Graduate School of Engineering and Management

Air Force Institute of Technology

Air University

Air Education and Training Command

In Partial Fulfillment of the Requirements for the

Degree of Master of Science in Engineering Management

John P. Richwine, BS

Captain, USAF

March 2014

AFIT-ENV-14-M-55

MODELING ULTRAVIOLET (UV) LIGHT EMITTING DIODE (LED) ENERGY PROPAGATION IN REACTOR VESSELS

John P. Richwine, BS

Captain, USAF

Approved:

_____//SIGNED//_____	11 March 2014
Michael R. Grimaila, Ph.D., CISM, CISSP (Chairman)	Date
_____//SIGNED//_____	11 March 2014
Lt Col LeeAnn Racz, Ph.D., P.E. (Member)	Date
_____//SIGNED//_____	11 March 2014
Michael E. Miller, Ph.D. (Member)	Date
_____//SIGNED//_____	11 March 2014
Alfred E. Thal, Jr., Ph.D. (Member)	Date

Abstract

The United States Environmental Protection Agency's (EPA) National Homeland Security Research Center (NHSRC) is concerned with both accidental and intentional releases of chemicals into waste streams. Certain chemicals may be detrimental to the effectiveness of municipal wastewater treatment plants. This can lead to reduced capability or costly damage to the plant. The NHSRC is researching methods to pre-treat waste streams to counter undesired chemicals before they are introduced to wastewater treatment plants. One of these methods includes an Advanced Oxidation Process (AOP) which uses ultraviolet (UV) energy and hydrogen peroxide (H_2O_2) to create hydroxyl radicals (·OH) that can neutralize harmful chemicals. Recent advancements in Ultra Violet Light Emitting Diodes (UV LEDs) are making it possible to use energy from these sources instead of traditional UV energy sources.

This research effort focuses on the modeling and simulation of UV LED energy sources for the purpose of providing the ability to predict the efficiency of different reactor vessel geometries. The model is used to evaluate the irradiance present at any point within a test reactor. When coupled with a suitable AOP production rate equation, the model provides insight into tradeoffs when designing a UV reactor suitable for AOP. When coupled with a suitable pathogen kill rate equation, the model provides insight into tradeoffs when designing a UV reactor suitable for pathogen extermination. Finally, simulated results are compared to measurements collected in actual laboratory experiments.

Table of Contents

Page

Abstract iii

Table of Contents iv

List of Figures vii

List of Tables ix

List of Equations xi

I. Introduction 1

Background 1
Problem Statement 3
Research Objectives/Questions/Hypotheses 3
Research Methodology 4
Assumptions/Limitations 5
Implications 5
Preview 6

II. Literature Review 7

Chapter Overview 7
Water Disinfection 7
Chlorine Disinfection *7*
UV Disinfection *7*
DNA Disruption *9*
Advanced Oxidation Process (AOP) *10*
Inactivation *11*
Mercury Lamp and LED Bulb Characteristics 13
Mercury Lamps *13*
UV LEDs *15*
Efficiency *16*
Lifespan *17*
Wavelength *20*
Warm Up Time *20*
Pulsing *21*
Advantages and Disadvantages *24*
Modeling and Simulation 25
Modeling Approaches *25*
Design Factors *26*
Multiple Bulbs *27*

Dose *27*
Collimated Beam *27*
Modeling and Simulation Environments 28
Chapter Summary 28

III. Methodology 30

Chapter Overview 30
Data Point Representation 30
Coordinate Systems 31
Modeling Concepts and Equations 32
Emission Angle *32*
Intensity *34*
Normalized Intensity *36*
Irradiance *38*
Absorption *40*
Spherical to Cartesian Coordinates *40*
Bulb Array *41*
Limit Bulb Array *41*
Pathogen Inactivation *42*
MATLAB 43
Graphing in MATLAB *43*
Reactor Vessel Optimization 44
Chapter Summary 44

IV. Data and Results 45

Chapter Overview 45
Baseline 45
Global Variables 48
Emission Angle 53
Intensity 57
Normalized Intensity 58
Irradiance 60
Absorption 63
Spherical to Cartesian Conversion 65
Bulb Array 66
Limit Bulb Array 67
Pathogen Inactivation 67
DNA Disruption – Batch *67*
AOP - Flow *72*
Graphing 74
Reactor Vessel Optimization 81
DNA Disruption Conclusions *82*
AOP Conclusions *84*
Batch Reactor Conclusions *84*

Fluid Flow Reactor Conclusions *85*
Concepts for Future Flow Reactor Designs 86
Fluid Flow *86*
Pipe Designs *86*
Rectangular Designs *88*
Modular Design *89*
Chapter Summary 89

V. Conclusions 90

Chapter Overview 90
Conclusions of Research 90
Significance of Research 93
Limitations 94
Recommendations for Future Research 94
Tune Model *94*
Optimize Reactor Vessels *95*
Summary 95

Appendix 96

MATLAB Code 96
Overall Model *96*
Variables *98*
Irradiance *100*
Absorption *102*
Conversion *102*
Re-Order *103*
Graph Single *104*
Bulb Offset *105*
Cut *105*
Dose Batch *106*
Graph Batch *108*
Dose Flow *109*
Graph Dose *111*

List of Figures

Page

Figure 1: Electromagnetic Spectrum (*UVC LED disinfection.*2013)..... 8

Figure 2: UVC DNA Disruption (*UVC LED disinfection.*2013)..... 10

Figure 3: Typical Fluence-Log Inactivation Response Curve (Mamane-Gravetz & Linden, 2005)..... 13

Figure 4: Spectral Emittance of Low Pressure Mercury UV Lamp (solid line) and Medium-Pressure Mercury UV Lamp (dashed line) (Bolton & Linden, 2003) 14

Figure 5: Mercury Lamp with Parallel Flow (Taghipour & Sozzi, 2005)..... 15

Figure 6: Mercury Lamp with Perpendicular Flow (Hofman et al., 2007)..... 15

Figure 7: Achieved and Projected LED Performance (Shur & Gaska, 2010) 17

Figure 8: Power Drop of a SET 265 nm LED at 20 mA over 100 hours (Kneissl, Kolbe, Wurtele, & Hoa, 2010) 19

Figure 9: Warm-up Time for UV LEDs (■) Versus Low Pressure Lamps (▲) (C. Chatterley, 2009) 21

Figure 10: Output Power Versus Current for CW and Pulsed Modes of Operation for DUV LEDs (Shur & Gaska, 2010)..... 23

Figure 11: Output Optical Power of Single-Chip LEDs and LED Lamps for CW and Pulsed Modes (Shur & Gaska, 2010) 24

Figure 12: MPSS, MSSS, and Radial Model Emittance Patterns (Liu et al., 2004)..... 26

Figure 13: Cartesian and Spherical Coordinate Systems..... 31

Figure 14: Surface Area of Sphere Contained by Solid Angle..... 35

Figure 15: Spherical Cap with Elevation Rings and Points..... 37

Figure 16: Vessel 46

Figure 17: LED Plate with LED Spacing 47

Figure 18: Typical Angular Diagram, Air 54

Figure 19: Averaged Angular Diagram, Air..... 55

Figure 20: Averaged Angular Diagram, Water..... 56

Figure 21: Radiant Intensity versus Emission Angle, Air 58

Figure 22: Radiant Intensity versus Emission Angle, Water 58

Figure 23: Area Associated with Singular Point 61

Figure 24: Ring Area 62

Figure 25: Single Bulb, 300 μW, Top a=0 cm^{-1}, Middle Left a=0.01 cm^{-1}, Middle Right a=0.077 cm^{-1}, Bottom Left a=0.171 cm^{-1}, Bottom Right a=0.266 cm^{-1} 65

Figure 26: Tran's Set Up (Tran, 2014) 69

Figure 27: Duckworth's Set Up (Duckworth, 2014) 73

Figure 28: Bulb at 300 μW with Nested Shoulder, Linear, and Tailing Regions 75

Figure 29: Bulb Array at 300 μW with Nested Shoulder, Linear, and Tailing Regions . 75

Figure 30: Single Bulb 0.1 to 1 mW/cm2, Top Left 180 μW, Top Right 300 μW, Bottom Left 567 μW, Bottom Right 1200 μW 76

Figure 31: Single Bulb 1 to 200 mW/cm2, Top Left 180 μW, Top Right 300 μW, Bottom Left 567 μW, Bottom Right 1200 μW 77

Figure 32: Single Bulb 200 to 1000 mW/cm2, Top Left 180 μW, Top Right 300 μW, Bottom Left 567 μW, Bottom Right 1200 μW 78

Figure 33: Bulb Array 0.1 to 1 mW/cm2, Top Left 180 μW, Top Right 300 μW, Bottom Left 567 μW, Bottom Right 1200 μW 79

Figure 34: Bulb Array 1 to 200 mW/cm2, Top Left 180 μW, Top Right 300 μW, Bottom Left 567 μW, Bottom Right 1200 μW 80

Figure 35: Bulb Array 200 to 1000 mW/cm2, Top Left 180 μW, Top Right 300 μW, Bottom Left 567 μW, Bottom Right 1200 μW 81

Figure 36: Pipe Reactor Design with 4 Bulb Array 87

Figure 37: 2, 3, and 4 Bulb Arrays for Pipe Reactors 87

Figure 38: Rectangular Reactor Design 88

List of Tables

Page

Table 1: Summary of Microbial and DBP Rules (U.S. Environmental Protection Agency (EPA), 2006) 12

Table 2: UV Dose Requirements (mJ/cm^2) (U.S. Environmental Protection Agency (EPA), 2006) 12

Table 3: Typical Start-up and Restart Times for Mercury Lamps[1] (U.S. Environmental Protection Agency (EPA), 2006) 21

Table 4: UV Mercury Lamps, UV LED Bulbs, and Visible LED Bulb Advantages and Disadvantages 25

Table 5: Bulb Spacing [inches, (centimeters)] 48

Table 6: Vessel Parameters 49

Table 7: Bulb Array Offset Dimensions 49

Table 8: Bulb and Fluid Characteristics 50

Table 9: Batch Variables 50

Table 10: Flow Variables 51

Table 11: Graphing Variables 51

Table 12: Fluence Log Inactivation Regions 51

Table 13: Spherical Coordinates 52

Table 14: Cartesian Coordinates 53

Table 15: Normalized Radiant Intensity Minimum, Maximum, and Averaged 54

Table 16: Emission Angle in Air and Water Compared to Average Radiant Intensity 56

Table 17: Intensity Results 57

Table 18: Absorption Coefficients for Common Types of Water (Kneissl et al., 2010) 64

Table 19: Batch Experiment Results 69

Table 20: Log Reduction for 64s Batch Experiment 70

Table 21: Log Reduction for 129s Batch Experiment 71

Table 22: Flow Dose with Varying Bulb Output Power 74

Table 23: Percent Volume Associated with Shoulder, Log-Linear, and Tailing Regions82

Table 24: Percent Volume Associated with Shoulder, Log-Linear, and Tailing Regions for 3000 μW..... 83

List of Equations

Page
Equation 1: Cartesian Coordinates to Spherical Coordinate 'r' 32
Equation 2: Cartesian Coordinates to Spherical Coordinate ‘azimuth' 32
Equation 3: Cartesian Coordinates to Spherical Coordinate 'elevation' 32
Equation 4: Spherical Coordinates to Cartesian Coordinate 'x' 32
Equation 5: Spherical Coordinates to Cartesian Coordinate 'y' 32
Equation 6: Spherical Coordinates to Cartesian Coordinate 'z' 32
Equation 7: Snell's Law 33
Equation 8: Snell's Law with LED and Medium Identified 33
Equation 9: Snell's Law with LED Constant and Medium Identified 33
Equation 10: Solid Angle 34
Equation 11: Surface Area of Sphere Contained by Specified Solid Angle 34
Equation 12: Intensity 35
Equation 13: Converting Intensity Equation to Limited Solid Angle 36
Equation 14: Intensity Limited to Solid Angle 36
Equation 15: Sum Normalized Intensity on Layer 38
Equation 16: Percent Intensity at Each Point 38
Equation 17: Intensity at Each Point 38
Equation 18: Irradiance 38
Equation 19: Mercury Lamp Irradiance 39
Equation 20: LED Bulb Irradiance 39
Equation 21: Beer-Lambert Law 40

Equation 22: Absorption Attenuation Factor 40
Equation 23: Log Reduction 42
Equation 24: Snell's Law Rearranged for Water Angle 55
Equation 25: Snell's Law Solved for Water Angle 55
Equation 26: Intensity Limited to Solid Angle 57
Equation 27: Intensity Equation Reduced with Emission Angle in Water 57
Equation 28: Normalized Intensity at Point 59
Equation 29: Normalized Intensity at Layer 60
Equation 30: Percent Intensity at Point 60
Equation 31: Intensity at Point 60
Equation 32: Elevation Half Step 62
Equation 33: Ring Area for Elevation = 0 62
Equation 34: Ring Area for Elevation > 0 63
Equation 35: Point Area for Elevation = 0 63
Equation 36: Point Area for Elevation > 0 63
Equation 37: Irradiance 63
Equation 38: Absorption 64
Equation 39: Dose-Log Inactivation for 269 nm LED Bulbs 67

MODELING ULTRAVIOLET (UV) LIGHT EMITTING DIODE (LED) ENERGY PROPAGATION IN REACTOR VESSELS

I. Introduction

Background

The United States Environmental Protection Agency's (EPA) National Homeland Security Research Center (NHSRC) is concerned with both accidental and intentional releases of chemicals into waste streams. Certain chemicals may be hazardous to municipal wastewater treatment plants that normally dispose of that wastewater. This can lead the plants to not accept contaminated wastewater due to decreased plant efficiency or increased plant costs to dispose of the harmful chemicals.

One method to neutralize chemicals of concern is through Advanced Oxidation Processes (AOP). One such process uses ultraviolet (UV) energy to decompose hydrogen peroxide (H_2O_2) to create hydroxyl radicals (·OH). The hydroxyl radicals then neutralize the hazardous chemicals.

A second UV disinfection method is DNA disruption. This method uses UV energy to directly alter DNA of targeted pathogens. This process deactivates the pathogen and prevents it from reproducing.

The AOP and DNA disruption is optimal for UV energy that is in a wavelength range 240-280 nanometers (nm). This requirement drives the selection of possible UV energy sources. Currently, UV energy is primarily produced through low pressure mercury lamps. Unfortunately, low pressure mercury lamps have many drawbacks. Mercury lamps are physically large. Their start up time prevents pulsing. The bulbs are

costly and have short lifespans. Additionally, the lamps contain a hazardous material that must be properly disposed.

Light Emitting Diodes (LEDs) were discovered in the fall of 1961 by Bob Biard and Gary Pittman (Edison tech center LEDs and OLEDs.2013). In their efforts to try to make a laser, they tested a tunnel diode and found a drop in resistance. Using an infrared detector, they discovered that the devices lit up. In 1962, the first commercial LED, the SNX-100, was sold. LED's offer many advantages including that they are an energy efficient source of light for short distances, exhibit small power dissipation, are durable and shockproof compared to glass bulb lamps, and provide directional light. Since that time, visible LEDs have seen drastic improvements in efficiency, energy output, lifespan, and cost. Additionally, LEDs are available which emit energy across the visible light spectrum and into the infrared spectrum.

In the last decade, UV LEDs were developed that operate in the wavelengths needed in the AOP process. Advantages of UV LED use over low pressure mercury lamps include smaller size, minimal start up time, and no hazardous material. Projections show UV LEDs will follow similar improvements to visible LEDs, which will improve cost, lifetime, efficiency, and energy output. While there has been research investigating the characteristics of UV LED energy, little research focuses upon models of UV LED fluence in an AOP or DNA disruption processes. Also, research is lacking on UV LED applications in air versus water.

Problem Statement

UV energy is historically used in mercury lamp applications to treat water. Mercury lamps have multiple drawbacks that UV LEDs are able to solve. However, the physical design and energy distribution between mercury lamps and LEDs are different. A large amount of research exists on the design of energy distribution in mercury lamp UV systems. UV LEDs, however, are relatively new in this application. Individual characteristics of light and UV energy are well documented in literature. Despite this, there is a knowledge gap of how these characteristics interact and how a single model can describe the concentration of UV LED energy in a specific area.

This research effort focuses on modeling the characteristics of UV LED energy. This effort will be useful to more efficiently design a device to apply a specified UV dosage. Optimized vessel designs will lower operating costs and improve disinfection/oxidation rates.

Research Objectives/Questions/Hypotheses

The objective of this research is to create and validate mathematical models of energy propagation emitted by UV LEDs for the purpose of aiding in the design of AOP or DNA disruption reactor vessels. The model will enable a detailed analysis of different vessel designs to identify those which are optimal, and in turn identify which may be most effective in neutralizing harmful pathogens. The research presented in this thesis will answer the following research questions:

RQ1: What is an Advanced Oxidation Process (AOP) and DNA disruption? How are they different and similar? Also, how are they used for water disinfection?

RQ2: What sources of ultraviolet (UV) radiation have been used for the AOP and DNA disruption in water disinfection applications?

RQ3: What are the measures of UV energy distribution in a reactor vessel?

RQ4: What mathematical models can be used to calculate the distribution and absorption of UV Light Emitting Diode (LED) radiation as it propagates through different mediums?

RQ5: What tools can be used to simulate these models to calculate the UV energy present at any point within a UV reactor vessel?

RQ6: How do simulation results generated from the model compare to actual experimental results collected from the laboratory?

RQ7: What UV LED reactor designs are most efficient for water disinfection?

Research Methodology

The research methodology used in this thesis is modeling and simulation. First, the relevant UV and AOP literature is reviewed to identify governing equations. Second, a model is synthesized at the appropriate level of abstraction to calculate the UV energy present at any point within a reactor vessel based upon multiple factors including its geometry, the location and intensity of the UV radiation sources, and the medium in which the energy propagates. The model lacks an absorption coefficient for the contaminant/microbes present in the solution and calculations for reflectance. Third, a

simulation tool suitable for modeling UV energy propagation within a reactor vessel is selected and the relevant models of an actual UV reactor vessel are coded into the simulation tool. Simulations are conducted and the results are compared to actual measurements made in the laboratory. Finally, tradeoffs in the spacing of UV LEDs within the vessel are discussed based upon the desired dosage and flow requirements.

Assumptions/Limitations

The models of UV radiation used in this thesis assume that the UV radiation emitted by the sources is incoherent and that the impact of interference is negligible compared to the loss due to absorption during propagation. The research is limited to comparing the simulation results to actual laboratory measurements for only two different reactor vessel geometries. This research effort represents the initial modeling effort to understand UV energy propagation. There are factors which have been approximated in an effort to simplify the model. These factors need more study to determine their impact on the accuracy of the model.

Implications

The results from this research effort will provide a modeling and simulation capability that will aid in the design and analysis of UV LED reactor vessels. UV LEDs are still in their infancy and are projected to improve at rates similar to visible LEDs. Optimized vessel design enables UV LEDs to be effective at an early stage and reduce overall project costs. The variables within the model are easily altered to match new bulb specifications and design new vessel shapes. The model may also be useful in applications other than the AOP or DNA disruption. UV energy is also used in air

disinfection systems and multiple curing applications utilize UV energy in manufacturing settings. Other industries may benefit from this research by optimizing energy distribution and in turn reducing the power requirements and lowering system costs.

Preview

The next chapter, Chapter II, highlights the available literature on water disinfection/oxidation, mercury lamp and LED bulb characteristics, and modeling techniques for LED systems. Chapter III describes the methodology of forming the MATLAB based model. Chapter IV reports and discusses the results. Finally, Chapter V states the conclusions of this study and identifies areas for future research.

II. Literature Review

Chapter Overview

In this chapter, the primary methods of water disinfection along with the advantages, disadvantages, and the major points on how the methods work are presented. Next, the characteristics of UV mercury lamps and LED bulbs are discussed to provide context for their application in UV reactor designs. A review of modeling techniques and factors important in the design of water disinfection reactor vessels is then presented. Finally, modeling and simulation environments are discussed.

Water Disinfection

Chlorine Disinfection

Chlorine disinfection has been the primary method to disinfect water for many years in the United States. The process involves adding the optimal amount of chlorine to a water source. However, chlorine disinfection has a few disadvantages. These include introducing trihalomethane (THM) and haloacetic acid (HAA) as byproducts (Taghipour & Sozzi, 2005). Additionally, two main harmful pathogens, *Cryptosporidium* and *Giardia*, are chlorine resistant. Chlorine is also harmful to humans in high concentrations and leaves an undesired smell and taste in disinfected water.

UV Disinfection

UV energy is defined as the energy spectrum between 100 and 400 nm. This range is further broken down into VUV (vacuum UV), UVC, UVB, and UVA which consist of wavelengths between 100-200, 200-280, 280-315, and 315-400 nm respectively. The range 255-275 nm is proven to be the most effective range for DNA

destruction of harmful pathogens. This range is contained in the UVC range and is slightly higher than the energy output for low pressure mercury lamps (254 nm). Figure 1 shows the electromagnetic spectrum with a callout for UV and visible energy (*UVC LED disinfection.*2013; Wurtele et al., 2011).

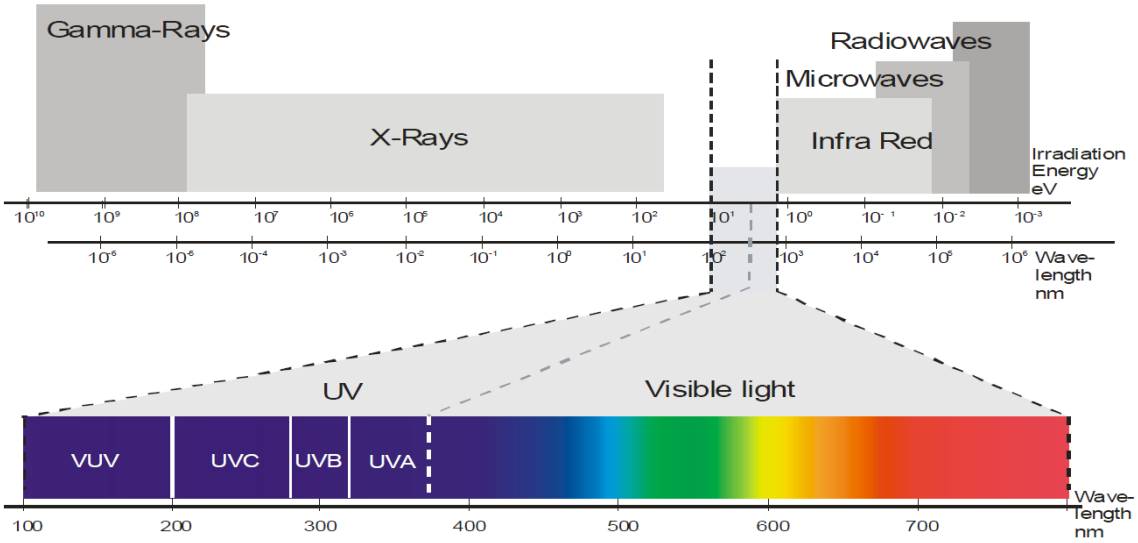

Figure 1: Electromagnetic Spectrum (*UVC LED disinfection.*2013)

There are two main disinfection methods associated with ultraviolet (UV) energy. The first utilizes the energy to directly deactivate the DNA of the pathogens, often called DNA disruption. The second method uses the energy in an advanced oxidation process (AOP) where the UV energy breaks down a chemical into radicals that neutralize the harmful pathogens (*UVC LED disinfection.*2013).

Both of the UV methods are used in disinfection processes to overcome disadvantages of chlorine systems. UV systems eliminate chlorine overdose issues and pose no threat of overdosing since overexposure of UV energy is not harmful when applied to water. UV disinfection systems reduce by-products and toxins introduced in

chlorine systems. Additionally, UV systems do not alter taste or smell of water (*UVC LED disinfection.*2013).

Despite the numerous advantages of UV over chlorine disinfection systems, there are a few disadvantages that affect UV systems. Sommer et. Al (2008) describe the complexity of measuring and calculating UV energy. UV fluence cannot be directly measured due to the intricacies of the system. Furthermore, UV lamp output, water flow, ultraviolet transmittance (UVT), and hydraulic properties of the vessel are all factors that complicate the system.

Lamps which output multiple wavelengths may increase the effectiveness of UV disinfection. UV LEDs are able to do this to maximize germicidal effects by combining bulb array patterns to create the right intensity and wavelength mix (C. Chatterley & Linden, 2010). One study showed that combining UVC and UVA energy at 280/365 and 280/405 nm more effectively disinfected bacterial counts in urban wastewater effluent than a single wavelength used alone (Chevremont, Farnet, Coulomb, & Boudenne, 2012; Oguma, Kita, Sakai, Murakami, & Takizawa, 2013)

DNA Disruption

DNA disruption uses UV energy to alter the DNA of pathogens to inactivate the targeted pathogen and prevent it from replicating (Figure 2). DNA disruption requires specific UV doses to inactivate different pathogens. The pathogens *Cryptosporidium* and *Giardia* are extremely resistant to chemicals such as chlorine, but correct doses of UV energy can inactivate these harmful pathogens (*UVC LED disinfection.*2013).

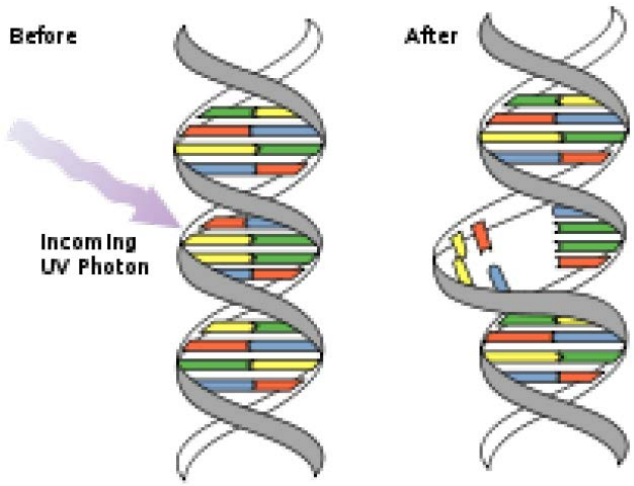

Figure 2: UVC DNA Disruption (*UVC LED disinfection*.2013)

DNA inactivation in water occurs in the 240-280 nm electromagnetic range. The most effective range for DNA UV absorption is known to be in the 260-265 nm range. This is based on the most commonly targeted pathogens. The range may shift, however, depending on the targeted pathogen. UV energy above and below this range still demonstrate efficient inactivation, however wavelengths higher than the UVC range required drastically higher dosages to achieve the same benefit (Bowker, Sain, Shatalov, & Ducoste, 2011; Oguma et al., 2013; Wurtele et al., 2011).

Advanced Oxidation Process (AOP)

An Advanced Oxidation Process utilizes UV energy to oxidize the target pathogens. AOP may also be used to oxidize chemicals of concern. This process requires applying the correct dose of UV energy to a solution to reduce a chemical to radicals that subsequently neutralize target pathogens. Chemicals are usually required to be added to the system. Two of the most common oxidants used in AOP systems are hydrogen peroxide (H_2O_2) and ozone (O_3) (Legrini, Oliveros, & Braun, 1993).

Alpert, Knappe, and Ducoste describe the reactions involved in the AOP process with hydrogen peroxide for the destruction of methylene blue. Their equations are all single ordered, but reactions occur to reform hydrogen peroxide from the ·OH radicals and also multiple byproducts. This may result in a non-linear relationship between input variables of UV energy, H_2O_2, and methylene blue and the resulting methylene blue concentration. Increasing the ·OH radical production may occur by using higher energy and H_2O_2 concentrations (Alpert, Knappe, & Ducoste, 2010; Coenen et al., 2013).

Inactivation

Pathogen inactivation is measured by log reduction. Method of disinfection, energy wavelength, pathogen type and intensity all factor into pathogen reduction. The log reduction requirements are typically driven by regulations in order to protect human health.

The US Environmental Protection Agency (EPA) regulates water disinfection in the United States. The Surface Water Treatment Rule (SWTR), Interim Enhanced Surface Water Treatment Rule (IESWTR), Long Term 1 Enhanced Surface Water Treatment Rule (LT1ESWTR), and Long Term 2 Enhanced Surface Water Treatment Rule (LT2ESWTR) are regulations set by the EPA. LT2ESWTR is currently being set in place and is scheduled to be completed by 1 October 2014. A summary of the regulations and their required log removal is shown in Table 1. Table 2 shows the EPA UV dose requirements for *Cryptosporidium*, *Giardia*, and viruses. It is important to note that the EPA report does not specify the wavelength used for the results in Table 2. However, mercury lamps (254 nm) were the predominant technology used at the time of publication in 2006 and are assumed to be used for this data. The relative dose suggests

that the 4 log reduction requirement for viruses may be the driving factor. This table suggests that *Cryptosporidium* and *Giardia* reduction are more easily achieved than virus reduction. Dose requirements may change with different applied wavelengths which may make either the *Cryptosporidium* or *Giardia* requirement the driving factor. Additionally, the results in Table 2 are based on DNA disruption and not an AOP system (U.S. Environmental Protection Agency (EPA), 2006).

Table 1: Summary of Microbial and DBP Rules (U.S. Environmental Protection Agency (EPA), 2006)

Surface Water Treatment Rules – Minimum Treatment Requirements[1]			
Regulation	***Giardia***	**Virus**	***Cryptosporidium***
SWTR	3-log removal and/or inactivation	4-log removal and/or inactivation	Not addressed
IESWTR and LT1ESWTR	No change from SWTR		2-log removal
LT2ESWTR	No change from SWTR		0- to 2.5-log additional treatment for filtered systems[2]
			2- or 3-log inactivation for unfiltered systems[2]

[1] The term "log" means the order of magnitude reduction in concentration; e.g., 2-log removal equals a 99% reduction, 3-log removal equals a 99.9% reduction, and 4-log removal equals a 99.99-percent reduction.
[2] Specific requirements for each plant depend on source water monitoring results and current treatment practices (40 CFR 141.710 – 141.712).

Table 2: UV Dose Requirements (mJ/cm^2) (U.S. Environmental Protection Agency (EPA), 2006)

Target Pathogens	**Log Inactivation**							
	0.5	**1.0**	**1.5**	**2.0**	**2.5**	**3.0**	**3.5**	**4.0**
Cryptosporidium	1.6	2.5	3.9	5.8	8.5	12	15	22
Giardia	1.5	2.1	3.0	5.2	7.7	11	15	22
Virus	39	58	79	100	121	143	163	186

[1] 40 CFR 141.720(d)(1)

Mamane-Gravetz and Linden report that many organisms follow a shoulder, log-linear, and tailing behavior at low, medium, and high fluence levels. This behavior is portrayed in Figure 3 with *Bacillus subtilis* spores as the target organism. This behavior is important due to the drastic increase in organism reduction after getting over the

shoulder. The tailing portion occurs when the organism is close to being completely disinfected (Mamane-Gravetz & Linden, 2005).

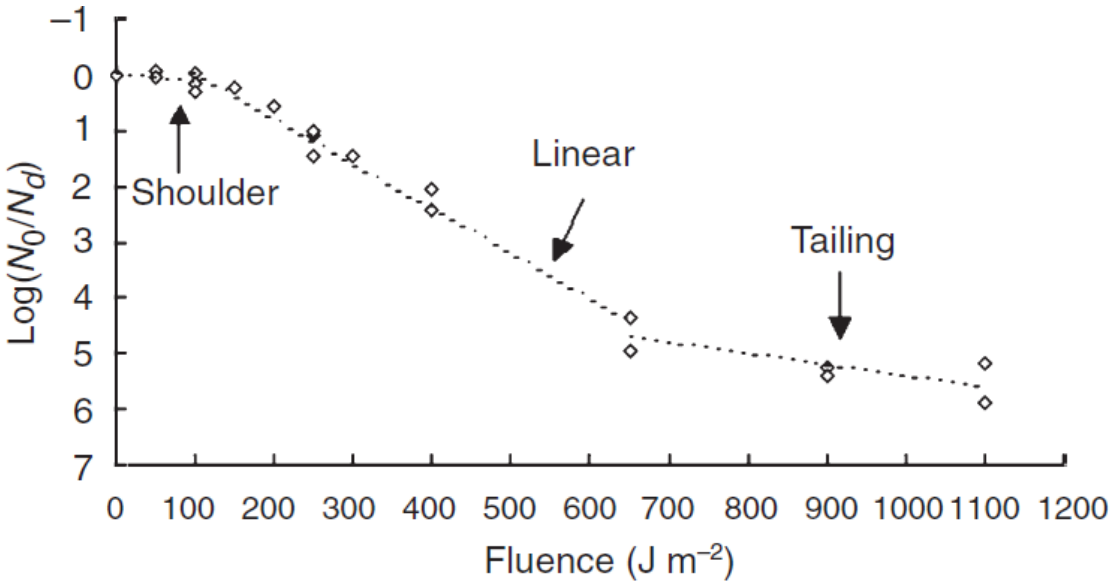

Figure 3: Typical Fluence-Log Inactivation Response Curve (Mamane-Gravetz & Linden, 2005)

Mercury Lamp and LED Bulb Characteristics

Mercury Lamps

Mercury lamps are the original source used in UV disinfection. They are an excellent source for high power but have numerous disadvantages. These include short lifespans, fragility, toxic waste, and large physical geometry (C. Chatterley, 2009).

Low pressure mercury lamps are restricted to emitting energy at a peak wavelength of 254 nm. Medium pressure mercury lamps emit energy over a broader spectrum, which ranges from 220-440 nm. Output power from a sample low pressure mercury lamp and medium pressure mercury lamp are shown in Figure 4. Both types of mercury lamps are specific with the spectrum of energy emitted and cannot be designed for different wavelengths. The medium pressure lamps cover a larger energy spectrum,

however only a small range of the energy emitted is effective for germicidal disinfection (Boyjoo, Ang, & Pareek, 2013; Liu, Ducoste, Jin, & Linden, 2004).

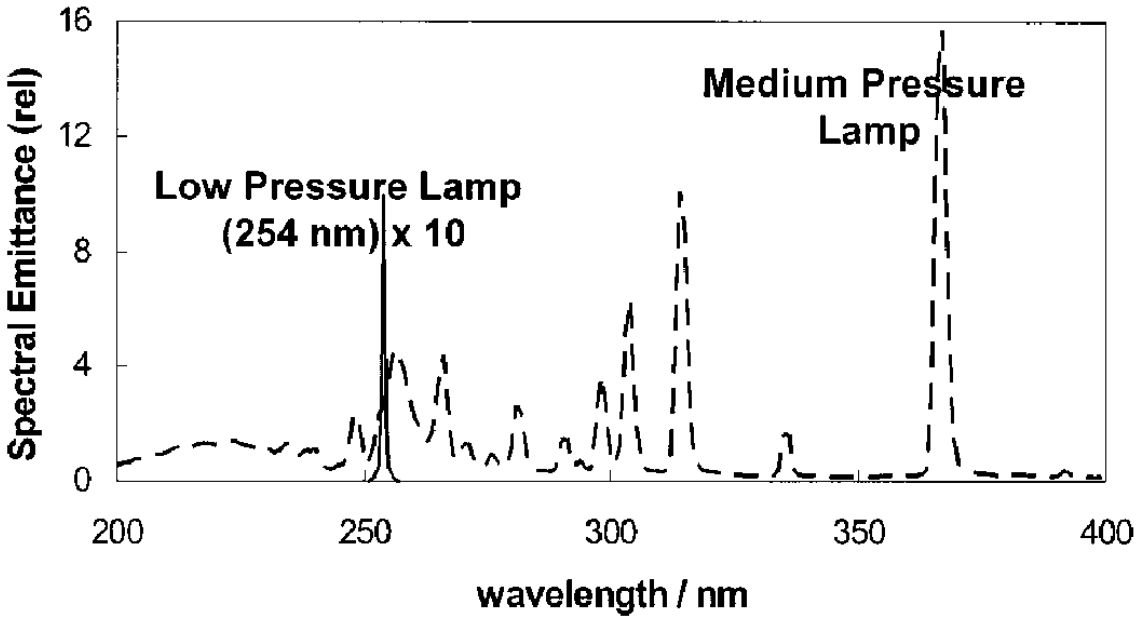

Figure 4: Spectral Emittance of Low Pressure Mercury UV Lamp (solid line) and Medium-Pressure Mercury UV Lamp (dashed line) (Bolton & Linden, 2003)

The physical geometry of mercury lamps limits the design choices when used in disinfection systems. The lamps are typically placed in line with fluid flow in a pipe, as shown in Figure 5, or are placed perpendicular to the flow, as shown in Figure 6, and arranged to maximize power throughout a cross section of the fluid flow. Figure 6 also shows the quartz sleeves that are normally used to encase mercury lamps within a disinfection system (Hofman et al., 2007; Taghipour & Sozzi, 2005).

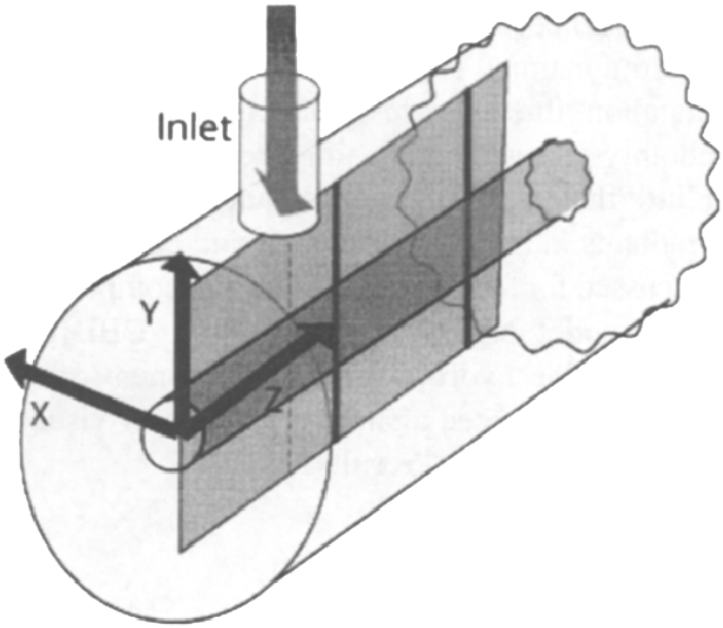

Figure 5: Mercury Lamp with Parallel Flow (Taghipour & Sozzi, 2005)

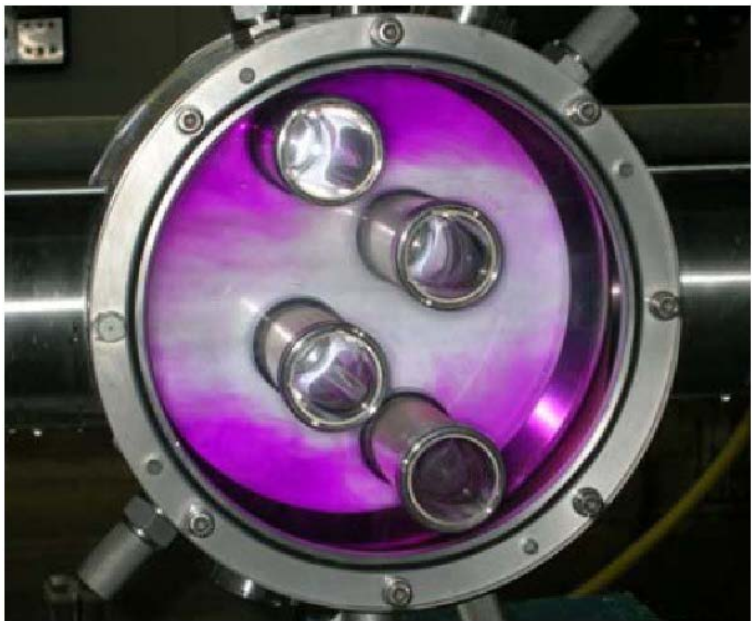

Figure 6: Mercury Lamp with Perpendicular Flow (Hofman et al., 2007)

UV LEDs

Studies are currently limited for UV LEDs and their application in either batch or flow through designs. This is primarily due to the novelty of the technology and limited

power output of UV LED bulbs. UV LEDs are expected to see large improvements in power, efficiency, and lifespan similar to the improvements seen in visible light LEDs in the past two decades. UV LEDs already provide the benefits of a small form factor, no toxic waste, and selectable wavelength over mercury lamps. Projections predict power, efficiency, and lifespan to match or exceed mercury lamps in the near future. Shur and Gaska predict UV LED applications will take off as performance of these bulbs increase (C. Chatterley & Linden, 2010; Oguma et al., 2013; Shur & Gaska, 2010; Yu et al., 2013; Yu, Achari, & Langford, 2013).

Efficiency

Low pressure mercury lamps are around 35-38% energy efficient. A 2010 study by Shur and Gaska reveals that UV LEDs are currently less than 2% efficient, with 280 nm bulbs having the highest efficiency rate and efficiency decreasing at shorter wavelengths. The internal efficiency of UV LEDs is between 15 and 70%; however, internal absorption and internal reflection create a maximum of 2% wall plug efficiency. The authors state that visible LEDs have resolved this problem and expect UV LEDs to follow as shown in Figure 7. Visible LEDs currently exceed an efficiency of 75%, more than twice the efficiency of mercury lamps (Bettles, Schujman, Smart, Liu, & Schowalter, 2007; Shur & Gaska, 2010).

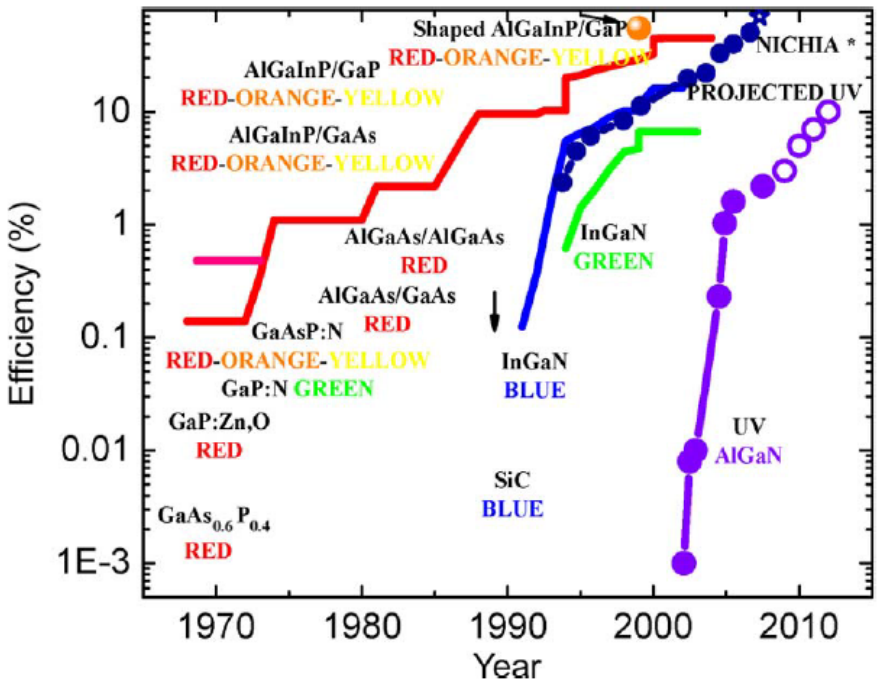

Figure 7: Achieved and Projected LED Performance (Shur & Gaska, 2010)

The efficiency growth rate is incredible for visible LEDs. Visible LEDs are the most used type of LEDs on the market today. They are the most researched and have significantly improved since the early 1990's. Their efficiency has improved at an average rate of 20 times per decade, which is due to advances in semiconductor and packaging technology. There is a consensus among researchers that UV LEDs will follow with similar success as visible LEDs, and the applications for UV LEDs will take off with the improved technology (Bettles et al., 2007; C. Chatterley & Linden, 2010; Je Wook Jang, Seung Yoon Choi, & Kon Son, 2011; Paisnik, Poppe, Rang, & Rang, 2012; Shur & Gaska, 2010).

Lifespan

The lifespan of conventional lighting is often based on catastrophic failure. Mature LEDs, on the other hand, are not prone to catastrophic failure and instead

progressively degrade over time. This changes the efficiency of the bulb and alters the wavelength of the emitted energy (Je Wook Jang et al., 2011; Lenk & Lenk, 2011).

In visible light LEDs, yellowing of the lens, which is often formed from an epoxy, changes the efficiency of the bulb and may also change the wavelength emitted. This occurs from exposure to heat and light. As yellowing increases, LEDs have a degradation effect that decreases light efficiency and changes the wavelength produced by the bulb. Furthermore, UV wavelengths lead to a greater yellowing effect than visible light when the same lens materials are applied. In addition to reduced transmission of the optics, the LEDs may become less efficient due to charge trapping or other mechanisms which affect the LEDs efficiency in converting electrons to photons. Multiple studies show that thermal stress is the main cause of this type of LED degradation (Lenk & Lenk, 2011; Narendran, Gu, Freyssinier, Yu, & Deng, 2004; Paisnik et al., 2012; Tang et al., 2012).

Since LEDs do not fail catastrophically, a common definition for LED failure is based off of a specified drop in efficiency, which is normally a drop in the 30-50 percent range. Some types of LEDs are able to be used up to 100,000 hours. However, studies show that UV LEDs are currently limited to much shorter lifespans often less than 1,500 hours. These lifespans are also associated with a large drop in efficiency of around 40 percent after 100 hours of use followed by almost constant output power until the bulb is no longer effective, shown in Figure 8 (Je Wook Jang et al., 2011; Wurtele et al., 2011).

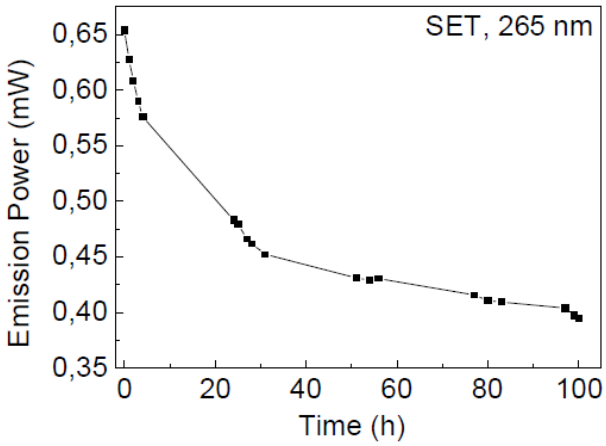

Figure 8: Power Drop of a SET 265 nm LED at 20 mA over 100 hours (Kneissl, Kolbe, Wurtele, & Hoa, 2010)

The source of heat in LED applications is caused from the efficiency of LEDs and ambient temperature. UV LEDs typically output less than 2% of the input power, while the remainder of this energy is dissipated as heat. This requires that the majority of the energy introduced to the bulb needs to be managed as heat and dissipated to the surrounding environment to adequately control the temperature. Less heat will be introduced to the system as the efficiency of UV bulbs improves, resulting in longer lifespans and greater power output (Narendran et al., 2004; Paisnik et al., 2012; Shur & Gaska, 2010).

Even though mercury lamps have been in use for many more years than UV LEDs, they have lifespans of around 8,000 to 10,000 hours. This equates to around 1 year of useful life. Mercury lamp lifespans are currently greater than UV LED lifespans but this ratio is projected to favor UV LEDs in the future (Bettles et al., 2007; C. Chatterley, 2009).

Wavelength

Studies show that about 265 nm UV energy has the maximum germicidal effect for DNA disruption. Wavelengths of 365 nm require a much higher dose (on the order of 30,000 times) over 254 nm UV energy. Also the gap between 265 nm and 310 nm energy corresponds to inactivation reduction of 6 orders of magnitude (C. Chatterley & Linden, 2010).

One particular advantage to take note of is the ability of LEDs to produce a range of wavelengths within the UV-C range while low pressure mercury lamps are restricted to 254 nm. LEDs are typically considered to be a single wavelength, instead of consisting of a spectrum of energy (Bettles et al., 2007; Wurtele et al., 2011).

Warm Up Time

Table 3 shows a sample of start-up and restart times for mercury lamps according to tests from the EPA. Both low-pressure and medium-pressure mercury lamps require a start-up time to reach full power. On the other hand, UV LEDs do not require a start-up or restart time. They start at a higher power and decrease to their 'maximum' power over 10 minutes. Figure 9 shows a comparison of start-up power conducted by Chatterley. The increased initial power of around 7% for UV LEDs may result in benefits of pulsing the bulb (C. Chatterley, 2009; U.S. Environmental Protection Agency (EPA), 2006).

Table 3: Typical Start-up and Restart Times for Mercury Lamps[1] (U.S. Environmental Protection Agency (EPA), 2006)

Lamp Type	Cold Start[2]	Warm Start[3]
LPHO	total time: 4 – 7 minutes (min) (0 – 2 min warm-up plus 4 – 5 min to full power)	total time: 2 – 7 min (0 – 2 min warm-up plus 2 – 5 min to full power)
MP	total time: 1 – 5 min (No warm-up or cool down plus 1 – 5 min to full power[4])	total time: 4 – 10 min (2 – 5 min cool down plus 2 – 5 min to full power[4])

[1] Information shown in table is compiled from Calgon Carbon Corporation, Severn Trent, Trojan, and WEDECO. Contact the manufacturer to determine the start-up and restart times for specific equipment models.
[2] A cold start occurs when UV lamps have not been operating for a significant period of time.
[3] A warm start occurs when UV lamps have just lost their arcs (e.g., due to voltage sag).
[4] 60 percent intensity is reached after 3 min.
Source: Cotton et al. (2005)

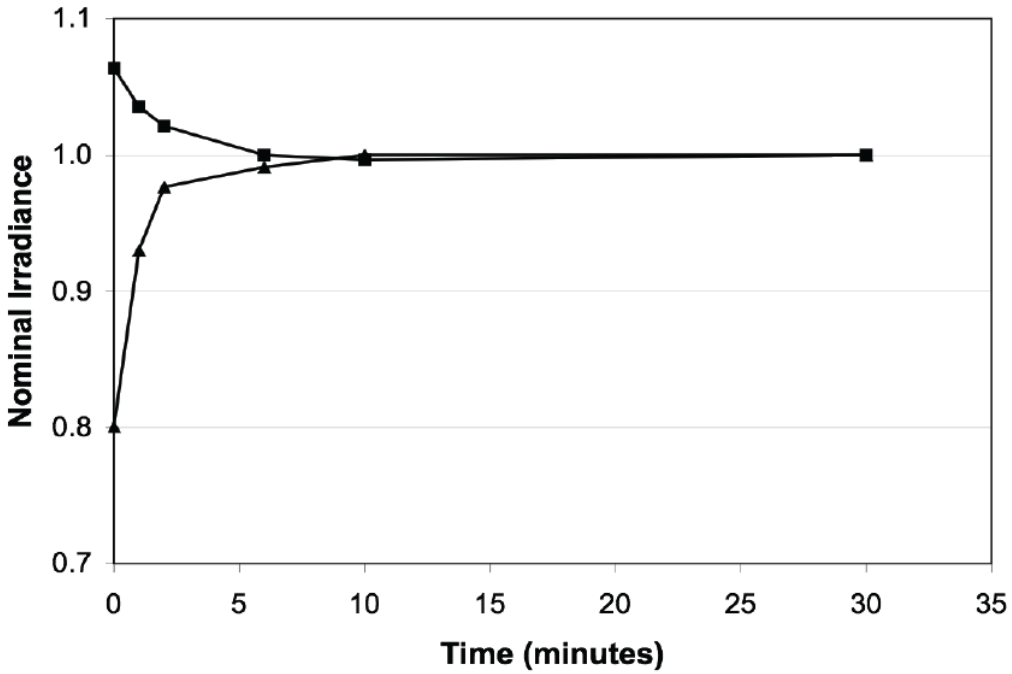

Figure 9: Warm-up Time for UV LEDs (■) Versus Low Pressure Lamps (▲) (C. Chatterley, 2009)

Pulsing

Pulsing light may decrease energy usage for a desired disinfection rate. A study shows UVA-LEDs with a stable current at 0.5 amps utilizes more than 10 times the energy of a 10 ms on to 100 ms off pulse rate for the same type bulb with a 1 amp current

for the same disinfection rate of E. coli in air. This research suggests that pulsing might be beneficial due to the higher power used in the pulsed bulb than the steady state experiment (Gadelmoula et al., 2009).

Shur and Gaska confirm that pulsing LEDs may provide higher power outputs from the system. Figure 10 shows how a smaller pulsed duty cycle provides higher power than larger duty cycles and continuous width (CW) operations. Pulsing LEDs increases the output power by limiting heat generation within the LED package (Shur & Gaska, 2010).

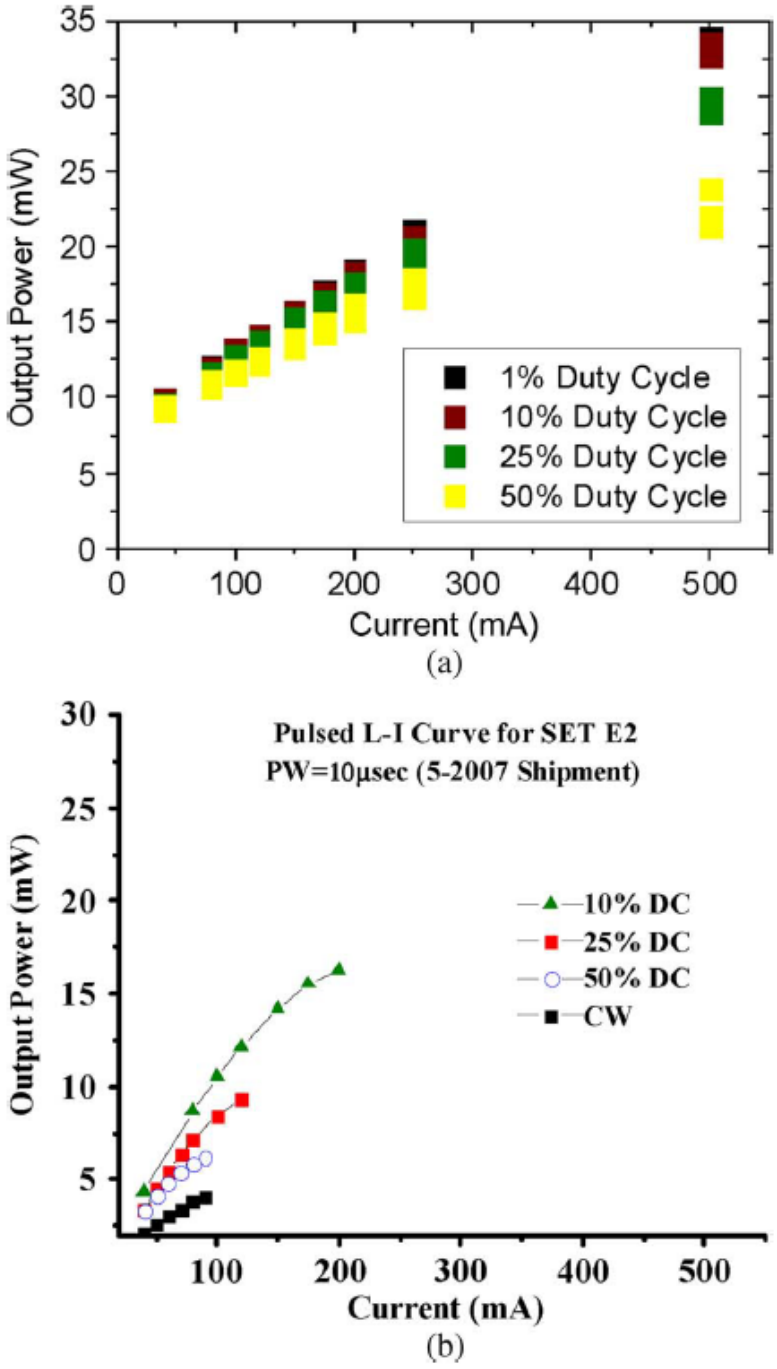

Figure 10: Output Power Versus Current for CW and Pulsed Modes of Operation for DUV LEDs
(Shur & Gaska, 2010)

Figure 11 compares single LED bulbs with an array of LED bulbs (called lamp in the diagram, not to be confused with mercury lamps used elsewhere in this document). The single chips have a much greater difference in power between pulsed and continuous

operations than the multiple bulb configuration. This may be mainly due to the heat generated by the bulb array. A better heat sink or increasing the bulb efficiency to reduce heat generation may supply better results for LED arrays (Shur & Gaska, 2010).

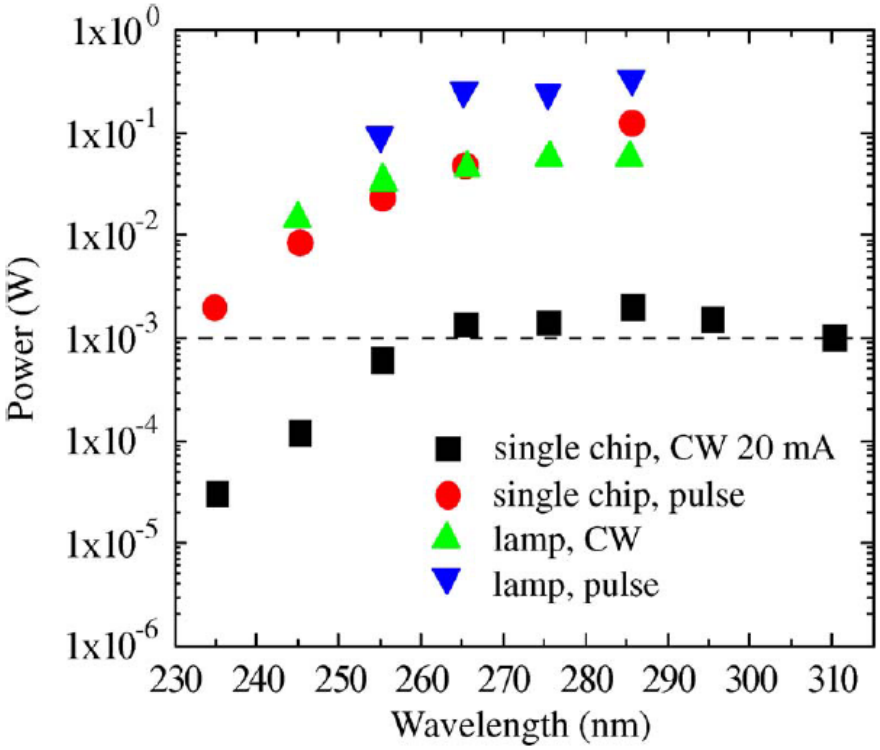

Figure 11: Output Optical Power of Single-Chip LEDs and LED Lamps for CW and Pulsed Modes (Shur & Gaska, 2010)

Advantages and Disadvantages

The advantages and disadvantages for UV mercury lamps and UV LED bulbs are currently mixed. The current advantages of UV LED bulbs include no toxicity from mercury, robustness, compact form factor, immediate start-up, ability to pulse, and ability to tune the wavelength. The remaining factors, power, efficiency, and lifespan, currently are advantageous in UV mercury lamps over UV LED bulbs. However, the technological advances in visible LED bulbs show projections for UV LED bulbs to soon exceed the

specifications for UV mercury lamps. Table 4 lists the current advantages and disadvantages for the mercury lamps and LED bulbs discussed.

Table 4: UV Mercury Lamps, UV LED Bulbs, and Visible LED Bulb Advantages and Disadvantages

	UV Mercury Lamps	UV LED Bulbs	Visible LED Bulbs
Power	15 W	Order of μW-mW	N.D.
Efficiency	33-38%	<2%	>75%
Lifespan	8,000-10,000 Hours	1,500 hours	100,000 Hours
Toxic by mercury	Yes	No	No
Fragile	Yes	No	No
Compact Form Factor	No	Yes	Yes
No Start Up Time	No	Yes	Yes
Ability to Pulse	No	Yes	Yes
Tune Wavelength	No	Yes	Yes

Modeling and Simulation

Modeling Approaches

Multiple point source summation (MPSS), multiple segment source summation (MSSS), and line source integration (LSI) are all methods to model mercury bulbs. MPSS is the process of splitting a linear mercury lamp into n equally spaced point sources. Each point source has 1/n watts associated with it. Fluence rate is uniformly distributed (Lambertian) in all directions from the point. Bolton (2000) expanded on the MPSS modeling method and created the MSSS method, which more accurately describes the behavior of UV energy emitting from mercury lamps near the ends of the lamp and the lamp surface. The LSI model is the MPSS model as the number of points, n, approaches infinity. It is a continuous calculation based on the location along the mercury lamp. Figure 12 shows the energy pattern emitted from the MPSS, MSSS, and radial methods (Bolton, 2000; Liu et al., 2004).

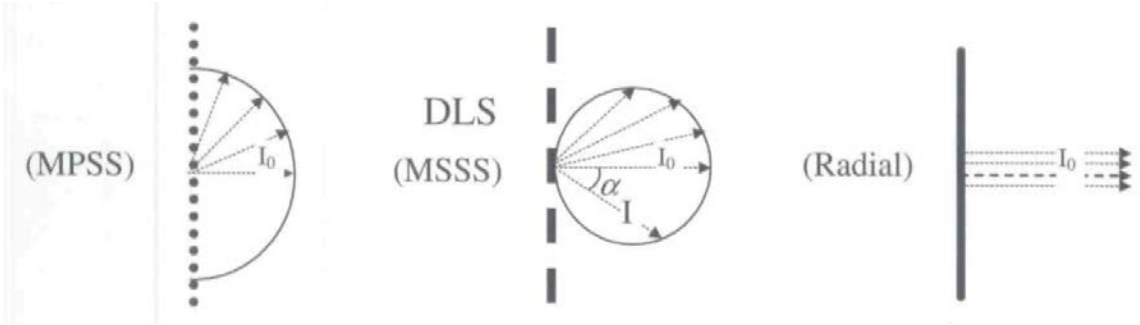

Figure 12: MPSS, MSSS, and Radial Model Emittance Patterns (Liu et al., 2004)

Mercury lamps are often modeled using a Lambertian emittance pattern. A Lambertian pattern is where emitted energy is constant independent of viewing angle (Dereniak & Boreman, 1996). These energy sources are straightforward to model due to limited changes in energy intensity. A good example is the incandescent light bulb. It emits energy equally in all directions. Some mercury lamp models assume the lamp is an infinite length and follow a Lambertian pattern. This radial method does not take into account deviations at the ends of the lamp. The MPSS, MSSS, and LSI models help solve this issue.

Design Factors

Crystal IS lists 3 important design factors to consider when choosing UV water disinfection. They are water quality, water flow rate, and pathogen(s) to be inactivated. Water quality determines the UV transmittance through the medium. Higher transmittance produces better results. This is due to less turbidity, which absorbs less UV energy. Water flow rate determines the exposure time, the lower the flow rate, the longer the exposure which results in a greater log inactivation or requires higher lamp output. Pathogens have different resistances to UV energy. The more resistant the pathogen the

more energy is required. AOP is dependent on reactions between the UV energy, oxidant and target pathogens (*UVC LED disinfection.*2013).

Multiple Bulbs

Bulb layout is driven by the efficiency and uniformity requirements previously discussed. The most efficient design requires a uniform energy array across the disinfection interface. Additionally, the strength of the LEDs determines bulb spacing. Higher output LEDs allow larger intervals between bulbs. Tighter spacing requirements increases heat produced, which decreases energy efficiency. Altering the heat sink may counter this effect for tightly spaced arrays (Wurtele et al., 2011).

Dose

The applied dose is the irradiance multiplied by exposure. There is currently no method to directly measure contact time between an energy source and flowing water. However, contact time is influenced by the flow rate and hydrodynamics, which can be used to determine an approximate contact time (Wurtele et al., 2011).

Collimated Beam

Due to the low output power of UV LEDs, researchers often use a collimated beam experiment to compare low and medium pressure mercury lamps to LED bulbs. In this approach, multiple LED bulbs, sometimes on the order of 30, are placed in an array to overlap the bulb's fields of view to increase the irradiance. The goal of a collimated beam is to produce parallel rays that form a uniform intensity over a given area. However, the distribution of energy may prevent a uniform intensity. A uniform beam of energy may be used to determine the log reduction associated with a given dose at specific wavelengths (Blatchley III, 1997; Bolton, 2000; Bowker et al., 2011).

Modeling and Simulation Environments

Modeling and simulation is a method used to optimize designs prior to manufacture. This method allows fewer device iterations, which, in turn reduces costs associated with prototypes and experimentation. Multiple software platforms are available for modeling and simulating physics based environments. Mathematica, MATLAB, and COMSOL Multiphysics are three platforms that are suited for this use (COMSOL multiphysics.2014; MATLAB - the language of technical computing.2014; Wolfram mathematica 9.2014).

Each of these programs provides a suitable modeling and simulation environment. They each have optional add-ons that aid in the modeling and simulation in domain specific fields. Mathematica is built around programming in the mathematical domain. It has many of the basics to start a theory based model. Similar to Mathematica, COMSOL Multiphysics also offers a platform based in physical equations. One of the main advantages of this program is the fluid modules. Arrays and matrices form the framework for MATLAB. This program is designed to handle large quantities of data and manipulate data through matrix operations. Each program offers two and three-dimensional plots that aid in producing graphics to represent results created from the program.

Chapter Summary

The advantages and disadvantages of chlorine disinfection, DNA disruption, and the advanced oxidation process are introduced. UV disinfection offers many advantages over chlorine disinfection technology. Next, the differences between mercury lamps and

LED bulbs are discussed. Finally, modeling approaches and factors are discussed. The next chapter discusses the methodology used to model UV LEDs.

III. Methodology

Chapter Overview

In this chapter, the process used to conduct the research is presented. First, a model of irradiance in a 3-dimensional space is introduced and discussed. The concepts and equations necessary to conduct the research are identified and discussed. An environment is selected as a vehicle to conduct the modeling and simulation of UV reactor vessels. Finally, issues related to the modeling of UV energy propagation are discussed.

Data Point Representation

When modeling a UV reactor vessel, it is necessary to identify all locations within a three-dimensional space. For this research, data points are represented in both the spherical and Cartesian coordinate systems. Data points are initialized in a local spherical system which enables calculations based off of distance away from a point source. The Cartesian coordinate system is then used to locate individual point sources in an array and is required for generation of three dimensional plots.

The resolution of a model is directly affected by the number and spacing of the initial data points. The greater number of data points in the needed range results in a higher resolution for the model. The trade-off for higher resolution is longer computing times or lack of computing memory to complete the operation.

Coordinate Systems

Use of both the Cartesian and spherical coordinate systems eases calculations. A right hand Cartesian system is used and below shows the relationship between this system and the spherical system used throughout this thesis. The azimuth is the angle in the x-y plane that is measured counterclockwise starting on the x-axis. The elevation is the angle measured from the x-y plane to the z axis. The spherical coordinate r is the distance from the origin to the specified point.

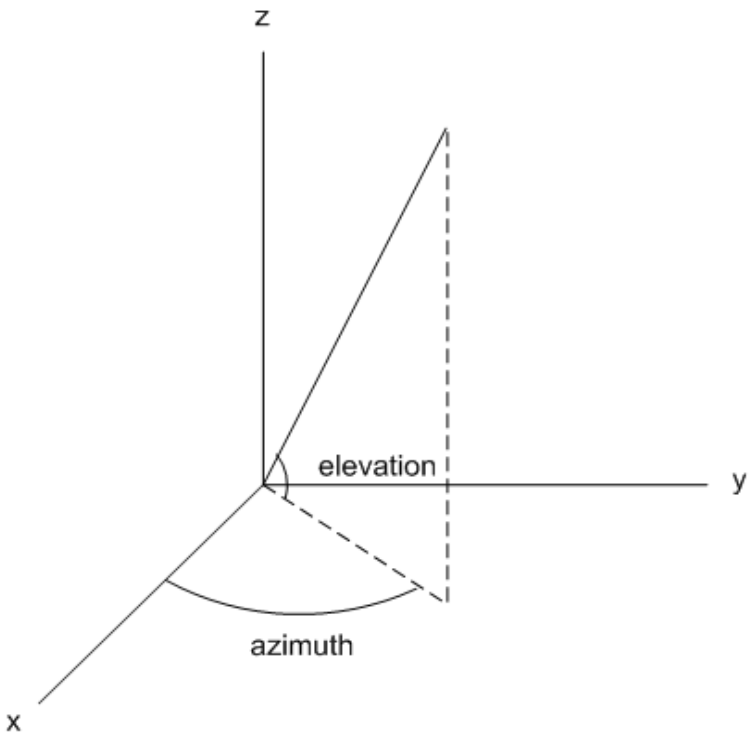

Figure 13: Cartesian and Spherical Coordinate Systems

The equations necessary to convert between the coordinates are shown below in equations 1 through 6.

Cartesian to Spherical

$$\mathbf{r} = \sqrt{\mathbf{x^2} + \mathbf{y^2} + \mathbf{z^2}} \quad (1)$$

Equation 1: Cartesian Coordinates to Spherical Coordinate 'r'

$$\boldsymbol{azimuth} = \boldsymbol{tan^{-1}}(\frac{\boldsymbol{y}}{\boldsymbol{x}}) \quad (2)$$

Equation 2: Cartesian Coordinates to Spherical Coordinate 'azimuth'

$$\boldsymbol{elevation} = \boldsymbol{tan^{-1}}(\frac{\boldsymbol{z}}{\sqrt{\boldsymbol{x^2}+\boldsymbol{y^2}}}) \quad (3)$$

Equation 3: Cartesian Coordinates to Spherical Coordinate 'elevation'

Spherical to Cartesian

$$\boldsymbol{x} = \boldsymbol{r} * \boldsymbol{cos}(\boldsymbol{elevation})\,\boldsymbol{cos}(\boldsymbol{azimuth}) \quad (4)$$

Equation 4: Spherical Coordinates to Cartesian Coordinate 'x'

$$\boldsymbol{y} = \boldsymbol{r} * \boldsymbol{cos}(\boldsymbol{elevation})\,\boldsymbol{sin}(\boldsymbol{azimuth}) \quad (5)$$

Equation 5: Spherical Coordinates to Cartesian Coordinate 'y'

$$\boldsymbol{z} = \boldsymbol{r} * \boldsymbol{sin}(\boldsymbol{elevation}) \quad (6)$$

Equation 6: Spherical Coordinates to Cartesian Coordinate 'z'

Modeling Concepts and Equations

Emission Angle

The emission angle of LEDs is used to describe energy propagation. This angle is used to describe the intensity of energy associated at a specific angle from the center of the energy transmission. The emission angle is also used to calculate area, later used to determine irradiance.

The emission angle of LEDs restricts the bulbs from projecting a Lambertian energy pattern. These bulbs differ from a Lambertian source in two ways. The first difference is that the energy pattern is restricted to a conical pattern. The second

difference is the intensity is dependent on the angle from the center of the beam. Most manufacturers publish data on the energy pattern emitted by their products. The specification sheets normally report the emittance pattern through air. A conversion is needed to determine the emission angle of a LED bulb in a medium other than air. Snell's law, shown in Equation 7, calculates the refracted angle when energy enters a new medium (Halliday, Resnick, & Walker, 2005).

$$\boldsymbol{n_1 \sin \theta_1 = n_2 \sin \theta_2} \quad (7)$$

Equation 7: Snell's Law

The variables on the left hand side of the equation describe the LED bulb and the variables on the right hand side describe the characteristics of air when applied to the LED bulb and air interface. The index of refraction, *n*, is readily available for air and the manufacturer provides the emission angle in air. The index of refraction and internal angle of energy within the LED is not known, but the left hand side of the equation may be represented by a constant since these values do not change when introducing a new medium. This transforms Equation 7 into Equation 8, and can be reduced to Equation 9.

$$\boldsymbol{n_{bulb} \sin \theta_{bulb} = n_{medium} \sin \theta_{medium}} \quad (8)$$

Equation 8: Snell's Law with LED and Medium Identified

$$\boldsymbol{Constant_{LED} = n_{medium} \sin \theta_{medium}} \quad (9)$$

Equation 9: Snell's Law with LED Constant and Medium Identified

Equation 9 can be solved for $Constant_{LED}$ and now be applied to a new medium to determine the emission angle in a medium other than that specified by the manufacturer.

Intensity

Intensity is measured in watts emitted from a light source per steradian. Steradians are a measurement of solid angle where a complete sphere contains 4π steradians. Equation 10 calculates the solid angle, steradians, from the surface area of a sphere contained from the angle and the radius of the sphere. The units of area and radius must cancel (Dereniak & Boreman, 1996).

$$\boldsymbol{\omega = \frac{A}{r^2}} \qquad (10)$$

Equation 10: Solid Angle

Where:

ω = solid angle [steradians]

A = contained surface area of sphere

r = radius of sphere

Equation 11 aides in determining the surface area of a sphere and is represented in Figure 14 (Lindeburg, 2011).

$$\boldsymbol{A = 2\pi r^2(1 - \cos\theta_0)} \qquad (11)$$

Equation 11: Surface Area of Sphere Contained by Specified Solid Angle

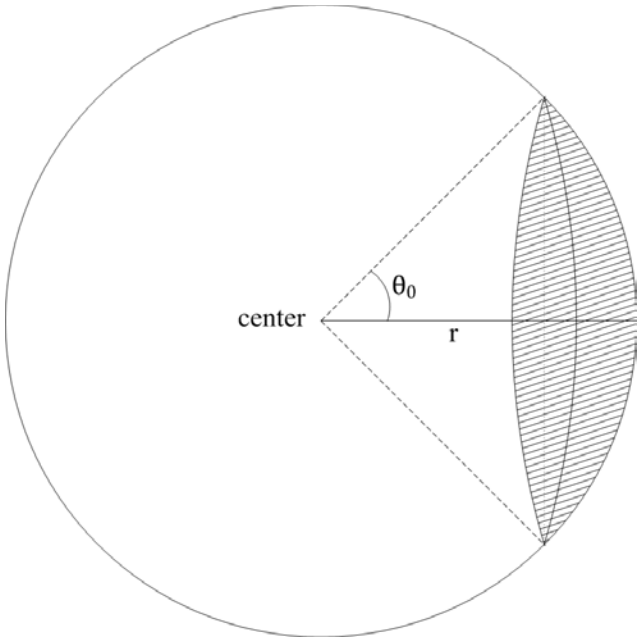

Figure 14: Surface Area of Sphere Contained by Solid Angle

From the definition of intensity the following equation is used.

$$\boldsymbol{I = \frac{P}{\omega}} \qquad (12)$$

Equation 12: Intensity

Where:

I = intensity [W/st]

P = power [W]

Combining equations 10, 11, and 12, Equation 14 is formed through operations in Equation 13 to calculate intensity.

$$\boldsymbol{I = \frac{P}{\omega} = \frac{P}{A/r^2} = \frac{P}{2\pi r^2(1-\cos\theta_0)/r^2} = \frac{P}{2\pi(1-\cos\theta_0)}} \quad (13)$$

Equation 13: Converting Intensity Equation to Limited Solid Angle

$$\boldsymbol{I = \frac{P}{2\pi(1-\cos\theta_0)}} \quad (14)$$

Equation 14: Intensity Limited to Solid Angle

Normalized Intensity

The energy pattern in LEDs is not evenly spread within the emission angle. The maximum intensity is near the center point and diminishes towards the extent of the viewing angle. Normalized radiant intensity is the common way to describe the energy propagated within a emission angle. The intensity is split into *n* points within the emission angle at a common distance from the light source. The maximum point is used in the denominator to describe the normalized intensity of energy seen at any given angle.

Intensity must be un-normalized to accurately describe the intensity at a given point. This begins by associating each distance away from the point source as a separate layer. At any radius away from the LED, the power on that layer is equal to the power output of the bulb minus the power that is absorbed by the medium between the source and that layer. Figure 15 shows an example of a layer at a given radius away from the LED.

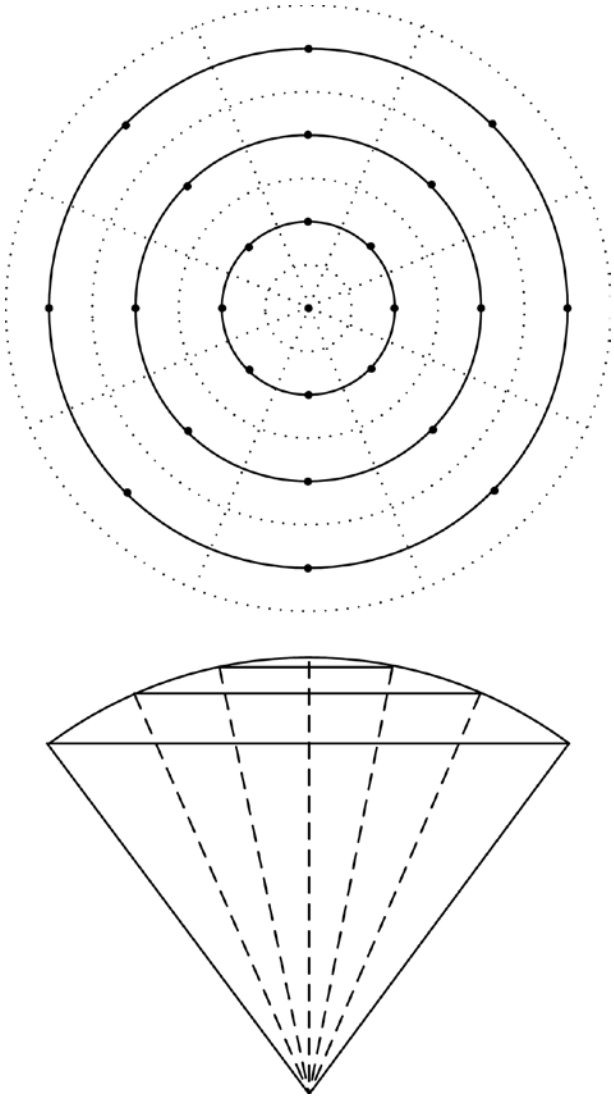

Figure 15: Spherical Cap with Elevation Rings and Points

Each layer is segmented into rings that represent elevations away from the LED's centerline. Each ring is divided into a specific number of segments represented by a point in the center of that segment. Increasing the number of rings and points on each ring increases the accuracy of the model.

Each ring is evenly spaced between the centerline and the extent of the emission angle. Rings are measured by an elevation angle away from the centerline. The manufacturer's specifications are used to fit a line to their data to determine the

normalized intensity at any given location on a layer based on the angle from the centerline.

Next, the sum of normalized intensity by all the points on one layer is calculated. Then the normalized intensity at each point on the layer is divided by the sum of normalized intensity on the layer to determine the percent intensity at each point on the layer. Finally, the percent intensity at each point is multiplied by the intensity on the layer to determine the intensity at each point. This process is shown in equations 15 through 17.

$$\sum \boldsymbol{normalizedintensity}_{\boldsymbol{layer}} = \sum \boldsymbol{normalizedintensity}_{\boldsymbol{points\ on\ layer}} \quad (15)$$

Equation 15: Sum Normalized Intensity on Layer

$$\%\boldsymbol{intensity}_{\boldsymbol{point}} = \frac{\boldsymbol{normalizedintensity}_{\boldsymbol{point}}}{\sum \boldsymbol{normalizedintensity}_{\boldsymbol{layer}}} \quad (16)$$

Equation 16: Percent Intensity at Each Point

$$\boldsymbol{intensity}_{\boldsymbol{point}} = \%\boldsymbol{intensity}_{\boldsymbol{point}} * \boldsymbol{intensity}_{\boldsymbol{layer}} \quad (17)$$

Equation 17: Intensity at Each Point

Irradiance

Irradiance (E) of light is the intensity that is emitted on a surface. For a Lambertian source, irradiance is calculated based off of the intensity of energy and distance from the light source. The irradiance decreases exponentially with distance, as seen in Equation 18. Milliwatts per square centimeter are typical units for irradiance in ultraviolet LED applications (Bolton, 2000; Dereniak & Boreman, 1996).

$$\boldsymbol{E} = {}^{\boldsymbol{I}}/_{\boldsymbol{r^2}} \quad (18)$$

Equation 18: Irradiance

Where:

E = Irradiance [W/m^2]

I = Intensity [W/ω]

r = distance [m]

This equation is useful with mercury lamps. Equation 18 above is converted into Equation 19 below. In this equation, intensity is reduced to power and 4π is placed in the denominator, representing the number of steradians in a complete sphere. This allows a user to directly input the typical specification, Watts, directly from the manufacturer's specification sheet for a mercury lamp (Bowker et al., 2011; Dereniak & Boreman, 1996).

$$\boldsymbol{E = \frac{P}{4\pi r^2}} \quad (19)$$

Equation 19: Mercury Lamp Irradiance

A rough estimation of LED bulbs is based off of Equation 19 above. Equation 20 accounts for the limited angle that is projected from an LED source. This assumes Lambertian properties within the emission angle of the LED and equally distributes the power in that area (Bowker et al., 2011).

$$\boldsymbol{E = \frac{P}{2\pi r^2(1-\cos(\theta_0))}} \quad (20)$$

Equation 20: LED Bulb Irradiance

These equations are firmly based on power per square area. Since an LED is not a Lambertian source and the energy propagated from an LED is not uniformly distributed, these equations do not accurately describe the energy density at specific points for a non-Lambertian energy spread. The correct approach is to determine the irradiance associated with each point. This process involves calculating the intensity

throughout the volume to be modeled and the area associated with that volume. Dividing the intensity at a point by the area at that point results in irradiance at that point.

Absorption

The Beer-Lambert law describes absorption through a medium. The law states that absorption is constant through a uniform material and can be calculated with an absorption constant and the path length. Equations 21 and 22 show how absorption affects irradiance (Liu et al., 2004; Beer's law.).

$$\boldsymbol{E = E_0 U} \quad (21)$$

Equation 21: Beer-Lambert Law

Where:

E_0 = irradiance without absorption

U = absorption attenuation factor

$$\boldsymbol{U = e^{-a(\lambda)l}} \quad (22)$$

Equation 22: Absorption Attenuation Factor

Where:

$a(\lambda)$ = absorption coefficient at a specific wavelength [1/m]

l = path length [m]

The absorption factor may be applied before or after distributing the intensity across all points on a layer. Doing this after un-normalizing the intensity allows the model to use the same intensity across the area covered by each layer.

Spherical to Cartesian Coordinates

At this point the coordinates need to be converted from spherical to Cartesian coordinates. Local spherical coordinates up to this point enable the energy to be evenly

distributed and solved at numerous steps away from the bulb. However, three dimensional plots often require evenly spaced Cartesian coordinates.

Since the data points are originally set up in spherical coordinates, the Cartesian coordinates are not evenly spaced. The un-spaced Cartesian coordinates are rounded to the nearest evenly spaced grid location to allow graphing volume data. Moving these points reduces the accuracy of the model, but decreasing the step size between points reduces this effect.

After the Cartesian coordinates are moved, they must be arranged into increasing coordinate value since they are still ordered based off of the original spherical coordinates. Another operation is performed to move the points into the correct sequence.

Bulb Array

After the coordinate system is converted from spherical to Cartesian coordinates, the bulb array is arranged. UV energy is additive and a simple point source summation can detail the energy pattern emitted on a surface or in a volume. The LED bulb model is reproduced for each LED in the array and offset from the center of the vessel to place the LEDs in the correct locations (Blatchley III, 1997; Bolton, 2000; Bowker et al., 2011).

Limit Bulb Array

The bulb array matrix is now limited to the vessel dimensions. The irradiance matrix is set to zero for points that fall outside the extents of the vessel size. The array is also limited to the fluid height for batch experiments that do not fill the vessel.

Pathogen Inactivation

Pathogen inactivation is calculated based off of the log reduction in a solution. This is reported as a log reduction, calculated by Equation 23. The initial and final concentrations are needed to determine the pathogen inactivation in a solution. Empirical methods are often used to determine the dose associated with the log reduction. UV dose is the summation of the integral of UV irradiance with respect to time (Wurtele et al., 2011).

$$\boldsymbol{logReduction = log\left(\frac{concentrationInitial}{concentrationNew}\right)} \quad (23)$$

Equation 23: Log Reduction

DNA disruption and AOP dose to log inactivation calculations differ. DNA disruption follows the shoulder, log-linear, and tailing regions introduced in Chapter II. DNA repair occurs in the shoulder region. The log reduction rate is slower in this region than the log-linear region. The log-linear region has the greatest contaminant reduction associated with it. The tailing region follows this region. The contaminant reduction rate slows in this region due to the sparse number of contaminants. The EPA reports the dose summation is valid for DNA disruption in the range of 1-200 mW/cm^2. UV dose is not affected by long exposure over a smaller irradiance or shorter exposure over a longer irradiance in this range. This range corresponds to the log-linear region (Mamane-Gravetz & Linden, 2005; U.S. Environmental Protection Agency (EPA), 2006).

AOPs do not follow the shoulder, log-linear, and tailing regions. Multiple equations govern the creation of radicals during UV irradiation. The radicals either neutralize the target pathogen, reform to the original oxidant, or react to form byproducts (Alpert et al., 2010; Coenen et al., 2013).

The process for batch and flow experiments is to first calculate the UV dose at each point. The second step is to calculate the log inactivation at each point. This calculation is conducted by fitting a line to data obtained to show the relationship between concentration reduction and dose. Next, the new concentration is calculated at each point. A mixing rate is introduced to this process to account for stirring that occurs in batch experiments. Assumptions must be made for flow experiments regarding fluid flow.

MATLAB

The governing equations used in this research were coded into MATLAB. The main advantage this program offers over the other possible choices is the ability to compute large matrices. This is required to set up a suitable three-dimensional coordinate space so that the irradiance could be calculated for each point in the system. MATLAB also has robust graphics capabilities that allow visualization of this data. The program is relatively easy to program, with built in functions and the ability to easily code additional functions. Finally, MATLAB is readily available in the research environment.

Graphing in MATLAB

Graphing in MATLAB requires an evenly spaced three dimensional grid and corresponding matrix with volume data. The grid size needs to be large enough to cover the irradiated area and the vessel volume. The grid needs to be capable of covering a large area if the design calls for multiple bulbs. Three dimensional graphs are used to show the overall irradiance effect in the vessel.

Reactor Vessel Optimization

Optimum reactor vessel geometry is dependent on output power and shape of energy propagation. The goal is to maximize the log-linear region in the reactor. The optimum size of the reactor is driven by the output power and the bulb array. The required log reduction and dose to reduction rate drive the flow rate, or duration for batch experiments.

Chapter Summary

In this chapter, the information required to understand how to duplicate the research effort was presented. The governing principles and concepts of UV energy propagation were identified, key equations used in the modeling activity were selected, and an environment suitable for implementing and simulating the models was selected. In the next chapter, the results of the application of the research methodology are presented.

IV. Data and Results

Chapter Overview

In this chapter, the research methodology presented in Chapter III is applied to model and simulate the UV energy distribution in two different UV reactor vessel designs. The results from the simulation are analyzed and compared to experimental results collected from a real-world experiment. Strengths and weaknesses of the modeling and simulation effort in terms of accuracy and efficiency are identified. The referenced MATLAB model throughout this chapter is located in the Appendix.

Baseline

The baseline for the model was based upon a UV reactor vessel and LED array created by Spencer (Spencer, 2014). This vessel was used for both batch and flow through experiments using *Bacillus globigii* (formerly known as *Bacillus subtilis* var. *niger*) spores and methylene blue (indicator dye), respectively. The batch experiments disinfected the water (inactivated spores via DNA disruption) while the flow through experiments used an AOP process with hydrogen peroxide to generate hydroxyl radicals. The vessel had an interior diameter of 2.87 inches with a depth of 3 inches and was made of polished stainless steel (Figure 16).

Figure 16: Vessel

The bulb array consisted of 7 LEDs configured in an array on the bottom plate of the vessel. One bulb was centered with the remaining 6 bulbs placed equally along a 1 inch (2.54 cm) radius from the center. The physical dimensions of the LED array are shown in Figure 17. Once configured, the bottom and top plates were bolted to the bottom and top of the vessel.

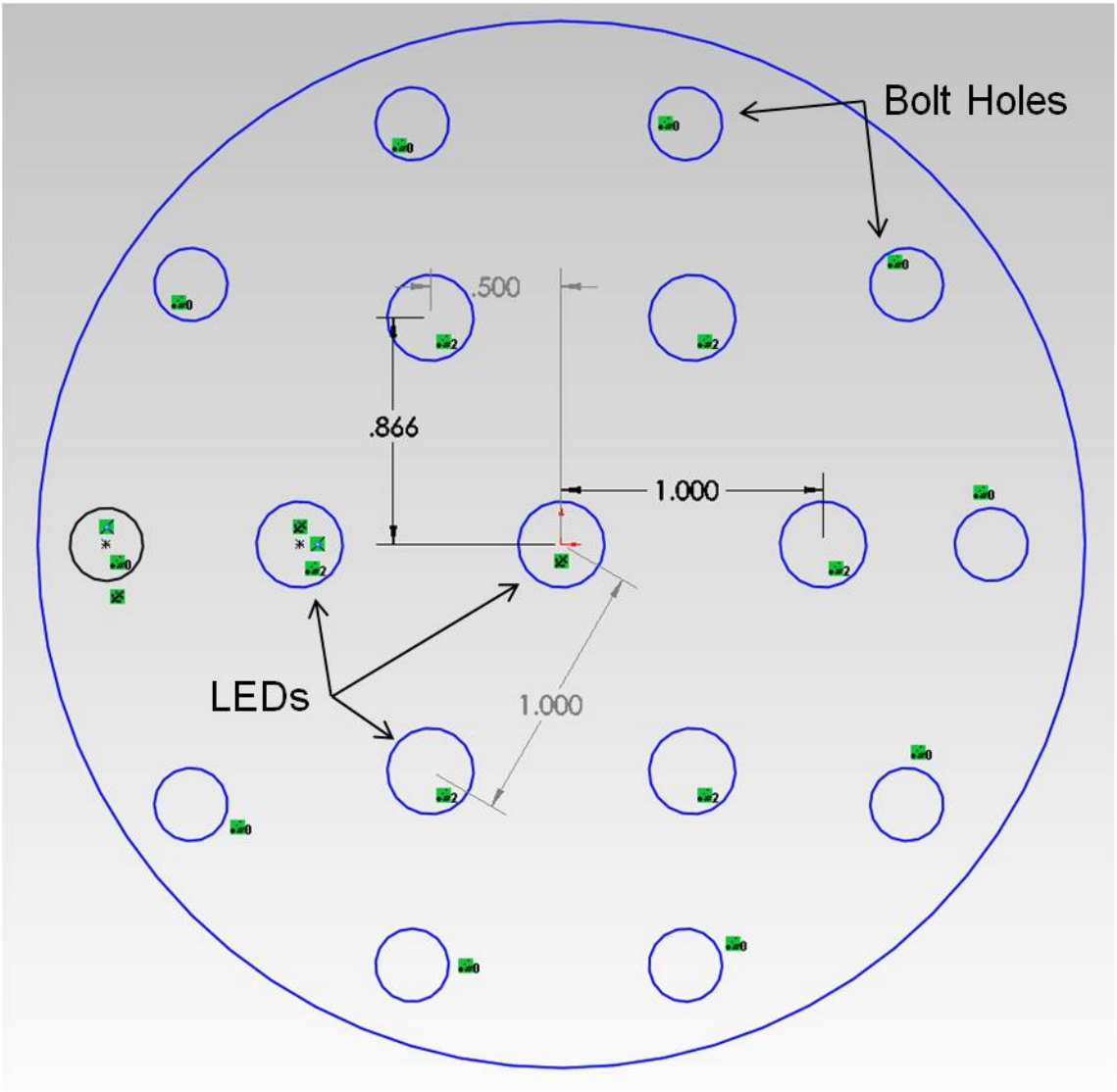

Figure 17: LED Plate with LED Spacing

The vessel was designed using the English coordinate system. However, the metric system is used throughout this document. The Cartesian system is initialized with the (x, y) reference with the zero coordinate set at the center bulb. The following table shows the bulb spacing in both English and in the International System of Units (SI) metric units.

Table 5: Bulb Spacing [inches, (centimeters)]

Bulb	x	y
1	0, (0)	0, (0)
2	1, (2.54)	0, (0)
3	0.5, (1.27)	-0.866, (-2.20)
4	-0.5, (-1.27)	-0.866, (-2.20)
5	-1, (-2,54)	0, (0)
6	-0.5, (-1.27)	0.866, (2.20)
7	0.5, (1.27)	0.866, (2.20)

The LEDs used were SETi UVTOP260 TO-39 FW (UVTOP260 manufacturer's specification sheet.). The manufacturer's specification sheet stated that this type of LED had a minimum and typical optical power of 180 and 300 μW at 20 mA, respectively. Several LEDs obtained from SETi averaged 567 μW on the Quality Control Inspection Report from SETi (*QC inspection report.*2013). Measurements from the spectrometer found the bulbs to have an initial power output of around 1200 μW. All power results were measured at 20 mA. The emission angle from the center of the bulb was typically 60 degrees in air. This LED had a minimum peak wavelength of 260 nm, typical wavelength of 265 nm and a maximum wavelength of 270 nm. The manufacturer's specification sheet did not state the lifespan or degradation pattern for the LED.

Global Variables

In this section, the development of the MATLAB model is discussed in detail. The model was initialized with a set of global variables. The variables were categorized into vessel parameters, bulb array, bulb and fluid characteristics, batch variables, flow variables, graphing variables, fluence log inactivation regions, spherical coordinates, and

Cartesian coordinates. The first seven categories were set by the user. The last two categories set up the spherical and Cartesian systems to populate data.

The vessel parameters, shown in Table 6, describe the shape of a cylindrical reactor. The '*radius*' was set to the interior radius of the system and '*vesselHeight*' was set to the interior height of the reactor.

Table 6: Vessel Parameters

Vessel Parameters	Value
radius	3.6449 cm
vesselHeight	7.62 cm

Table 7 lists the location of the individual bulbs in the system. The term '*offsetDimensions*' placed the bulbs on the bottom plate in the reactor. This variable allowed any number of bulbs by passing the variable through a 'for loop' in the '*bulbOffset*' function.

Table 7: Bulb Array Offset Dimensions

Bulb Array	Value
offsetDimensions	[-2.54,0; -1.27,2.20; -1.27,-2.20; 0,0; 1.27,2.20; 1.27,-2.20; 2.54,0] cm

The bulb and fluid characteristics drove the irradiance calculations and are shown in Table 8. The emission angle, '*va*', was calculated based off of the medium and the manufacturer's specification. Power, '*p*', was set to the power of the bulb. The absorption coefficient, '*a*', was set for the specific wavelength and fluid turbidity. The values are discussed later in this chapter.

Table 8: Bulb and Fluid Characteristics

Bulb and Fluid Characteristics	Value
va	39.72 degrees
p	180, 300, 567, or 1200 μW
a	.01 cm^{-1}

The batch variables, shown in Table 9, are specific to a previous experiment (Tran, 2014). The initial concentration, '*concentrationInitial*', was the same for each of the batch trials. The experiment time, '*time*', was set for one of the two experiment durations. Mix time, '*mixTime*', was set from 1 to the duration with intervals every five seconds. The fluid height, '*fluidHeightBatch*', was set to the distance that encases 100 ml of solution.

Table 9: Batch Variables

Batch Variables	Value
concentrationInitial	$7x10^6$ cfu/ml
time	64 or 129 seconds
mixTime	1 to time
fluidHeightBatch	2.396 cm

Similar to the batch variables, the flow variables, shown in Table 10, were specific to a separate recent experiment (Duckworth, 2014) experiments. The flow rate, '*flowRate*', was set by default to 1.4 mL/min. The fluid height, '*fluidHeightFlow*', was set to the vessel height to account for a full reactor (7.62 cm).

Table 10: Flow Variables

Flow Variables	Value
flowRate	1.4 mL/min
fluidHeightFlow	7.62 cm

Table 11 shows the graphing variables, which allowed the user to specify a space that encompasses the reactor and change the step size. The step size increased and decreased the space between the data points which affected the resolution of the model.

Table 11: Graphing Variables

Graphing Variables	Value
stepSize	0.1 cm
xGridMin	-10 cm
xGridMax	10 cm
yGridMin	-10 cm
yGridMax	10 cm
zGridMin	0 cm
zGridMax	10 cm

The fluence log inactivation variables, shown in Table 12, allowed for calculations and graphs for each of the regions. The log linear and tailing minimums are not stated since they are equal to the shoulder and log linear regions, respectively.

Table 12: Fluence Log Inactivation Regions

Fluence Log Inactivation Regions	Value
shoulderMin	100 μW/cm^2
shoulderMax	1,000 μW/cm^2
logLinearMax	200,000 μW/cm^2
tailingMax	1,000,000 μW/cm^2

Two coordinate systems were also initialized. The first was a localized spherical system used for individual LED bulbs, shown in Table 13. This required values for azimuth, elevation, and r. The 'linspace' command was used to set equally spaced values between a minimum and maximum value. The number of points could be set to the default of 100 or the points could be increased or decreased to produce the desired resolution/model run time trade off. Azimuth is set to -179 to 180 degrees with 360 steps. Elevation was set to provide the points between the emission angle and the center of the beam with 100 steps. Since MATLAB's spherical system measured elevation from the x-y axis up to the z axis and the center of the beam was considered zero emission angle, (90 – emission angle) was set for the minimum value and 90 was set to the maximum value. The term '*r*' was set to cover the needed distance. This was determined by the vessel geometry to ensure irradiance is calculated for every point within the vessel. In this case, '*r*' was set from 0.1 to 10 cm with 100 steps. This covered the distance from the LED plate to the opposite side of the vessel for the entire emission angle. This dimension did not start at zero to avoid division of zero in the irradiance calculations.

Table 13: Spherical Coordinates

Spherical Coordinates	
azInitial	-179 to 180 degrees, 360 steps
elInitial	va to 90 degrees, 100 steps
rInitial	0.1 to 10 cm, 100 steps
az	azimuth array of 3D spherical space
el	elevation array of 3D spherical space
r	radius array of 3D spherical space

The second coordinate system was a global Cartesian system, shown in Table 14. This system consisted of x, y, and z coordinates that represented the three dimensional

space of the vessel in .1 cm increments. An evenly spaced Cartesian coordinate system was required to graph volume data in MATLAB.

Table 14: Cartesian Coordinates

Cartesian Coordinates	
x1	-10 to 10 cm, 201 steps
y1	-10 to 10 cm, 201 steps
z1	0 to 10 cm, 101 steps
xGraph	x array of 3D Cartesian space
yGraph	y array of 3D Cartesian space
zGraph	z array of 3D Cartesian space

The data points for each coordinate system were combined to form a matrix for the azimuth, elevation, and r and x, y, and z for the spherical and Cartesian coordinate systems respectively. This was completed using MATLAB's 'meshgrid' function. Calculations were based off of this initial spherical matrix to determine irradiance at all of the points within the matrix. The initial Cartesian matrix was used to plot results.

Emission Angle

The SETi specification sheet for their flat window bulb stated that the emission angle, angle between the center of the energy propagation and extents, in air was typically 60 degrees. They also gave their typical angular diagram, which is displayed in Figure 18. The power/radiant intensity was the expected normalized value by the manufacturer and is further discussed in the next two sections.

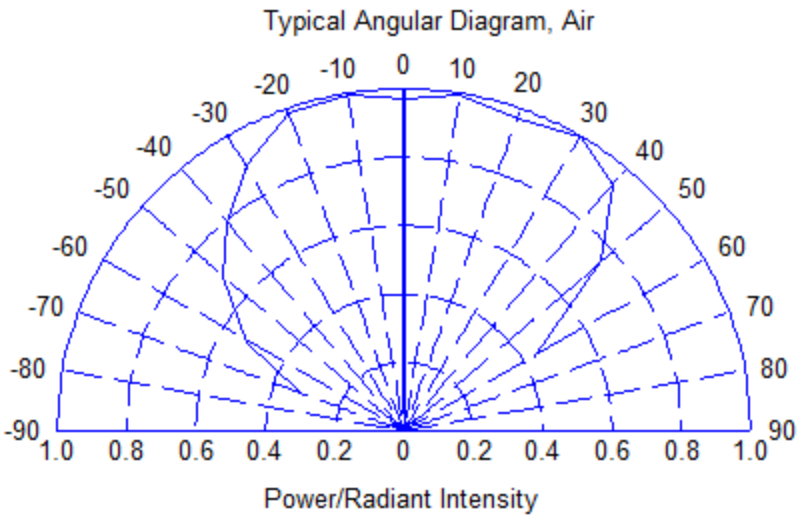

Figure 18: Typical Angular Diagram, Air

Table 15 lists the minimum, maximum, and calculates the average value for each angle reported by the manufacturer.

Table 15: Normalized Radiant Intensity Minimum, Maximum, and Averaged

Angle (Degrees)	Radiant Intensity Minimum	Radiant Intensity Maximum	Radiant Intensity Average
0	0.96	0.96	0.96
10	0.98	1	0.99
20	0.96	0.98	0.97
30	0.88	0.99	0.935
40	0.78	0.94	0.86
50	0.68	0.72	0.7
60	0.44	0.49	0.465
70	0	0.34	0.17

The averaged radiant intensity was plotted against the emission angle to depict the expected intensity from a SETi flat window LED bulb in air, shown in Figure 19.

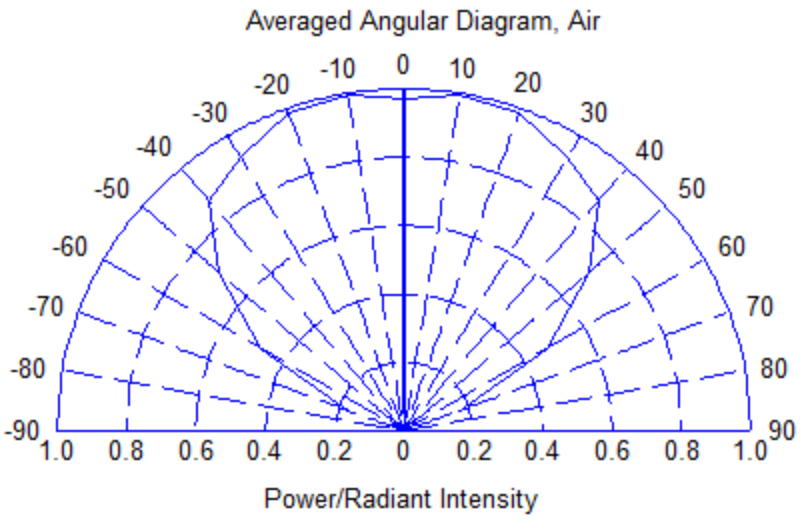

Figure 19: Averaged Angular Diagram, Air

Snell's law was used to calculate the emission angle and shift the power/radiant intensity ratio from air to the correct angle for water. This was done by rearranging and substituting the mediums into Equation 9, from Chapter III, to obtain Equation 24.

$$\boldsymbol{\theta_{water}} = \mathbf{sin^{-1}}\left(\frac{\boldsymbol{n_{air}}}{\boldsymbol{n_{water}}}\ \mathbf{sin}\,\boldsymbol{\theta_{air}}\right) \qquad (24)$$

Equation 24: Snell's Law Rearranged for Water Angle

The values for the index of refraction for air and water were 1.0002967 and 1.3556, respectively, at 270 nm (Polyanskiy, 2013). Solving for the typical emission angle for SETi flat window bulbs, the emission angle was 39.72° in water.

$$\boldsymbol{\theta_{water}} = \mathbf{sin^{-1}}\left(\frac{\mathbf{1.0002967}}{\mathbf{1.3556}}\ \mathbf{sin}\,\mathbf{60°}\right) \quad = \mathbf{39.72°} \qquad (25)$$

Equation 25: Snell's Law Solved for Water Angle

Table 16 shows the emission angle in water associated with the emission angle in air and the average radiant intensity correlated to those angles.

Table 16: Emission Angle in Air and Water Compared to Average Radiant Intensity

Angle (Air) (Degrees)	Angle (Water) (Degrees)	Radiant Intensity Average
0	0	0.96
10	7.36	0.99
20	14.62	0.97
30	21.65	0.935
40	28.31	0.86
50	34.42	0.7
60	39.72	0.465
70	43.9	0.17

The averaged angular diagram for water was produced from the data in Table 16. This is shown in Figure 20. The energy spread was reduced in water from that in air. This created a higher intensity and lessens the effects of absorption in water, which is discussed later in this chapter.

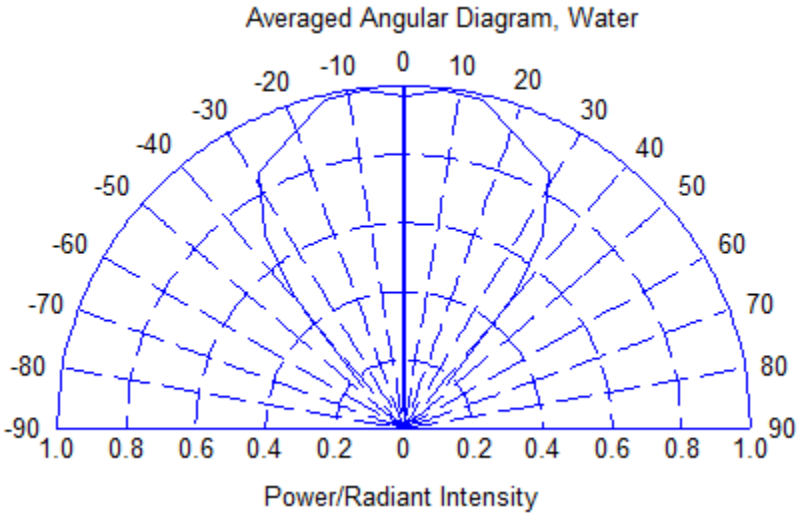

Figure 20: Averaged Angular Diagram, Water

Intensity

The intensity was calculated from Equation 14 introduced in Chapter III. This was the total intensity at each layer away from the bulb. The emission angle of 39.72 in water was used to determine the intensity in water.

$$\boldsymbol{I = \frac{P}{2\pi(1-\cos\theta_0)}} \quad (26)$$

Equation 26: Intensity Limited to Solid Angle

$$\boldsymbol{I = \frac{P}{2\pi(1-\cos 39.72)} = \frac{P}{1.4503\ st}} \quad (27)$$

Equation 27: Intensity Equation Reduced with Emission Angle in Water

The power values of 180, 300, 567, and 1200 μW were used for the minimum manufacturer's specifications, typical manufacturer's specifications, measured power by the manufacturer's quality inspection report, and measured power in the laboratory, respectively. The power and intensity are shown in Table 17. It is important to note that the minimum power stated by the manufacturer was 60 percent of the typical power. This agreed with the 40 percent reduction in the first 100 hours of operation time for UV LEDs discussed in Chapter II (Kneissl et al., 2010).

Table 17: Intensity Results

	Manufacturer's Specifications		Measured	
	Minimum	Maximum	Manufacturer	Lab
Power	180 μW	300 μW	567 μW	1200 μW
Intensity	124.11 μW/st	206.85 μW/st	390.95 μW/st	827.41 μW/st

The next section discusses un-normalizing the intensity for each layer to describe the intensity at specific points within the bulb's emission angle.

Normalized Intensity

The normalized radiant intensity was plotted against the emission angle for air and water in Figures 21 and 22. A line was fit to the data to obtain an equation that described the normalized radiant intensity for any angle between zero and the extent of the emission angle.

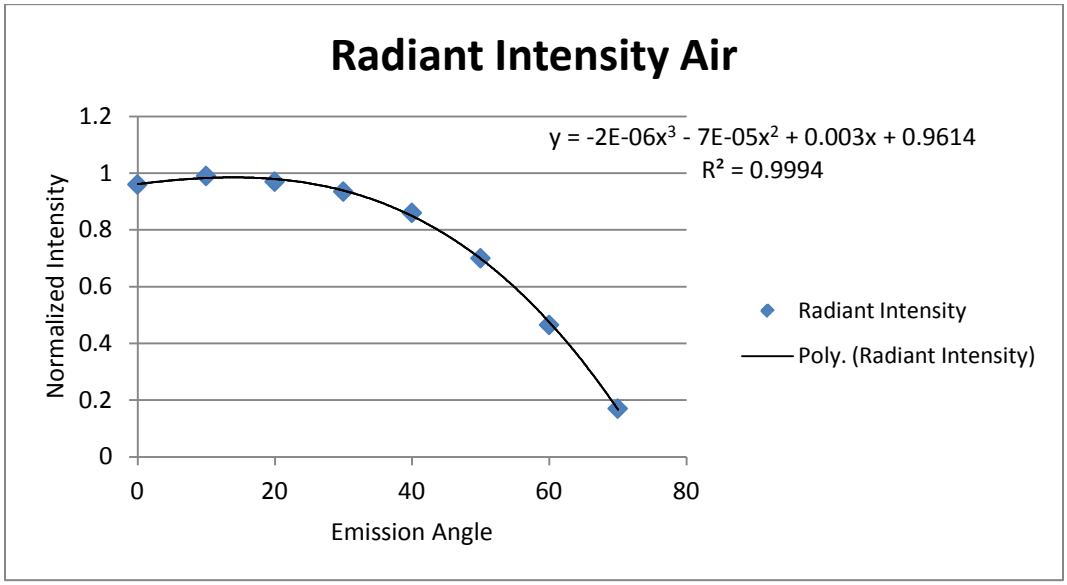

Figure 21: Radiant Intensity versus Emission Angle, Air

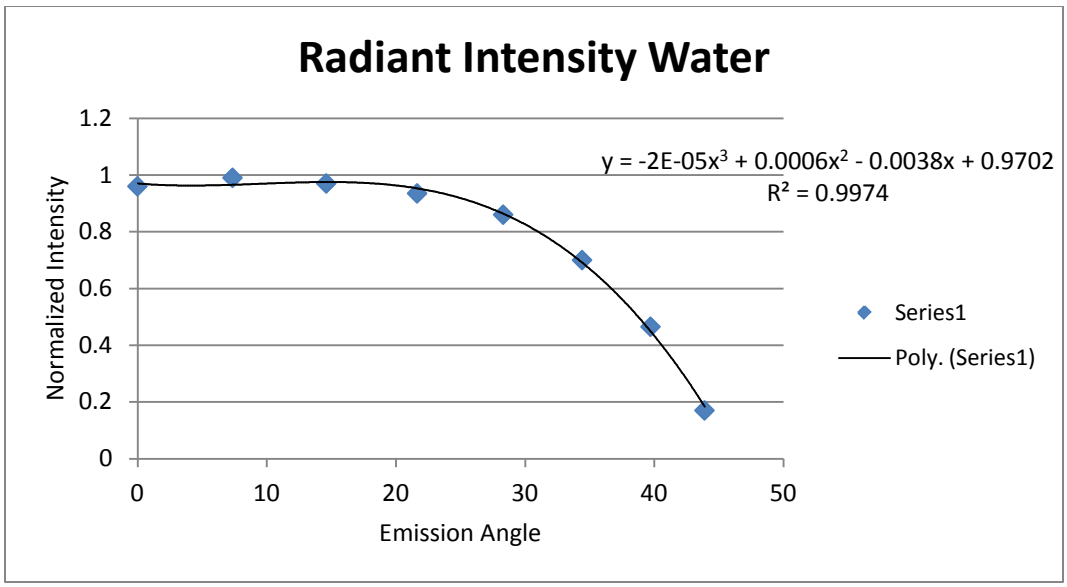

Figure 22: Radiant Intensity versus Emission Angle, Water

The SETi flat window bulb was stated to have a 60° emission angle in air, which was a 39.72° emission angle in water. This was a smaller angle than obtained in experiments from Spencer (2014), which was found to be 46° for 270 nm at 20 mA in water. This resulted in a 6.28° difference between the theoretical value and actual value. Extending the equation in Figure 22 resulted in an angle of 47.5° at the zero radiant intensity point. The differences between these angles may be explained by a number of reasons. First, the manufacturer may have stated the angle to be slightly smaller than typically seen to reduce tolerances needed in manufacturing the bulbs. Another possibility is that the intensity was set higher than what is detected by Spencer's experiment. Extending the line to the zero intensity point was not valid since there was no data that proved the fit line in Figure 22 was accurate outside the data provided by the manufacturer. Due to the inability to measure the intensity at these extents, the model assumed the intensity ended at an angle of 39.72 degrees since the stated emission angle in air by the manufacturer was 60 degrees. This ensured that the emission angle was not overstated. A larger emission angle increases the area of incident energy on each layer, and decreases the energy at each point in that layer.

The angle with each point was calculated by subtracting the array '*el*' from 90 degrees. The new array '*angle*' was now used in the following equation, obtained from Figure 22, to calculate the normalized intensity at each point.

$$\boldsymbol{normalizedIntensityAtPoint} = \boldsymbol{-2 * 10^{-5}(angle^3) + 6 * 10^{-4}(angle^2) - 3.8 * 10^{-3}(angle) + .9702} \quad (28)$$

Equation 28: Normalized Intensity at Point

The '*normalizedIntensityAtPoint*' array accounted for the center point (when *el* = 90) for each azimuth angle called in the initialization of the spherical coordinate system.

This array was passed through a filter that kept one azimuth angle when elevation was 90 degrees at the original value. The remaining azimuth points were set to 0.

The next step calculated the intensity at each point. This operation started by summing the normalized intensity on each layer.

$$\boldsymbol{normalizedTotatlIntensityAtLayer} = \sum \boldsymbol{normalizedIntensityAtPoint} \quad (29)$$

Equation 29: Normalized Intensity at Layer

Next, the normalized intensity at each point was divided by the total intensity for the respective layer. This resulted in an array that represented the percent of intensity at each point.

$$\boldsymbol{percentIntensityPoint} = \frac{\boldsymbol{normalizedIntensityAtPoint}}{\boldsymbol{normalizedTotalIntensityAtLayer}} \quad (30)$$

Equation 30: Percent Intensity at Point

This array was multiplied by the intensity to calculate the intensity associated with each point.

$$\boldsymbol{intensityAtPoint} = \boldsymbol{percentIntensityPoint} .* \boldsymbol{intensity} \quad (31)$$

Equation 31: Intensity at Point

Irradiance

The next step was to calculate irradiance from intensity. This was accomplished by dividing the intensity at a point by the area associated with that point. Figure 23 shows the area associated with a singular point. This area was curved when viewed in a Cartesian system. The tributary area was the area covered halfway between the point and the points on the next rings, and halfway between the closest points on the same ring. The center point differed by accounting for the area halfway between the center point and

the next ring. Not only did the intensity drop as a point is closer to the extent of the energy propagation, but the area associated with the point also increased. These factors work together to reduce the irradiance closer to the extent of the emission angle.

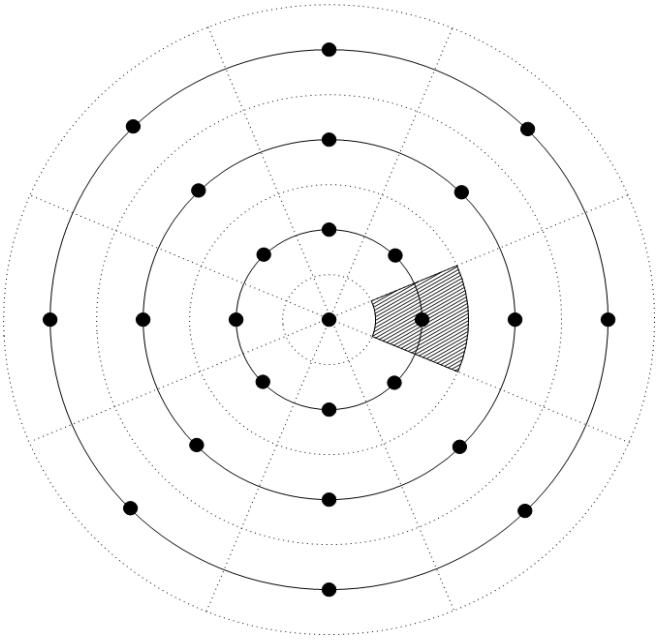

Figure 23: Area Associated with Singular Point

The area for each ring was calculated before the area for each point. Figure 24 shows the area associated with each ring. The inner ring was calculated with Equation 11 in Chapter III. The remaining rings were calculated in a similar manner. For example the first ring, as shown in the middle of Figure 24, was calculated by subtracting the center area from the area including the first ring and the center area.

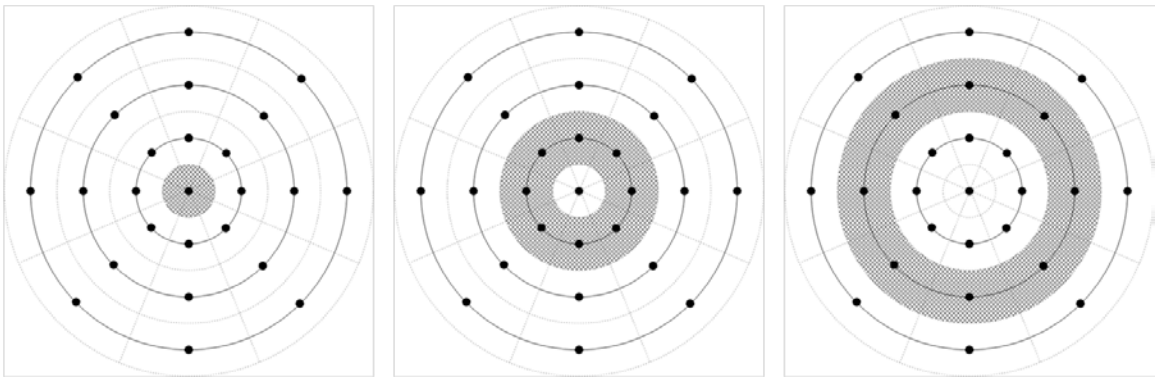

Figure 24: Ring Area

This process was started by calculating the half step angle between the defined elevation angles. Equation 32 shows this step.

$$\boldsymbol{halfStep} = \frac{(\boldsymbol{el}(\mathbf{2},\mathbf{1},\mathbf{1}) - \boldsymbol{el}(\mathbf{1},\mathbf{1},\mathbf{1}))}{\mathbf{2}} \quad (32)$$

Equation 32: Elevation Half Step

Next the ring area was calculated. A 'for loop' ran through each point in the intensity matrix. If the elevation angle was zero, the ring area was simply the area covered by the half step between the center point and the first ring. For all other elevation angles, the ring area was the area covered by the area of the ring elevation minus a half step subtracted from the area of the ring elevation plus a half step. These equations are shown below.

For elevation = 0:

$$\boldsymbol{ringArea} = \mathbf{2}\boldsymbol{\pi r}^{\mathbf{2}}(\mathbf{1} - \mathbf{cos}(\boldsymbol{halfStep})) \quad (33)$$

Equation 33: Ring Area for Elevation = 0

For elevation > 0:

$$\boldsymbol{ringArea = 2\pi r^2((1 - \cos(el + halfStep)) - (1 - \cos(el - halfStep)))} \quad (34)$$

Equation 34: Ring Area for Elevation > 0

The next step after determining the ring area was to split each ring into the number of azimuth points per ring. For the inner circle, this was one since there was only a singular center point. The remaining rings had the same number of user defined points in each ring. These equations are shown below.

For elevation = 0:

$$\boldsymbol{pointArea = ringArea} \quad (35)$$

Equation 35: Point Area for Elevation = 0

For elevation > 0:

$$\boldsymbol{pointArea = \frac{ringArea}{\#\ of\ azimuth\ angles}} \quad (36)$$

Equation 36: Point Area for Elevation > 0

Finally, the point intensity matrix was divided by the point area matrix to yield irradiance at each point.

$$\boldsymbol{irradiance = \frac{intensityAtPoint}{pointArea}} \quad (37)$$

Equation 37: Irradiance

Absorption

Absorption was now factored into the irradiance matrix. The absorption attenuation factor U was multiplied by irradiance. The absorption constant was approximately 0.01 cm^{-1} for 269 nm UV energy in unfiltered deionized water. This was done by the following operation (Kneissl et al., 2010).

$$absorption = irradiance * e^{-a*r} \quad (38)$$

Equation 38: Absorption

Table 18 shows absorption coefficients for four types of water used in an experiment to test UV LED disinfection rates. These constants show that tap water, surface water, and secondary effluent absorb much more energy than deionized water. Figure 25 shows the effect of altering the absorption coefficient. The absorption constant was first set to 0 to show the effect of no absorption. Then the absorption rate was stepped through the absorption values for deionized water, tap water, surface water, and secondary effluent. It is clear that absorption greatly reduces the effect of an LED bulb (Kneissl et al., 2010).

The table also showed that filtered water has a lower absorption coefficient than unfiltered water. Suspended solids in unfiltered water cause this effect. In addition to increasing the absorption coefficient, suspended solids may also build up residue within the vessel. This may decrease reflection from the vessel walls and energy output from the bulbs (Lenk & Lenk, 2011; Wurtele et al., 2011).

Table 18: Absorption Coefficients for Common Types of Water (Kneissl et al., 2010)

	Parameter	Unit	Deionised Water (DI)	Tap Water (TW)	Surface Water (SW)	Secondary Effluent (SE)
unfiltered	A (254)	[1/m]	1.1	8.8	19	29.2
	A (269)	[1/m]	n.a.	7.7	17.1	26.6
filtered	A (254)	[1/m]	0.8	8.5	17.6	28.2
	A (269)	[1/m]	n.a.	7.5	15.7	25.7

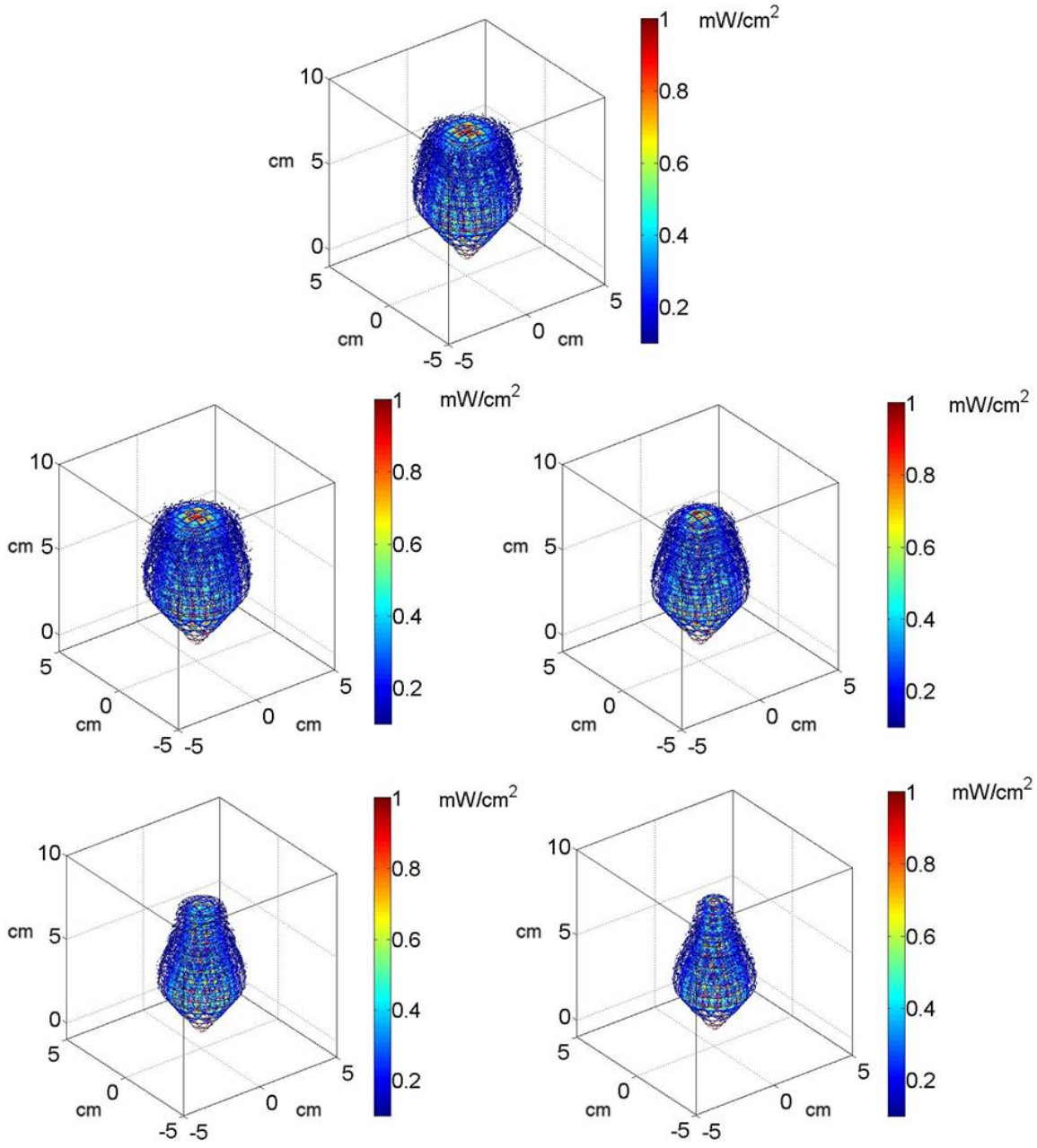

Figure 25: Single Bulb, 300 µW, Top a=0 cm^{-1}, Middle Left a=0.01 cm^{-1}, Middle Right a=0.077 cm^{-1}, Bottom Left a=0.171 cm^{-1}, Bottom Right a=0.266 cm^{-1}

Spherical to Cartesian Conversion

Three operations were performed to convert the spherical coordinates used up to this point into a Cartesian system that was able to be used in MATLAB to plot in three

dimensions. The first process was a simple conversion of spherical to Cartesian coordinates. After this was completed, the Cartesian coordinates were moved to the closest 0.1 cm interval. Finally the matrices were reordered to allow the x, y, and z coordinates to be arranged in increasing value.

MATLAB's '*sph2cart*' command was used to convert the spherical coordinates to Cartesian coordinates. Azimuth and elevation were first converted to radians, as required by MATLAB. The output of this command was x, y, and z matrices that was ordered according to the initial spherical system.

The function '*conversion*' was used to move the x, y, and z coordinates to the closest 0.1 cm grid. This function stepped through each data point in the x, y, and z coordinate matrices and moves the coordinate to the closest grid location. This movement introduced error into the model. A smaller grid size reduced the error, but resulted in a longer computing time if adequate computing memory was even available.

Finally, the function '*reOrder*' was used to rearrange the Cartesian coordinate and irradiance matrices to order the coordinates in increasing value. Each data point was called and stepped through a 0.1 cm grid. The irradiance at a point was added to the re-ordered matrix when the x, y, and z coordinates matched the correct grid location. At this point the irradiance matrix was set up for MATLAB's three dimensional graphing functions.

Bulb Array

The function '*bulbOffset*' was used to add multiple bulbs. The metric units for the LEDs in Table 5, above, were used for the LED placement. The function rounded the

units to the closest 0.1 cm interval to use the same spacing requirement as used in the coordinate conversion steps. The function added one LED at a time with the x and y displacement. The intensity for each point in the multiple LED array was summed into a matrix named '*multipleBulbs*'.

Limit Bulb Array

The function '*cut*' was used to limit the irradiance matrix to inside the vessel and for the fluid height in the vessel. The function called each point in the matrix passed into the function. The value of irradiance at any point was set to zero if the radius of the point from the center of the vessel was greater than the radius of the vessel, or the height of the point exceeded the fluid height of the system. The fluid height variable must be set equal to the vessel height for flow through systems.

Pathogen Inactivation

DNA Disruption – Batch

The dose-log inactivation equation for *Bacillus subtilis* spores was obtained from experiments conducted by Wurtele et. al and is shown in Equation 39. This equation was obtained from data taken from 117 to 233 J/m^2. 'Dose' was measured in J/m^2 (Wurtele et al., 2011).

$$\boldsymbol{Log\ Inactivation = 0.0133\ dose + 0.5547} \quad (39)$$

Equation 39: Dose-Log Inactivation for 269 nm LED Bulbs

This equation did not account for the shoulder and tailing regions. Instead it only represented the log-linear region. The MATLAB code was adjusted for this by limiting dose to only be valid at or above 117 J/m^2. This threshold was chosen since that was the

smallest data point recorded in the experiment. If a lower limit was not selected, then a dose of 0 J/m^2 would calculate to a log reduction of 0.5547 when there should be no log reduction.

Mix time was defined as the time required for the solution to completely mix and re-initialize as a singular concentration due to the stirrer in the vessel. The calculations behind the log reduction assumed that the fluid was relatively stable during the mix time and averaged with the rest of the solution after each mix period. One final mix period was performed for the remainder when experiment times were not evenly divisible by the mix time.

Tran's (2014) experiments consisted of measuring the log reduction of *bacillus globigii* spores in a batch environment. The reactor vessel was placed on an orbital shaker to mix the solution in the reactor without introducing a mixing device within the vessel. The reactor was oriented with the bulb plate on the bottom and the bulbs facing up. A solution of deionized water and spores with an initial concentration of $7x10^6$ was used to fill the vessel with 100 ml. This resulted in a calculated fluid height of 2.396 cm in the vessel. Figure 26 shows the set up for Tran's experiments. Tran ran multiple trials with durations of 64 and 129 seconds. Table 19 shows the log reduction associated with both duration times.

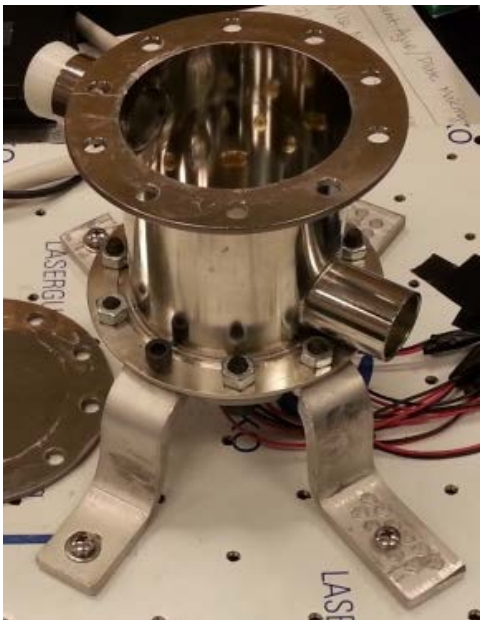

Figure 26: Tran's Set Up (Tran, 2014)

Table 19: Batch Experiment Results

Duration	Log Kill
64 s	.5-.6
129 s	1.5

Table 20 shows the log reduction results for various mix times and power outputs for an experiment duration of 64 seconds. The highlighted cells correspond to the results obtained from Tran's experiments. This suggests that a mix time of between 55 and 64 seconds is proper to match Tran's results with the theoretical values, depending on the actual power output from the bulbs.

Table 20: Log Reduction for 64s Batch Experiment

	Power (μW)			
Mix Time	180	300	567	1200
1	4.3830	5.9283	8.9287	14.9112
5	2.4120	3.3983	3.9658	4.2148
10	1.8441	2.0840	2.2309	2.3098
15	1.3706	1.5134	1.6094	1.6509
20	1.1030	1.2065	1.2883	1.3240
25	0.9402	0.9744	0.9917	1.0047
30	0.8051	0.8911	0.9588	0.9947
32	0.6461	0.6605	0.6660	0.6739
35	0.6469	0.6596	0.6655	0.6737
40	0.6468	0.6586	0.6655	0.6733
45	0.6419	0.6545	0.6650	0.6721
50	0.6291	0.6508	0.6640	0.6713
55	0.6030	0.6349	0.6584	0.6695
60	0.4913	0.5655	0.6306	0.6598
64	0.3315	0.3310	0.3369	0.3391

Table 21 shows the same results for experiment duration of 129 seconds. This data shows that a mix time of around 30 to 35 seconds is appropriate.

Table 21: Log Reduction for 129s Batch Experiment

	Power (μW)			
Mix Time	180	300	567	1200
1	8.8344	11.9493	17.9970	30.0554
5	4.8511	6.8274	7.9436	8.4332
10	3.6395	4.0046	4.1956	4.3084
15	2.6926	2.8633	2.9526	2.9906
20	2.1575	2.2494	2.3105	2.3368
25	1.7611	1.8727	1.9525	2.0015
30	1.5615	1.6187	1.6514	1.6781
35	1.2944	1.3189	1.3310	1.3467
40	1.2541	1.2969	1.3231	1.3435
45	0.9843	0.9948	1.0025	1.0137
50	0.9801	0.9938	1.0038	1.0144
55	0.9739	0.9877	1.0040	1.0116
60	0.9339	0.9675	0.9952	1.0084
64.5	0.6630	0.6662	0.6738	0.6782
65	0.6630	0.6662	0.6738	0.6782
70	0.6622	0.6661	0.6737	0.6780
75	0.6619	0.6662	0.6731	0.6780
80	0.6608	0.6662	0.6728	0.6775
85	0.6607	0.6660	0.6720	0.6768
90	0.6594	0.6672	0.6713	0.6763
95	0.6572	0.6660	0.6714	0.6761
100	0.6545	0.6652	0.6707	0.6759
105	0.6527	0.6638	0.6700	0.6749
110	0.6464	0.6595	0.6695	0.6730
115	0.6337	0.6552	0.6672	0.6717
120	0.6063	0.6394	0.6606	0.6699
125	0.4944	0.5699	0.6328	0.6602
129	0.3344	0.3370	0.3389	0.3392

Since the mix times are a rough generalization of fluid flow in the batch reactor, the mixing rate for the 64 second and 129 second experiments do not match. A program or process that adequately calculates fluid flow in a batch reactor is needed.

AOP - Flow

Radical production may follow a linear relationship with input variables of UV energy and oxidant concentration. The rate of change is dependent on the specific applied energy and the oxidant type. Little research is available in this area, which mainly describes a rate constant based off of a starting concentration and an overall dose. Literature does not state if AOPs follow a linear dose to log-reduction curve or if regions are present as in DNA disruption. This research calculated the total dose applied within the reaction vessel for the flow through experiments.

The flow through experiments were set up with the solution entering the vessel through the inlet pipe on the bottom of the vessel. Then the solution traveled through the vessel and exited by the discharge pipe located on the top of the vessel. The LED plate faced horizontally along the reactor on the side closer to the discharge pipe. Duckworth's (2014) set up is shown in Figure 27.

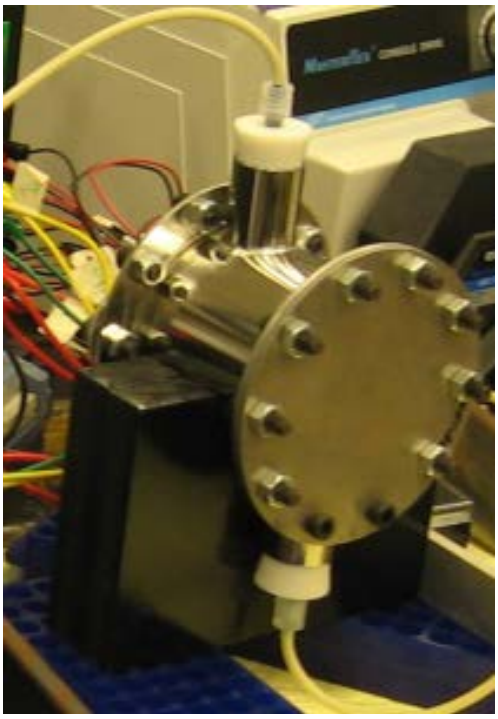

Figure 27: Duckworth's Set Up (Duckworth, 2014)

A basic dose calculation for flow was conducted to determine the dose that was exposed to the solution flowing through the reaction vessel. This calculation represented the applied dose for flow that began at the inlet. This does not apply to the initial fluid in the vessel that started part way through the vessel, since when this process is applied in real world applications, the reactor may be primed with a neutralized solution. The flow was also assumed to be laminar and constant through the vessel. The calculation used a flow rate of 1.4 mL/min to match the experiments conducted by Duckworth (2014). The total dose for each power output is reported in Table 22. The applied dose was between 6.42×10^{9} and 4.28×10^{10} mJ/cm^2. A more specific dose was not determined because the LEDs were not measured directly before or after testing.

Table 22: Flow Dose with Varying Bulb Output Power

	Dose (mJ/cm^2)
180 µW	6.42E+09
300 µW	1.07E+10
567 µW	2.02E+10
1200 µW	4.28E+10

Graphing

MATLAB's graphing function '*contourslice*' was used to visualize the three dimensional irradiance patterns. Graphs were called to show irradiance values of less than 1 mW/cm^2, 1-200 mW/cm^2, and greater than 200 mW/cm^2. These ranges were used to show the shoulder, linear, and tailing regions set forth by the EPA for DNA disruption. These ranges are useful in either batch or flow experiments for this reactor vessel.

Figures 28 and 29 show a singular bulb and the bulb array with extents limited to the vessel dimensions at the three regions. Each region was nested inside each other. The log-linear region overlapped with adjacent bulbs in the bulb array configuration.

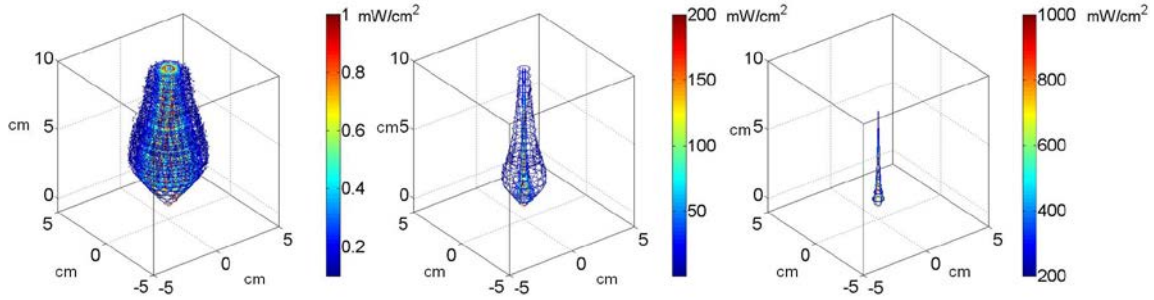

Figure 28: Bulb at 300 µW with Nested Shoulder, Linear, and Tailing Regions

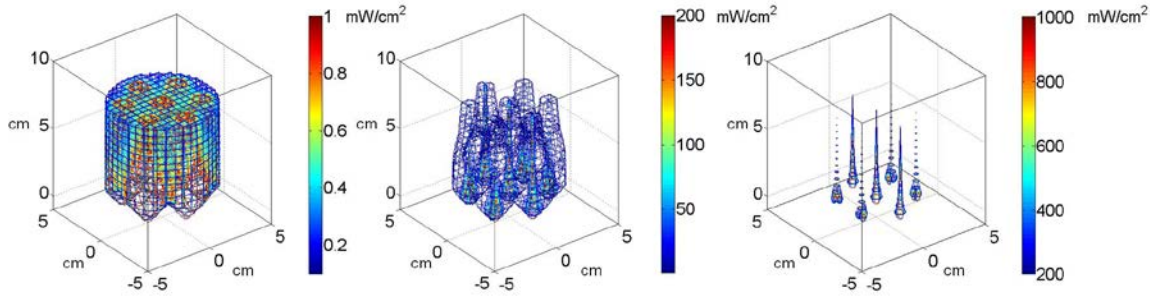

Figure 29: Bulb Array at 300 µW with Nested Shoulder, Linear, and Tailing Regions

Figures 30 to 32 show the shoulder, linear and tailing regions for a single SETi UVTOP260 TO-39 FW bulb. Each figure shows the bulb with the minimum and typical power specifications stated on the manufacturer's specification sheet on the top row followed by the average value measured by the manufacturer prior to shipment and the average value measured locally.

Figure 30 shows irradiance from 0.1 to 1 mW/cm^2 for a single LED limited to the height and radius of the vessel. This was in the shoulder region where DNA repair

occurs. The higher output power had a much greater effect than the minimum power stated by the manufacturer.

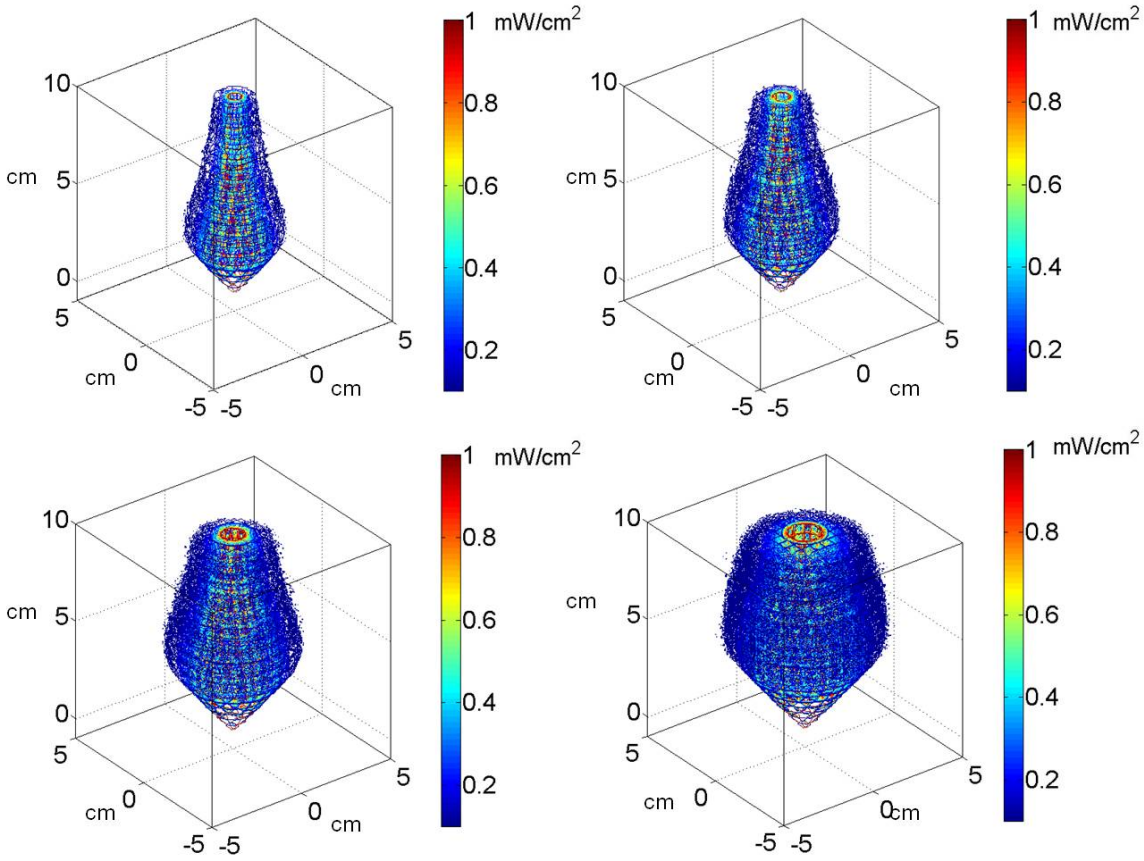

Figure 30: Single Bulb 0.1 to 1 mW/cm2, Top Left 180 µW, Top Right 300 µW, Bottom Left 567 µW, Bottom Right 1200 µW

Figure 31 shows the linear region, which was nested inside the shoulder region. This volume was where DNA repair did not occur and was inside the tailing region. The volume greatly changed for the different output power of the bulbs.

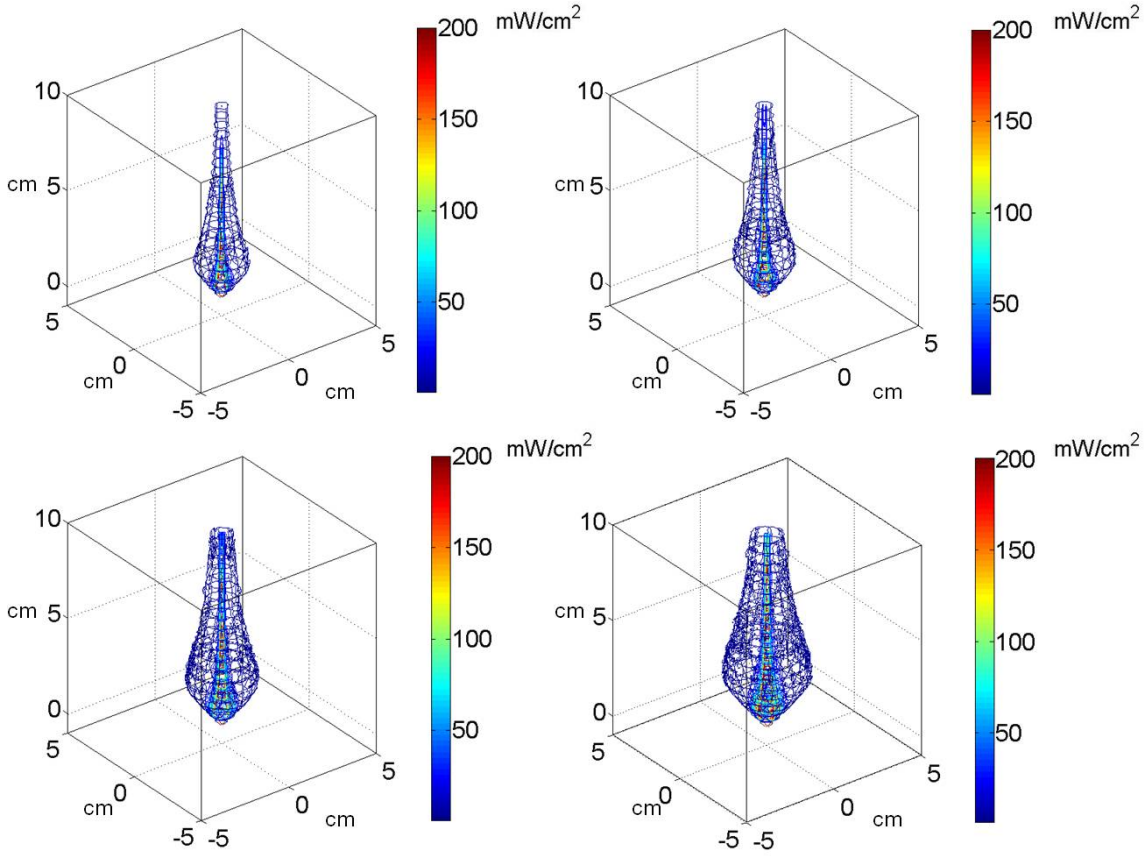

Figure 31: Single Bulb 1 to 200 mW/cm2, Top Left 180 µW, Top Right 300 µW, Bottom Left 567 µW, Bottom Right 1200 µW

Figure 32 shows the tailing region. This volume is nested within the linear region. This represents where the log kill rate slowed down due to the reduction of pathogens in the target solution. The high dose did little to further the contaminant reduction. However, reducing the dose in this area could only be performed by either limiting the output power or changing the characteristics of light propagation by the bulb. This volume was relatively small for the SETi UVTOP260 TO-39 FW bulbs and only slightly increases with the increased in output power.

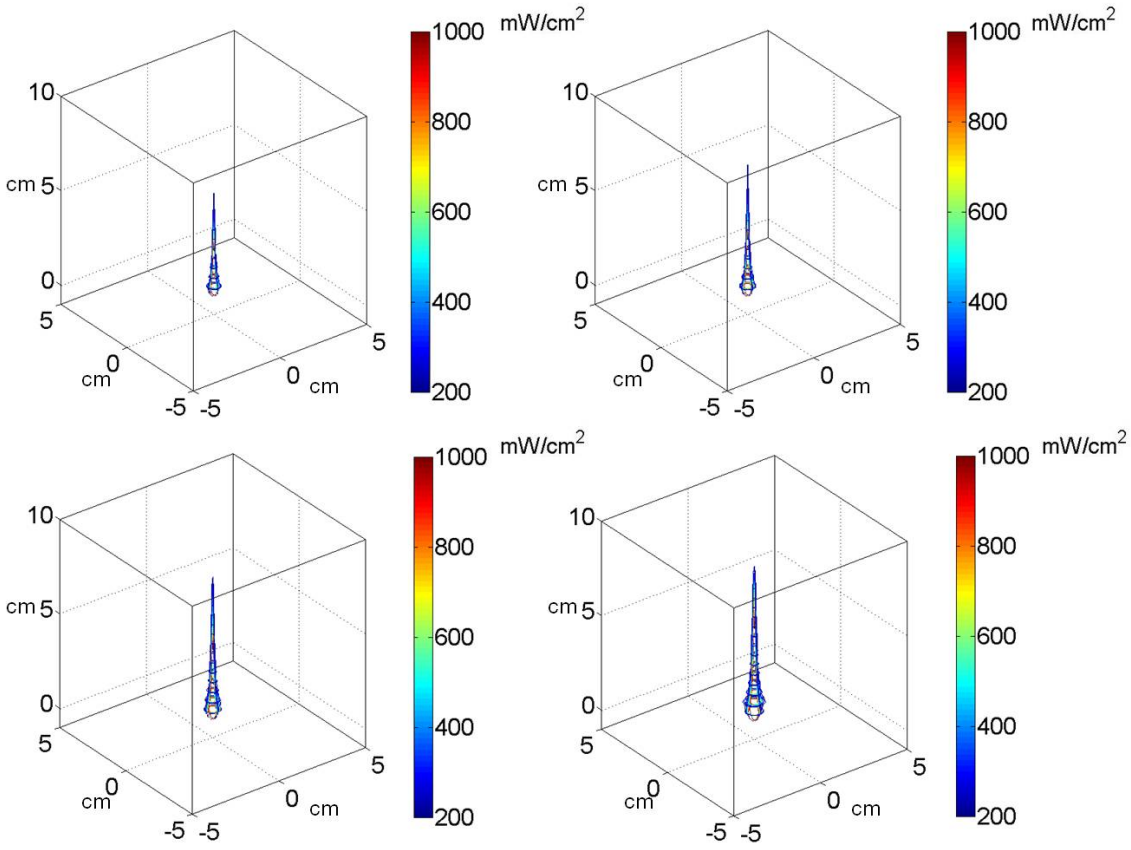

Figure 32: Single Bulb 200 to 1000 mW/cm2, Top Left 180 µW, Top Right 300 µW, Bottom Left 567 µW, Bottom Right 1200 µW

Figures 33 through 35 show the same regions for the bulb array. Figure 33 shows that almost all of the volume was covered by the minimum output power guaranteed by the manufacturer for the shoulder region. The only area outside this region was outside the emission angle of each bulb located at the bottom of the vessel.

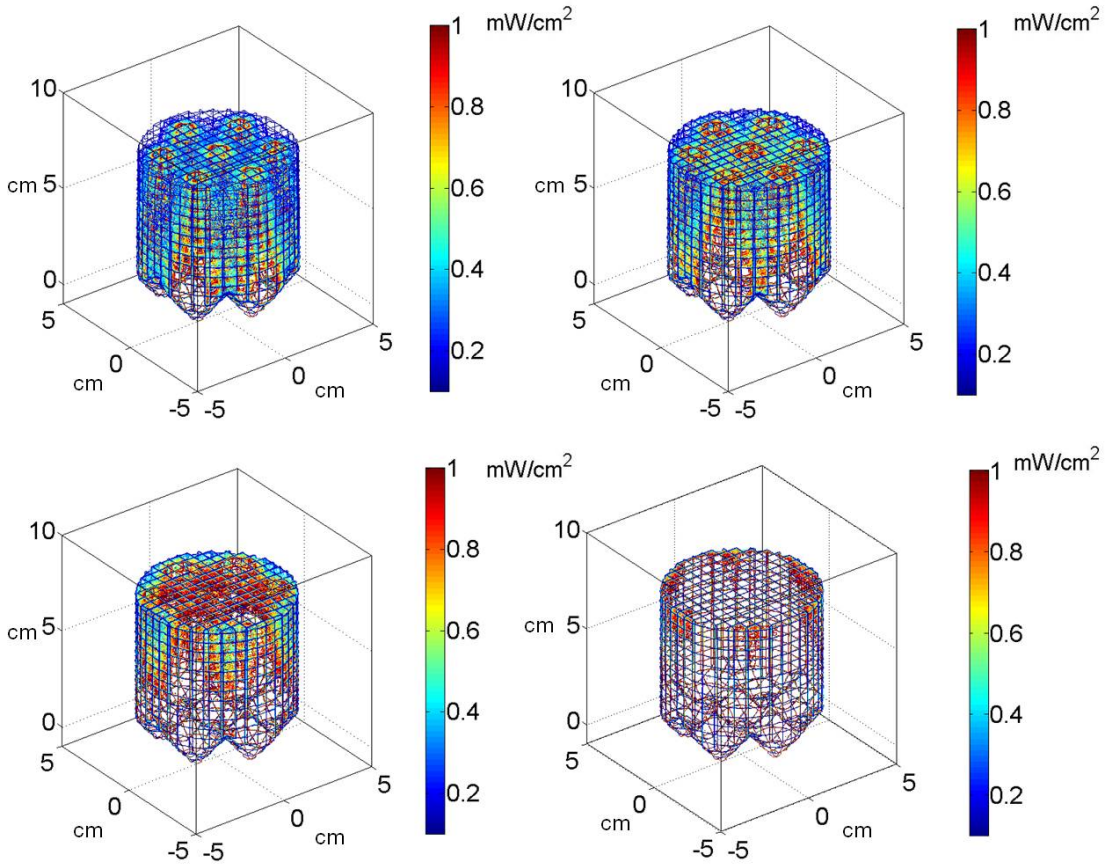

Figure 33: Bulb Array 0.1 to 1 mW/cm2, Top Left 180 µW, Top Right 300 µW, Bottom Left 567 µW, Bottom Right 1200 µW

Figure 34 shows the volume covered by the linear region in the multiple bulb configuration. The area increased as the power increased. The area between the energy propagation was almost nonexistent for the 567 µW power output and did not exist for the 1200 µW power output.

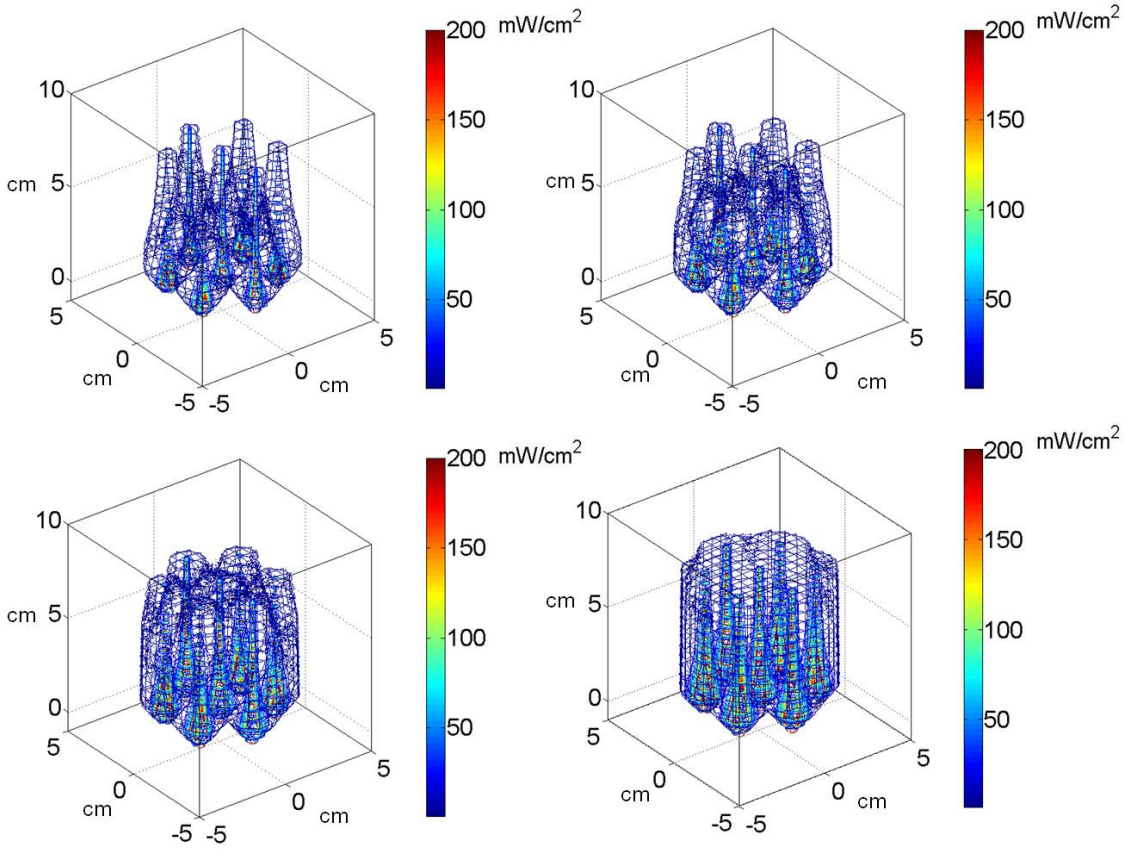

Figure 34: Bulb Array 1 to 200 mW/cm2, Top Left 180 µW, Top Right 300 µW, Bottom Left 567 µW, Bottom Right 1200 µW

The tailing region, shown in Figure 35, did not overlap between the energy propagated from the separate bulbs. This illustrates that the maximum log reduction in the vessel was not limited by overpowering due to the bulb array configuration, but from the individual bulbs themselves.

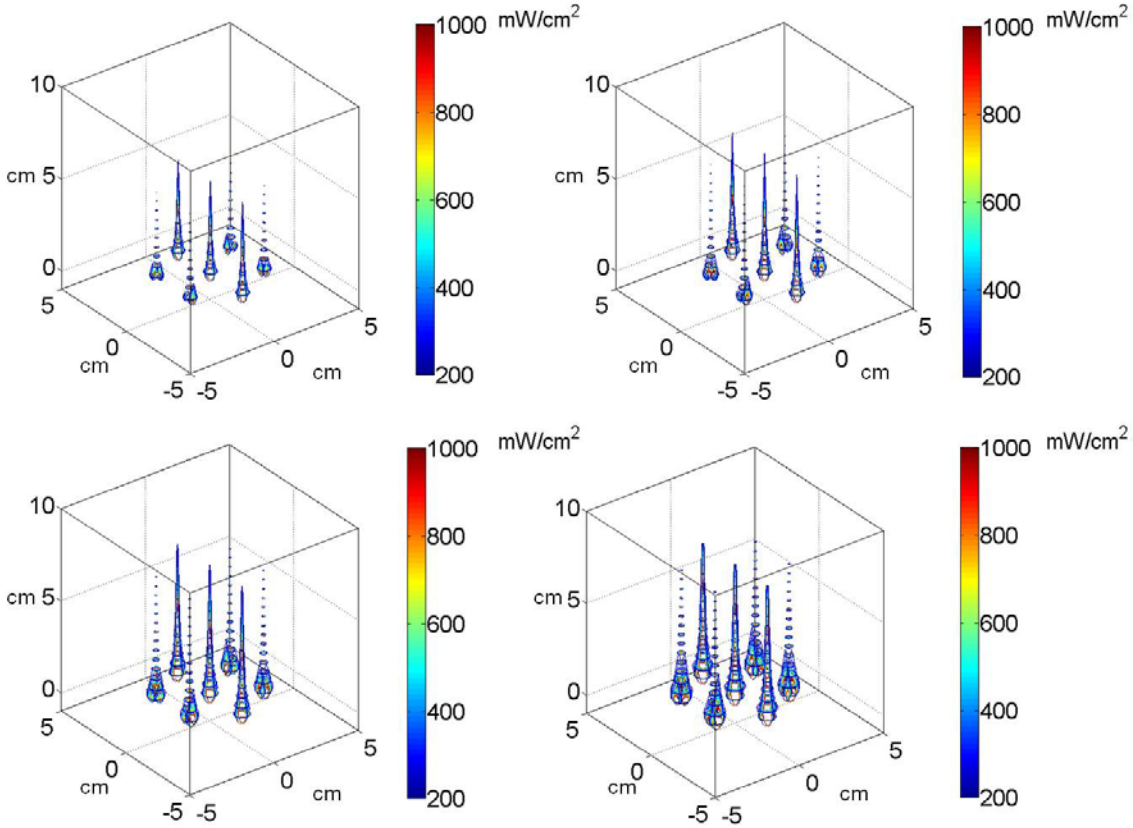

Figure 35: Bulb Array 200 to 1000 mW/cm2, Top Left 180 µW, Top Right 300 µW, Bottom Left 567 µW, Bottom Right 1200 µW

Reactor Vessel Optimization

The measures for DNA disruption and AOP are different. Reactor vessels for DNA disruption are optimized when they reach the greatest efficiency to neutralize target pathogens. DNA disruption followed a log reduction curve that had a shoulder, log-linear, and tailing regions. AOPs may lack the shoulder, log-linear, and tailing curve

where some regions are less effective than others. Batch and flow vessels may also alter the optimum design of the reactor.

DNA Disruption Conclusions

Reactor vessels are optimized for DNA disruption applications when the percent by volume for the log-linear region is the greatest. This ensures that the optimal dose range is present in the greatest volume of the vessel. Table 23 shows the percent by volume for the three regions for varying power output for the bulb array. The log-linear region greatly increased with the given power outputs while the tailing region slightly increased. Throughout this process, the shoulder region significantly decreased.

Table 23: Percent Volume Associated with Shoulder, Log-Linear, and Tailing Regions

	180 μW	
	Count	Percent
Shoulder	153432	55.49%
Log-Linear	120562	43.60%
Tailing	2534	0.92%

	300 μW	
	Count	Percent
Shoulder	105000	37.97%
Log-Linear	167901	60.72%
Tailing	3619	1.31%

	567 μW	
	Count	Percent
Shoulder	41384	14.97%
Log-Linear	229490	82.99%
Tailing	5646	2.04%

	1200 μW	
	Count	Percent
Shoulder	4284	1.55%
Log-Linear	262968	95.10%
Tailing	9268	3.35%

Table 24 shows results for the same bulb spacing and vessel size with a power output of 3000 μW. This illustrates that the vessel radius is smaller than the optimized radius for the same fluid height due to the decrease in the log-linear region when compared to bulbs with 1200 μW output power. The higher output bulbs provide a higher dose, but the energy output to disinfection rate is reduced.

Table 24: Percent Volume Associated with Shoulder, Log-Linear, and Tailing Regions for 3000 µW

	3000 µW	
	Count	Percent
Shoulder	330	0.12%
Log-Linear	257376	93.08%
Tailing	18814	6.80%

The bulb array was dependent on the power output of the bulbs and the ranges of the shoulder, log-linear, and tailing regions. The goal was to reduce the volume containing the shoulder region, while increasing the volume containing the log-linear region. The tailing region was where overpowering occurs, but this was a direct result from the bulb specifications. This goal results in a higher disinfection to energy output rate. The tailing region may be reduced by obtaining LEDs with a different energy spread. Otherwise, this region was accepted as a necessary less efficient volume than the log-linear region volume. However, the minimum this region should be in a reactor vessel was the size of this region for a single bulb, multiplied by the number of bulbs in the reactor. Co-locating bulbs on opposite plates to overlap the tailing region may provide data that shows a decrease in the tailing region, but this only further overpowers the tailing volume. A better approach is to not overlap the tailing regions for a single bulb. Design needs to ensure that the overlap of the energy spread does not produce excess volume in the tailing region.

Utilizing the same vessel shape, another LED plate may be used on the opposite side of the reactor to eliminate the void space near the bottom plate that receives no energy and increase the areas in the shoulder region. The two bulb plates may be designed to offset the bulbs so the tailing regions are not co-located. The energy pattern

also must be analyzed to reduce any excess tailing region volume. An ideal situation would involve LED bulbs that do not emit in the tailing region, which also creates an energy pattern fully in the log-linear region.

AOP Conclusions

The limited available literature on AOPs suggests that radical production is dependent on UV dose and initial oxidant concentration. Therefore, the optimal vessel design would involve applying the optimal UV and oxidant doses to reach a given contaminant reduction for every fluid path in the vessel.

Batch Reactor Conclusions

Batch and flow applications affect reactor design. These applications greatly differ in how dose is applied and in fluid movement within the reactor. Batch reactors may be best suited for small scale home or individual water disinfection systems, while flow through reactors may be best suited for large scale commercial applications.

Batch reactor design must account for sediment and achieve an even dose throughout the vessel. Sediment in the reactor may block energy propagation. Depending on the sediment density, it may fall, suspend, or float in the reactor. Bulb placement may be decided based on the anticipated sediment in the reactor. For example, place the LEDs on the top of the vessel if the sediment tends to fall. In this case, the fluid may be placed in the reactor for a given time prior to disinfection to allow the sediment to collect prior to energizing the system. Another option is to filter the fluid to remove particles, which may also filter microbes. The batch experiments conducted by Tran (2014) shook the system since the LED array was placed on the bottom plate. This prevented the spores from collecting on the bottom plate which could increase the

absorption coefficient closer to the bulbs and increase the concentration of spores located in the system outside the emission angle of any of the bulbs. The orbital shaking also mixed the solution to spread the applied dose more evenly throughout the fluid. An even dose may be applied by arranging the LED array to provide an even intensity throughout the vessel. The gaps between the bulbs on a single plane may be eliminated by placing bulbs on multiple planes.

Fluid Flow Reactor Conclusions

Flow through reactor designs must account for fluid flow. The fluid path must be analyzed to correctly apply an energy distribution in the system to guarantee a minimum dose applied to every path through the reactor. A conservative method may involve determining the quickest path through the vessel and applying a minimum intensity throughout the vessel to achieve the required dose along this quickest path. Sediment collecting in the reactor may be an issue depending on flow velocity. Two methods to circumvent this are to increase the flow rate to not allow sediment collection and filter the fluid prior to entering the reactor, which may also filter the organisms.

Designing a system for laminar flow eases the process to build the correct bulb array. However, large flow requirements may prevent a laminar system from being possible. Pipe friction reduces the flow velocity around the reactor walls. This drives an uneven required spread of energy in the system since the contact time near the reactor walls is higher than the quicker velocity towards the center of the reactor.

Concepts for Future Flow Reactor Designs

Fluid Flow

The basics of fluid flow in a closed vessel involve laminar versus turbulent flow and flow velocity through the vessel. Laminar flow may be beneficial in flow through reactors due to more predictable flow paths. Whether the flow is laminar or turbulent depends on a few factors. The vessel shape and fluid velocity play a major role in this. Areas where the vessel changes shape may change laminar flow to turbulent flow. Flow velocity alone may also determine if a flow is laminar or turbulent through a constant geometry.

Internal wall friction prevents constant fluid flow. The flow is slower closer to the reactor walls and is the quickest in the middle of a flow through reactor. Smoother vessel walls reduce the velocity differences and provide a better surface for reflection.

Pipe Designs

Mercury lamp flow through reactors are traditionally based off of a pipe with mercury lamps in a quartz tube placed parallel or perpendicular to the flow, as discussed in Chapter II. LEDs are able to eliminate the need for the quartz tube interface in reactor vessels. The traditional pipe design may be used with LEDs around the exterior of the reactor. Figure 36 shows an example of this design with four evenly spaced bulbs around the outside of the pipe and the resulting fields of view with the SETi bulbs in water. The cross sectional four-bulb array may repeat along the length of the pipe and be rotated to level the irradiance field along the pipe.

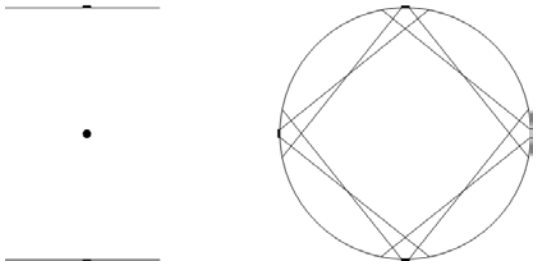

Figure 36: Pipe Reactor Design with 4 Bulb Array

The number of LEDs in the cross sectional array is only limited by the radius of the pipe and the size of the LEDs. Figure 37 shows the fields of view for two, three, and four LED bulb arrays in a pipe reactor. The two bulb array may have dead space, where no irradiance is present, shown in the shaded regions. Three or more bulbs in the same plane eliminate the dead space for the emission angle produced by SETi flat window bulbs in water. Each cross sectional array may also be offset along the length of the pipe to eliminate the dead space associated with two bulb arrays and level out the irradiance fields to provide a more constant dose for any linear path through the vessel.

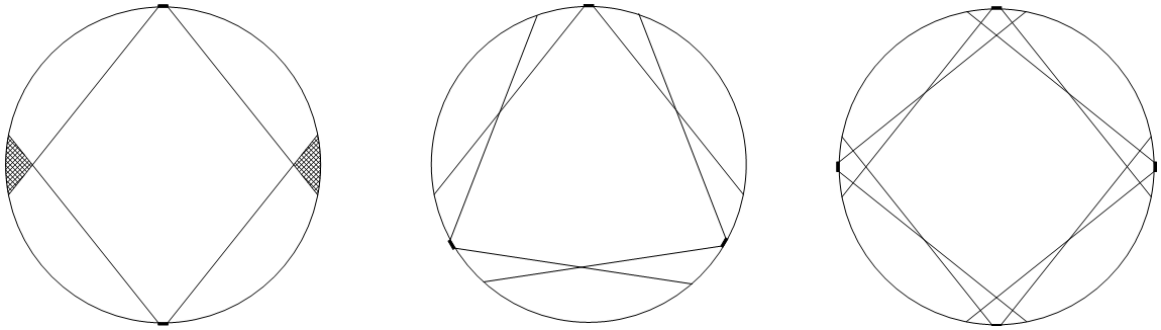

Figure 37: 2, 3, and 4 Bulb Arrays for Pipe Reactors

The spacing between the cross sectional arrays is determined by the required overlap to provide the minimum irradiance needed for either AOP or DNA disruption, and present contaminants. The length of the reactor and fluid velocity is determined based off of the radius of the reactor, required capacity, and disinfection requirements.

Manufacturing is one major drawback of pipe reactors with flat window LED bulbs. Placing a flat window on a curved surface requires high part tolerances. Rectangular designs ease LED installation.

Rectangular Designs

Utilizing bulb arrays on two reactor walls in rectangular designs eliminates dead space in the reactor. The arrays may be offset to eliminate peaks from the upper and lower arrays from overlapping. Figure 38 shows a general rectangular reactor design. The black circles represent LEDs on the upper reactor wall and red circles represent LEDs on the lower reactor wall.

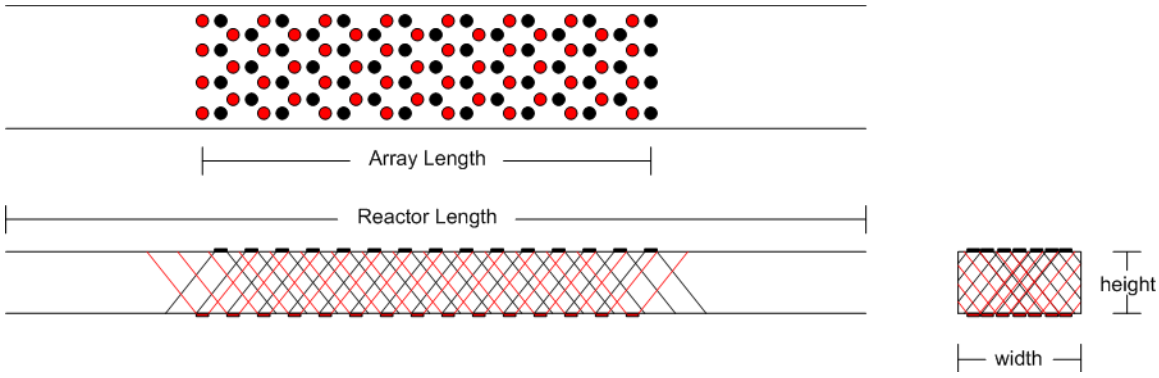

Figure 38: Rectangular Reactor Design

The LED bulb layout and spacing needs to be optimized based off of bulb characteristics, disinfection method, and inactivation requirements. The reactor height, reactor width and array length also need to be optimized to provide the required capacity. Normally, fluid is conveyed through circular pipes. A rectangular reactor may require a volume before and after the bulb array to allow the fluid to transition from a circular to rectangular geometry and provide a laminar flow through the volume exposed to UV energy.

Modular Design

In either pipe or rectangular designs, reactors may be split into modules to increase the uses for a single reactor. The modules may be designed in series or parallel. The series designs allow separate bulb arrays to operate as needed. Parallel designs may open reactor chambers as needed. The bulb arrays may be placed sequentially or overlap to provide the needed flexibility throughout the system's life.

Modular designs allow a single system to increase dose based when required. These designs also enable systems to increase or decrease inactivation capacity based off of need. This flexibility also changes energy usage to either slow or speed up the system to prevent shutting the system down, while not wasting energy by overpowering slow fluid velocities.

Chapter Summary

In this chapter, the data and results from the modeling and simulation are presented. This work is compared to results collected from laboratory experiments and differences are noted. The next chapter presents conclusions from this research and concepts for future reactor designs with LED bulbs.

V. Conclusions

Chapter Overview

This chapter explains the main conclusions of this research stream, followed by why it is important. Next, research limitations are stated. Finally, recommendations for future research are presented.

Conclusions of Research

This research presented a methodology to model UV LEDs in reactor vessels. Energy propagation patterns were used to determine irradiance in a reaction vessel for both batch and flow experiments. The irradiance patterns were used to illustrate how to optimize vessels to achieve log reduction requirements by both DNA disruption and AOP methods. The initial research questions are answered below.

RQ1: What is an Advanced Oxidation Process (AOP) and DNA disruption? How are they different and similar? Also, how are they used for water disinfection?

Chapter II discusses AOP and DNA disruption in more detail. The AOP involves adding a chemical that breaks down into radicals when the optimal wavelength of energy is applied. These radicals subsequently react with the contaminants to transform them. In Duckworth's (2014) research, hydrogen peroxide (H_2O_2) was converted by UV energy into hydroxyl radicals (·OH), which reacted with methylene blue, an indicator dye. DNA disruption affects the chemical structure of the targeted pathogens. This neutralizes the pathogen and prevents reproduction from occurring.

RQ2: What sources of ultraviolet (UV) radiation have been used for the AOP and DNA disruption in water disinfection applications?

This question is also addressed in Chapter II. Mercury lamps are the predominant UV energy source due to their high power output and market availability. UV LEDs are an emerging technology for water disinfection. They are relatively new, have low power output, and have short lifespans. Many experts agree that UV LEDs will follow the advancements of visible light LEDs and improve in the coming years.

RQ3: What are the measures of UV energy distribution in a reactor vessel?

Chapter II discusses the measures of UV energy distribution. The measures are different for DNA disruption and AOPs. DNA disruption follows a shoulder, log-linear, and tailing regions. The log-linear region has the most efficient disinfection rate of the three regions. Literature suggests that radical formation has a linear relationship with UV energy in an AOP. More research is needed to show the relationship between radical concentration and organic oxidation.

RQ4: What mathematical models can be used to calculate the distribution and absorption of UV Light Emitting Diode (LED) radiation as it propagates through different mediums?

Chapter III describes the equations and models used to determine energy propagation. LED energy propagation is vastly different than the predominant mercury lamp technology in water disinfection. The basic mercury lamp models assume

Lambertian attributes, which do not describe LED energy propagation. Modeling LED energy propagation involves un-normalizing the manufacturer's specifications for energy distribution and calculating the energy and area associated with each point in the reactor. Absorption is applied based on the distance away from the energy source. Different mediums change the absorption coefficient and the emission angle of the LEDs.

RQ5: What tools can be used to simulate these models to calculate the UV energy present at any point within a UV reactor vessel?

Chapters II and III discuss the tools that can be used to model UV energy. MATLAB is excellent to manipulate data arrays to calculate energy distribution, but lacks fluid flow capability. COMSOL Multiphysics offers fluid modules to account for fluid flow through a reactor. This platform may be best to optimize LED bulb arrangement for fluid flow through a reactor.

RQ6: How do simulation results generated from the model compare to actual experimental results collected from the laboratory?

Chapter IV discusses the results obtained from the laboratory and the model. The batch experiments utilize DNA disruption which has better dose-log reduction equations in literature. A mix time was applied to the model to generalize the effect of mixing in the vessel. However, the mix time for the 64 and 129 second duration experiments did not match. The limited equation from literature for these experiments also restricts the accuracy of the model. The flow through experiments utilize AOP to generate hydroxyl

radicals. Further research needs to be conducted to fill the knowledge gap of dose to hydroxyl radical production to properly model the results.

RQ7: What UV LED reactor designs are most efficient for water disinfection?

Chapter IV discusses optimized reactor designs. The application drives design choices for batch or flow, while disinfection method determines vessel geometry. The required flow determines if batch or flow is appropriate. Smaller scale systems may be best in batch applications since the reactor is less complex. On the other hand flow systems may be used to treat larger quantities of fluid. DNA disruption or AOP determines the optimal LED arrangement. DNA disruption seeks to optimize the log-linear region and optimal dose while AOP only seeks to optimize a constant dose to all of the fluid.

Significance of Research

This research addressed the difference in modeling UV LED bulbs compared to mercury lamps. Mercury lamps propagate energy following Lambertian behavior. This is not the case with LEDs. They have a limited emission angle that reduces in power towards the extent of this angle.

The presented methodology illustrated how to model energy propagation for LEDs to determine reactor vessel shape and size. This research is useful to create reactor vessels that replace mercury lamps with UV LEDs. The approach may also be used in other UV LED applications, such as curing in a manufacturing setting.

Limitations

The main limitations of this research are limited knowledge of energy outputs throughout the experiments conducted in the laboratory, log reduction rates compared to applied dose, and fluid flow. The actual output power was not known for the multiple experiments due to exponential output power degradation in the first 100 hours of run time. This research based the applied dose to log reduction rate of *Bacillus subtilis* spores on data that only describes the log-linear region. Assumptions were made to supplement the data for the shoulder and tailing regions. Finally, fluid flow through the vessel was not addressed. Assumptions were made that constant, laminar flow occurred throughout the vessel for flow applications and a generalization for mix rate in batch applications.

Recommendations for Future Research

Follow on research is necessary to tune the model for specific water disinfection applications and optimize reactor vessels. These research streams are described below.

Tune Model

1) Collimated Beam Experiments: The model can be applied with these experiments to determine the log reduction function, dependent on dose, for various contaminants. The trials need to determine the shoulder, log-linear, and tailing regions along with the associated log reduction.
2) Fluid Flow: The model can be refined by accounting for fluid flow in reactor vessels. The fluid modules in COMSOL Multiphysics may be the correct tool.

Optimize Reactor Vessels

1) Compare UV LED Bulbs: A comparison of LED windows and power output can be performed to decrease the shoulder and tailing regions and optimize the log-linear region.
2) Optimize Reactor Vessel Shape: A comparison of reactor vessel shapes can be performed to determine optimized shapes for both batch and flow applications for single bulbs and various bulb arrays.
3) Optimize Reactor Vessel Size for Various Uses: A comparison of reactor vessel size can be optimized for various types of uses and quantities of contaminated fluid.
4) Pulsing: Pulsing has shown increased energy efficiency in UV disinfection systems. This may be researched with the previous research streams.

Summary

In this chapter, the conclusions of research are addressed along with the significance of the findings. Limitations to this research are addressed followed by recommendations for future research.

Appendix

MATLAB Code

Overall Model

```
% Sub Functions: intensity, absorption, conversion, re_order,
bulb_offset, addCylinder

clear
clc

%%%%%%%%%%%%%%%%%%%%%%%%%%%%%%%%%%%%%%%%
% Initializing

variables;

% End Initialization
%%%%%%%%%%%%%%%%%%%%%%%%%%%%%%%%%%%%%%%%


%%%%%%%%%%%%%%%%%%%%%%%%%%%%%%%%%%%%%%%%
% Calculate Irradiance with Aborption

irradiance = irradiance(az,el,r,va,p); % power function calculates
power at each spherical coordinate [uW/cm^2]

irradianceAbsorption = absorption(irradiance, a, r);

% End Irradiance Calculations
%%%%%%%%%%%%%%%%%%%%%%%%%%%%%%%%%%%%%%%%


%%%%%%%%%%%%%%%%%%%%%%%%%%%%%%%%%%%%%%%%
% Convert Spherical to Cartesian Coordinates, Move Cartesian
Coordinates to
% Closest Grid and ReOrder Matrix

[x,y,z] = sph2cart(deg2rad(az),deg2rad(el),r); %converts az, el, r
spherical coordinates to x, y, z cartesian coordinates

xMoved = conversion(x, stepSize); %moves x,y,z coordinates to closest
evenly spaced x,y,z grid, spaced .1 cm
yMoved = conversion(y, stepSize);
zMoved = conversion(z, stepSize);

irradianceOrdered = reOrder(irradianceAbsorption, xMoved, yMoved,
zMoved); %re-orders x,y,z, and intensity matrixes to later graph them
% 201x201x101 matrix representing x:-10:.1:10, y:-10:.1:10, z:0:.1:10
```

```
% End Spherical to Cartesian Conversion and ReOrder
%%%%%%%%%%%%%%%%%%%%%%%%%%%%%%%%%%%%%%


%%%%%%%%%%%%%%%%%%%%%%%%%%%%%%%%%%%%%%
% Graph Single Bulbs
graphSingle;
%%%%%%%%%%%%%%%%%%%%%%%%%%%%%%%%%%%%%%


%%%%%%%%%%%%%%%%%%%%%%%%%%%%%%%%%%%%%%
% Add Multiple Bulbs

bulbArray = bulbOffset(irradianceOrdered, offsetDimensions); % Add 6
bulbs to get 7 total

% End Multiple Bulbs
%%%%%%%%%%%%%%%%%%%%%%%%%%%%%%%%%%%%%%


%%%%%%%%%%%%%%%%%%%%%%%%%%%%%%%%%%%%%%%%%%%%%%%%%%%%%%%%%%%%%%%%%%%%%%%
%%%%%
% Batch

%%%%%%%%%%%%%%%%%%%%%%%%%%%%%%%%%%%%%%
% Limit Irradiance to Inside Container & Water Level
bulbArrayLimitedBatch = cut(bulbArray, xGraph, yGraph, zGraph, radius,
fluidHeightBatch);
%%%%%%%%%%%%%%%%%%%%%%%%%%%%%%%%%%%%%%


%%%%%%%%%%%%%%%%%%%%%%%%%%%%%%%%%%%%%%
% Calculate New Concentration
concentrationNew = doseBatch(bulbArrayLimitedBatch,
concentrationInitial, time, xGraph, yGraph, zGraph, radius,
fluidHeightBatch, mixTime);
%%%%%%%%%%%%%%%%%%%%%%%%%%%%%%%%%%%%%%


%%%%%%%%%%%%%%%%%%%%%%%%%%%%%%%%%%%%%%
% Calculate Log Kill in Vessel
logKill = log10(concentrationInitial / concentrationNew);
%%%%%%%%%%%%%%%%%%%%%%%%%%%%%%%%%%%%%%


%%%%%%%%%%%%%%%%%%%%%%%%%%%%%%%%%%%%%%
% Graph
graphBatch;
%%%%%%%%%%%%%%%%%%%%%%%%%%%%%%%%%%%%%%
%%%%%%%%%%%%%%%%%%%%%%%%%%%%%%%%%%%%%%%%%%%%%%%%%%%%%%%%%%%%%%%%%%%%%%%
%%%%%
```

```
%%%%%%%%%%%%%%%%%%%%%%%%%%%%%%%%%%%%%%%%%%%%%%%%%%%%%%%%%%%%%%%%%%%%%%%
%%%%%
% Dose

%%%%%%%%%%%%%%%%%%%%%%%%%%%%%%%%%%%%%%
% Limit Irradiance to Inside Container & Water Level
bulbArrayLimitedFlow = cut(bulbArray, xGraph, yGraph, zGraph, radius,
fluidHeightFlow);
%%%%%%%%%%%%%%%%%%%%%%%%%%%%%%%%%%%%%%

%%%%%%%%%%%%%%%%%%%%%%%%%%%%%%%%%%%%%%
% Calculate Flow Dose Regions
[doseTotal, doseShoulderTotal, doseLinearTotal, doseTailingTotal,
countShoulder, countLinear, countTailing] =
doseFlow(bulbArrayLimitedFlow, xGraph, yGraph, zGraph, radius,
fluidHeightFlow, flowRate, shoulderMax, logLinearMax, stepSize);
%%%%%%%%%%%%%%%%%%%%%%%%%%%%%%%%%%%%%%


%%%%%%%%%%%%%%%%%%%%%%%%%%%%%%%%%%%%%%
% Graph
graphDose;
%%%%%%%%%%%%%%%%%%%%%%%%%%%%%%%%%%%%%%

%%%%%%%%%%%%%%%%%%%%%%%%%%%%%%%%%%%%%%%%%%%%%%%%%%%%%%%%%%%%%%%%%%%%%%%
%%%%%
Model = 'DONE'
```

Variables

```
%%%%%%%%%%%%%%%%%%%%%%%%%%%%%%%%%%%%%%%%%%%%%%%%%%%%%%%%%
% User Input

%%%%%%%%%%%%%%%%%%%
% Vessel Parameters for Cylinder
radius = 3.6449; %cm
vesselHeight = 7.62; %cm
%%%%%%%%%%%%%%%%%%%

%%%%%%%%%%%%%%%%%%%
% Bulb Array
offsetDimensions = [-2.54,0;-1.27,2.20;-1.27,-2.20;0,0;1.27,2.20;1.27,-
2.20;2.54,0];
%%%%%%%%%%%%%%%%%%%

%%%%%%%%%%%%%%%%%%%
% Bulb and Fluid Characteristics
va = 39.72; %degrees
p = 567; %180, 300, 567, 1200 uW
a = .01; %1 per m for deionised water (DI) so .01 per cm to match units
of r in cm
%%%%%%%%%%%%%%%%%%%
```

```
%%%%%%%%%%%%%%%%%%%
% Batch Variables
concentrationInitial = 7E6; %cfu/ml
time = 64; %64 or 129 seconds
mixTime = 64; %seconds to remix batch to calculate log kill
fluidHeightBatch = 2.396; %cm, 2.396 for batch experiments, 7.62 for
flow through
%%%%%%%%%%%%%%%%%%%

%%%%%%%%%%%%%%%%%%%
% Flow Variables
flowRate = 1.4; % mL/min
fluidHeightFlow = 7.62; %cm
%%%%%%%%%%%%%%%%%%%

%%%%%%%%%%%%%%%%%%%
% User Input to size graphs
stepSize = .1; %cm

xGridMin = -10; %cm
xGridMax = 10; %cm

yGridMin = -10;
yGridMax = 10;

zGridMin = 0;
zGridMax = 10;
%%%%%%%%%%%%%%%%%%%



%%%%%%%%%%%%%%%%%%%
% Shoulder, Log-Linear, Tailing Regions
shoulderMin = 100; %uW/cm^2, used only for graphing
shoulderMax = 1000; %uW/cm^2 (1000 uW/cm^2 is 1 mW/cm^2)
logLinearMax = 200000; %uW/cm^2 (200000 uW/cm^2 is 200 mW/cm^2)
tailingMax = 1000000; %uW/cm^2, used only for graphing
%%%%%%%%%%%%%%%%%%%

% End User Input
%%%%%%%%%%%%%%%%%%%%%%%%%%%%%%%%%%%%%%%%%%%%%%%%%%%%%%%%%%%%%%%%%%%%%%%

%%%%%%%%%%%%%%%%%%%%%%%%%%%%%%%%%%%%%%%%%%%%%%%%%%%%%%%%%%%%%%%%%%%%%%%
% Set Up Spherical and Cartesian Space

%%%%%%%%%%%%%%%%%%%
%creates values for azimuth, elevation, and r
azInitial = linspace(-179,180, 360);  %degrees
elInitial = linspace((90-va),90, 100);  %degrees, limits elevation to
values within visual angle
rInitial = linspace(.1,zGridMax, 100);     %cm

[az,el,r] = meshgrid(azInitial,elInitial,rInitial);  %creates grid for
all az (degrees), el (degrees), and r (cm) values
```

```
%%%%%%%%%%%%%%%%%%%%

%%%%%%%%%%%%%%%%%%%%
% Size graphs
xSteps = ((xGridMax - xGridMin)/stepSize)+1; %cm
ySteps = ((yGridMax - yGridMin)/stepSize)+1;
zSteps = ((zGridMax - zGridMin)/stepSize)+1;

x1 = linspace(xGridMin,xGridMax,xSteps); %tenths
y1 = linspace(yGridMin,yGridMax,ySteps);
z1 = linspace(zGridMin,zGridMax,zSteps);

[xGraph,yGraph,zGraph] = meshgrid(x1,y1,z1); % creates x,y,z matrixes
to describe the points in the 'intensity' matrix
%%%%%%%%%%%%%%%%%%%%

%%%%%%%%%%%%%%%%%%%%%%%%%%%%%%%%%%%%%%%%%%%%%%%%%%%%%%%%%%%%%%%%%%%
```

Irradiance

```
% calculates irradiance [uW/cm^2] based off of evenly spaced azimuth,
elevation, and r


function [ irradiance ] = irradiance(az,el,r,va,p)

steradians = 2*pi*(1-cos(.5*(deg2rad(va)))); %calculates steradians
based off of visual angle

intensity = p/steradians; %calculates intensity based on power and
angle shown through [uW/st]

angle = 90-el; %calculates visual angle from center of light spread

normalizedIntensityAtPoint = -2E-5*(angle.^3) + 6E-4*(angle.^2) -
.0038*(angle) + .9702; %calculates normalized intensity value for each
visual angle

oSize = size(normalizedIntensityAtPoint);

% Set center point azimuths to 0 except 1 value
for i = 1:oSize(1);

    if el(i,1,1) == 90; %at 0 degrees from center (at center)
        normalizedIntensityAtPoint(i,2:oSize(2),1:oSize(3)) = 0; % set
normalized intensity to zero except first azimuth angle so this doesn't
add more than 1 point to center of beam
    end

end
```

```
azSize = size(az); %number of data points in each ring

normalizedTotalIntensityAtLayer = sum(sum(normalizedIntensityAtPoint));
%sums up intensity among all rings

percentIntensityPoint = normalizedIntensityAtPoint(:,:,:) ./
normalizedTotalIntensityAtLayer(:,:,1);  %percent intensity for each
ring

intensityAtPoint = percentIntensityPoint .* intensity; %calculates
intensity at each point at distance r from bulb


%%%%%%%%%%%%%%%%%%%%%%%%%%%%%%%%%%%%%%%%%%%%%%%%%%%
% compute area associated with each point

halfStep = (el(2,1,1) - el(1,1,1))/2;

areaSize = size(intensityAtPoint);

ringArea = zeros(areaSize(1), areaSize(2), areaSize(3));
pointArea = zeros(areaSize(1), areaSize(2), areaSize(3));

% Calculates Ring area
for i = 1:areaSize(1);
    for j = 1:areaSize(2);
        for k = 1:areaSize(3);

            if 90 - el(i,j,k) == 0;
                ringArea(i,j,k) = 2*pi*r(i,j,k)^2 * (1-
cos(deg2rad(halfStep))); %computes area associated with inner ring
(circle)
            else ringArea(i,j,k) = (2*pi*r(i,j,k)^2 * (1-cos(deg2rad(90
- el(i,1,1) + halfStep)))) - (2*pi*r(i,j,k)^2 * (1-cos(deg2rad(90 -
el(i,1,1) - halfStep)))); %computes area associated with all other
rings

            end

        end
    end
end

% Calculates Point Area
for i = 1:areaSize(1);
    for j = 1:areaSize(2);
        for k = 1:areaSize(3);

            if 90 - el(i,j,k) == 0;
```

```
                pointArea(i,j,k) = ringArea(i,j,k); %leaves inner ring
(circle) area at same value as ring (circle) area
            else pointArea(i,j,k) = ringArea(i,j,k) / azSize(2);
%divides all other rings area by number of azimuth angle to obtain area
per point

            end

        end
    end
end
%%%%%%%%%%%%%%%%%%%%%%%%%%%%%%%%%%%%%%%%%%%%%%%%%%%%

% Calculates Irradiance at each point
irradiance = intensityAtPoint ./ pointArea; %uW/cm^2

end
```

Absorption

```
function [ absorption ] = absorption(irradiance, a, r)

absorption = irradiance .* exp(-a .* r); %calculates intensity with
absorbance factored in

end
```

Conversion

```
% converts spherical to cartesian coordinates

function [ oMoved ] = conversion(o, stepSize)

oSize = size(o);

% step = .1; %tenths
newValue = -10:stepSize:10;

for i = 1:oSize(1);
    for j = 1:oSize(2);
        for k = 1:oSize(3);

            z = 1;

            while o(i,j,k) ~= newValue(z);

                if o(i,j,k) >= newValue(z)-.5*stepSize && o(i,j,k) <
newValue(z)+.5*stepSize;
                    o(i,j,k) = newValue(z);
                else z = z + 1;
```

```
                end

            end
        end
    end

end

oMoved = o(:,:,:);

end
```

Re-Order

```
% orders intensity points by increasing values of x,y, and z

function [ irradianceReorder ] = reOrder(irradiance, xMoved, yMoved,
zMoved)

intensSize = size(irradiance);

irradianceReorder = zeros(201,201,101); %tenths

for i = 1:intensSize(1);
    for j = 1:intensSize(2);
        for k = 1:intensSize(3);

            a = xMoved(i,j,k);
            b = yMoved(i,j,k);
            c = zMoved(i,j,k);

%             a1 = (a*100)+1001; %hundreths
%             b1 = (b*100)+1001;
%             c1 = (c*100)+1;

            a1 = (a*10)+101; %tenths
            b1 = (b*10)+101;
            c1 = (c*10)+1;

            irradianceReorder(round(a1),round(b1),round(c1)) =
irradiance(i,j,k) + irradianceReorder(round(a1),round(b1),round(c1));
%tenths, need round so indeces are not 1.00, 2.00 etc...
%             intensity(a+11,b+11,(c*10)+1) = intens(i,j,k) +
intensity(a+11,b+11,c+1); %whole numbers

        end
    end
end

end
```

Graph Single

```
%Single Bulb Graphs

vSingle = irradianceOrdered ./ 1000; %converts irradiance from uW to mW

%%%%%%%%%%%%%%%
figure
contourslice(xGraph,yGraph,zGraph,vSingle,[xGridMin:.5:xGridMax],[yGrid
Min:.5:yGridMax],[zGridMin:.5:zGridMax],linspace(shoulderMin/1000,shoul
derMax/1000, 10));%shoulder region, mW/cm^2 shows

axis([-5,5,-5,5,-1,10]); %changes axis
daspect([1,1,1]) %controls aspect ratio
box on
grid on
colorbar('FontSize',25)
%%%%%%%%%%%%%%%



%%%%%%%%%%%%%%%
figure
contourslice(xGraph,yGraph,zGraph,vSingle,[xGridMin:.5:xGridMax],[yGrid
Min:.5:yGridMax],[zGridMin:.5:zGridMax],linspace(shoulderMax/1000,logLi
nearMax/1000, 10));%log linear region, mW/cm^2 shows

axis([-5,5,-5,5,-1,10]); %changes axis
daspect([1,1,1]) %controls aspect ratio
box on
grid on
colorbar('FontSize',25)
%%%%%%%%%%%%%%%



%%%%%%%%%%%%%%%
figure
contourslice(xGraph,yGraph,zGraph,vSingle,[xGridMin:.5:xGridMax],[yGrid
Min:.5:yGridMax],[zGridMin:.5:zGridMax],linspace(logLinearMax/1000,tail
ingMax/1000, 10));%tailing region, mW/cm^2 shows

axis([-5,5,-5,5,-1,10]); %changes axis
daspect([1,1,1]) %controls aspect ratio
box on
grid on
colorbar('FontSize',25)
%%%%%%%%%%%%%%%
```

Bulb Offset

```
function [ multipleBulbs ] = bulbOffset(irradiance, offsetDimensions)

sizeIrradiance = size(irradiance);

sizeOffsetDimensions = size(offsetDimensions);

offsetX = round(10*offsetDimensions(:,1)');
offsetY = round(10*offsetDimensions(:,2)');

multipleBulbs =
zeros(sizeIrradiance(1),sizeIrradiance(2),sizeIrradiance(3));

% iteration for each bulb
for z = 1:sizeOffsetDimensions(1);

    % shifts bulb intensity in x-y plane
    for i = 30:sizeIrradiance(1)-30;
        for j = 30:sizeIrradiance(2)-30;
            for k = 1:sizeIrradiance(3);

                xOff = round(i+offsetX(z));
                yOff = round(j+offsetY(z));

                multipleBulbs(i,j,k) = multipleBulbs(i,j,k) +
irradiance(round(i-offsetX(z)),round(j-offsetY(z)),k);

            end
        end
    end

end

multipleBulbs;

end
```

Cut

```
function [reduced] = cut(irradiance, x, y, z, r, h)

Msize = size(irradiance);

for i = 1:Msize(1);
    for j = 1:Msize(2);
        for k = 1:Msize(3);

            if (x(i,j,k))^2 + (y(i,j,k))^2 >= r^2 || z(i,j,k) >= h;
                irradiance(i,j,k) = 0;
```

```
            else irradiance(i,j,k) = irradiance(i,j,k);

            end

        end
    end
end

reduced = irradiance;

end
```

Dose Batch

```
% Dose Batch

function [concentration] = doseBatch(irradiance, concentrationInitial,
time, xGraph, yGraph, zGraph, radius, fluidHeight, mixTime)

dose = irradiance .* mixTime; %dose per second .* s; %uJ/cm^2

doseJm2 = dose .* .01; %converts uJ/cm^2 to J/m^2

%equation to convert dose to log kill
logKill = (0.0133 .* doseJm2) + 0.5547; % J/m^2 application of gan....
wurtele

sizeLogKill = size(logKill);

for x = 1:sizeLogKill(1);
    for y = 1:sizeLogKill(2);
        for z = 1:sizeLogKill(3);

            if logKill(x,y,z) < 1.8847;
                logKill(x,y,z) = 0;
            else if logKill(x,y,z) > 5.5;
                    logKill(x,y,z) = 5.5;
                else logKill(x,y,z) = logKill(x,y,z);
                end
            end

        end
    end
end

concentrationMatrix = ones(sizeLogKill(1), sizeLogKill(2),
sizeLogKill(3));

concentrationMatrixCut = cut(concentrationMatrix, xGraph, yGraph,
zGraph, radius, fluidHeight);
```

```
sizeConcentraitonMatrixCut = size(concentrationMatrixCut);
count = 0;

for x1 = 1:sizeConcentraitonMatrixCut(1);
    for y1 = 1:sizeConcentraitonMatrixCut(2);
        for z1 = 1:sizeConcentraitonMatrixCut(3);

            if concentrationMatrixCut(x1,y1,z1) ~= 0;
                count = count + 1;
            else
            end

        end
    end
end

concentrationCycle = concentrationInitial * concentrationMatrixCut;

for i = 1:floor(time/mixTime);

    concentrationCycle = concentrationCycle .* concentrationMatrixCut;

    newConcentration = ((concentrationCycle) ./ (10.^logKill));

    averageConcentration1 = sum(sum(sum(newConcentration))) / count;
%100152 is the number of .1x.1x.1 cm cubes in Maj Tran's expirement

    concentrationCycle = averageConcentration1;

end

concentrationCycleEnd = concentrationCycle;

if round(time/mixTime) ~= (time/mixTime)

    dose2 = irradiance .* (((time/mixTime) -
floor(time/mixTime))*mixTime);
    dose2Jm2 = dose2 .* .01; %converts uJ/cm^2 to J/m^2
    logKill2 = (0.0133 .* dose2Jm2) + 0.5547; % J/m^2 application of
gan.... wurtele

    sizeLogKill2 = size(logKill2);

    for x = 1:sizeLogKill2(1);
        for y = 1:sizeLogKill2(2);
            for z = 1:sizeLogKill2(3);

                if logKill2(x,y,z) < 1.8847;
                    logKill2(x,y,z) = 0;
                else if logKill(x,y,z) > 5.5;
                        logKill(x,y,z) = 5.5;
```

```
                    else logKill(x,y,z) = logKill(x,y,z);
                    end
                end

            end
        end
    end

    concentrationCycle2 = concentrationCycleEnd *
concentrationMatrixCut;

    concentrationLastBatch = ((concentrationCycle2) ./ (10.^logKill2));

    averageConcentration2 = sum(sum(sum(concentrationLastBatch))) /
count; %100152 is the number of .1x.1x.1 cm cubes in Maj Tran's
expirement

    concentration = averageConcentration2;

else concentration = concentrationCycle;

end

end
```

Graph Batch

```
%Graphs Batch

vArrayBatch = bulbArrayLimitedBatch ./1000; %converts irradiance from
uW to mW

%%%%%%%%%%%%%%%%%%%%%
figure
contourslice(xGraph,yGraph,zGraph,vArrayBatch,[xGridMin:.5:xGridMax],[y
GridMin:.5:yGridMax],[zGridMin:.5:zGridMax],linspace(shoulderMin/1000,s
houlderMax/1000, 10));%shoulder region, mW/cm^2 shows

axis([-5,5,-5,5,-1,10]); %changes axis
daspect([1,1,1]) %controls aspect ratio
box on
grid on
colorbar('FontSize',25)
%%%%%%%%%%%%%%%%%%%%%



%%%%%%%%%%%%%%%%%%%%%
figure
contourslice(xGraph,yGraph,zGraph,vArrayBatch,[xGridMin:.5:xGridMax],[y
GridMin:.5:yGridMax],[zGridMin:.5:zGridMax],linspace(shoulderMax/1000,l
ogLinearMax/1000, 10));%log linear region, mW/cm^2 shows
```

```
axis([-5,5,-5,5,-1,10]); %changes axis
daspect([1,1,1]) %controls aspect ratio
box on
grid on
colorbar('FontSize',25)
%%%%%%%%%%%%%%%%%%%%%


%%%%%%%%%%%%%%%%%%%%%
figure
contourslice(xGraph,yGraph,zGraph,vArrayBatch,[xGridMin:.5:xGridMax],[y
GridMin:.5:yGridMax],[zGridMin:.5:zGridMax],linspace(logLinearMax/1000,
tailingMax/1000, 10));%tailing region, mW/cm^2 shows

axis([-5,5,-5,5,-1,10]); %changes axis
daspect([1,1,1]) %controls aspect ratio
box on
grid on
colorbar('FontSize',25)
%%%%%%%%%%%%%%%%%%%%%
```

Dose Flow

```
% Dose Flow

function [doseTotal, doseShoulderTotal, doseLinearTotal,
doseTailingTotal, countShoulder, countLinear, countTailing] =
doseFlow(irradiance, xGraph, yGraph, zGraph, radius, fluidHeightFlow,
flowRate, shoulderMax, logLinearMax, stepSize)

irradianceCut = cut(irradiance, xGraph, yGraph, zGraph, radius,
fluidHeightFlow);

rate = flowRate / 60; % converts mL/min to cm^3/s;

layerTime = pi * (radius^2) * stepSize / rate;

dose = irradianceCut .* layerTime; %dose per second .* s; %uJ/cm^2

doseTotal = sum(sum(sum(dose)));

sizeDose = size(dose);

doseShoulder = zeros(sizeDose(1), sizeDose(2), sizeDose(3));
doseLinear = zeros(sizeDose(1), sizeDose(2), sizeDose(3));
doseTailing = zeros(sizeDose(1), sizeDose(2), sizeDose(3));

for x = 1:sizeDose(1);
    for y = 1:sizeDose(2);
        for z = 1:sizeDose(3);
```

```
            if irradianceCut(x,y,z) < shoulderMax;
                doseShoulder(x,y,z) = dose(x,y,z);
            else
                if irradianceCut(x,y,z) >= shoulderMax &&
irradianceCut(x,y,z) < logLinearMax;
                    doseLinear(x,y,z) = dose(x,y,z);
                else
                    if irradianceCut(x,y,z) > logLinearMax;
                        doseTailing(x,y,z) = dose(x,y,z);
                    else
                    end

                end
            end

        end
    end
end


doseShoulderTotal = sum(sum(sum(doseShoulder)));

doseLinearTotal = sum(sum(sum(doseLinear)));

doseTailingTotal = sum(sum(sum(doseTailing)));


countShoulder = 0;
countLinear = 0;
countTailing = 0;

for x = 1:sizeDose(1);
    for y = 1:sizeDose(2);
        for z = 1:sizeDose(3);

            if doseShoulder(x,y,z) ~= 0; %uW/cm^2 (1 mW/cm^2)
                countShoulder = countShoulder + 1;
            else
            end

            if doseLinear(x,y,z) ~= 0; %uW/cm^2 (1 mW/cm^2)
                countLinear = countLinear + 1;
            else
            end

            if doseTailing(x,y,z) ~= 0; %uW/cm^2 (1 mW/cm^2)
                countTailing = countTailing + 1;
            else
            end
```

```
        end
    end
end

end
```

Graph Dose

```
%Graphs Dose

vArrayFlow = bulbArrayLimitedFlow ./1000; %converts irradiance from uW
to mW

%%%%%%%%%%%%%%%%%%%%%
figure
contourslice(xGraph,yGraph,zGraph,vArrayFlow,[xGridMin:.5:xGridMax],[yG
ridMin:.5:yGridMax],[zGridMin:.5:zGridMax],linspace(shoulderMin/1000,sh
oulderMax/1000, 10));%shoulder region, mW/cm^2 shows

axis([-5,5,-5,5,-1,10]); %changes axis
daspect([1,1,1]) %controls aspect ratio
box on
grid on
colorbar('FontSize',25)
%%%%%%%%%%%%%%%%%%%%%


%%%%%%%%%%%%%%%%%%%%%
figure
contourslice(xGraph,yGraph,zGraph,vArrayFlow,[xGridMin:.5:xGridMax],[yG
ridMin:.5:yGridMax],[zGridMin:.5:zGridMax],linspace(shoulderMax/1000,lo
gLinearMax/1000, 10));%log linear region, mW/cm^2 shows

axis([-5,5,-5,5,-1,10]); %changes axis
daspect([1,1,1]) %controls aspect ratio
box on
grid on
colorbar('FontSize',25)
%%%%%%%%%%%%%%%%%%%%%


%%%%%%%%%%%%%%%%%%%%%
figure
contourslice(xGraph,yGraph,zGraph,vArrayFlow,[xGridMin:.5:xGridMax],[yG
ridMin:.5:yGridMax],[zGridMin:.5:zGridMax],linspace(logLinearMax/1000,t
ailingMax/1000, 10));%tailing region, mW/cm^2 shows

axis([-5,5,-5,5,-1,10]); %changes axis
daspect([1,1,1]) %controls aspect ratio
box on
grid on
```

```
colorbar('FontSize',25)
%%%%%%%%%%%%%%%%%%%%%%
```

References

Alpert, S. M., Knappe, D. R. U., & Ducoste, J. J. (2010). Modeling the UV/hydrogen peroxide advanced oxidation process using computational fluid dynamics. *Water Research, 44,* 1797-1808.

Beer's law. Retrieved October 21, 2013, from http://teaching.shu.ac.uk/hwb/chemistry/tutorials/molspec/beers1.htm

Bettles, T., Schujman, S., Smart, J. A., Liu, W., & Schowalter, L. (2007). UV light emitting diodes - their applications and benefits. *International Ultraviolet Association, 9*(2), 11-15.

Blatchley III, E. R. (1997). Numerical modelling of UV intensity: Application to collimated-beam reactors and continuous-flow systems. *Water Research, 31*(9), 2205-2218. doi:http://dx.doi.org/10.1016/S0043-1354(97)82238-5

Bolton, J. R. (2000). Calculation of ultraviolet fluence rate distributions in an annular reactor: Significance of refraction and reflection. *Water Research, 34*(13), 3315-3324. doi:http://dx.doi.org/10.1016/S0043-1354(00)00087-7

Bolton, J. R., & Linden, K. G. (2003). Standardization of methods for fluence (UV dose) determination in bench-scale UV experiments. *Journal of Environmental Engineering, 129*(3), 209. Retrieved from http://search.ebscohost.com/login.aspx?direct=true&db=a9h&AN=9110067&site=ehost-live

Bowker, C., Sain, A., Shatalov, M., & Ducoste, J. (2011). Microbial UV fluence-response assessment using a novel UV-LED collimated beam system. *Water Research, 45*(5), 2011-2019. doi:http://dx.doi.org/10.1016/j.watres.2010.12.005

Boyjoo, Y., Ang, M., & Pareek, V. (2013). Light intensity distribution in multi-lamp photocatalytic reactors. *Chemical Engineering Science, 93*(0), 11-21. doi:http://dx.doi.org/10.1016/j.ces.2012.12.045

Chatterley, C. (2009). *UV-LED irradiation technology for point-of-use water disinfection in developing communities.* (Unpublished Master of Science Thesis). University of Colorado at Boulder,

Chatterley, C., & Linden, K. (2010). Demonstration and evaluation of germicidal UV-LEDs for point-of-use water disinfection. *Journal of Water & Health, 8*(3), 479-486. doi:10.2166/wh.2010.124

Chevremont, A., Farnet, A., Coulomb, B., & Boudenne, J. (2012). Effect of coupled UV-A and UV-C LEDs on both microbiological and chemical pollution of urban wastewaters. *Science of the Total Environment, 426*(0), 304-310. doi:http://dx.doi.org/10.1016/j.scitotenv.2012.03.043

Coenen, T., Van de Moortel, W., Logist, F., Luyten, J., Van Impe, J. F. M., & Degrève, J. (2013). Modeling and geometry optimization of photochemical reactors: Single- and multi-lamp reactors for UV–H2O2 AOP systems. *Chemical Engineering Science, 96*(0), 174-189. doi:http://dx.doi.org/10.1016/j.ces.2013.03.056

COMSOL multiphysics. (2014). Retrieved February 16, 2014, from http://www.comsol.com/

Dereniak, E. L., & Boreman, G. D. (1996). *Infrared detectors and systems*. New York: John Wiley & Sons, Inc.

Duckworth, K. L. (2014). *Ultraviolet light emitting diode use in advanced oxidation processes.* (Unpublished Master's Thesis). Air Force Institute of Technology

Edison tech center LEDs and OLEDs. (2013). Retrieved March 5, 2014, from http://www.edisontechcenter.org/LED.html

Gadelmoula, M., Lian, X., Maeda, M., Aihara, M., Mawatari, K., Hamamoto, A., Takahashi, A. (2009). Suitability of ultraviolet (A)- light emitting diode for air stream disinfection. *Journal of Medical Investigation, 56*, 150-156.

Halliday, D., Resnick, R., & Walker, J. (2005). *Fundamentals of physics* (7th ed.) John Wiley & Sons, Inc.

Hofman, J., Shao, L., Wols, B., Uijttewaal, W., IJpelaar, G., Beerendonk, E., & van Dijk, H. (2007). Design of UV reactors by CFD: Model development and experimental validation. *Kiwa Water Research*, Delft University of Technology.

Je Wook Jang, Seung Yoon Choi, & Kon Son, J. (2011). Degradation model of LED based on accelerated life test. Paper presented at the *Physical and Failure Analysis of Integrated Circuits (IPFA), 2011 18th IEEE International Symposium on the*, 1-4. doi:10.1109/IPFA.2011.5992771

Kneissl, M., Kolbe, T., Wurtele, M., & Hoa, E. (2010). *Development of UV-LED disinfection.* (No. D 2.5.13).Techneau.

Legrini, O., Oliveros, E., & Braun, A. M. (1993). Photochemical processes for water treatment. *Chemical Reviews, 93*, 671-698.

Lenk, C., & Lenk, R. (2011). *Practical lighting design with LEDs* (First Edition ed.) John Wiley & Sons, Inc.

Lindeburg, M. R. (2011). *Civil engineering reference manual for the PE exam* (12th ed.). Belmont CA: Professional Publications, Inc.

Liu, D., Ducoste, J., Jin, S., & Linden, K. (2004). Evaluation of alternative fluence rate distribution models. *Journal of Water Supply: Research & Technology-AQUA, 53*(6), 391-408. Retrieved from http://search.ebscohost.com/login.aspx?direct=true&db=a9h&AN=15032323&site=ehost-live

Mamane-Gravetz, H., & Linden, K. G. (2005). Relationship between physiochemical properties, aggregation and u.v. inactivation of isolated indigenous spores in water. *Journal of Applied Microbiology, 98*(2), 351-363. doi:10.1111/j.1365-2672.2004.02455.x

MATLAB - the language of technical computing. (2014). Retrieved Fabruary 16, 2014, from http://www.mathworks.com/products/matlab/?s_tid=brdcrb

Narendran, N., Gu, Y., Freyssinier, J. P., Yu, H., & Deng, L. (2004). Solid-state lighting: Failure analysis of white LEDs. *Journal of Crystal Growth, 268*(3–4), 449-456. doi:10.1016/j.jcrysgro.2004.04.071

Oguma, K., Kita, R., Sakai, H., Murakami, M., & Takizawa, S. (2013). Application of UV light emitting diodes to batch and flow-through water disinfection systems. *Desalination, 328*(0), 24-30. doi:http://dx.doi.org/10.1016/j.desal.2013.08.014

Paisnik, K., Poppe, A., Rang, T., & Rang, G. (2012). Physics related modeling of power LEDs. Paper presented at the *Electronics Conference (BEC), 2012 13th Biennial Baltic*, 57-60. doi:10.1109/BEC.2012.6376814

Polyanskiy, M. (2013). Refractive index database. Retrieved February 13, 2014, from http://refractiveindex.info/

QC inspection report. (2013). (No. 02-061313-DC ML).SETi Sensor Electronic Technology, Inc.

Shur, M. S., & Gaska, R. (2010). Deep-ultraviolet light-emitting diodes. *Electron Devices, IEEE Transactions on, 57*(1), 12-25. doi:10.1109/TED.2009.2033768

Sommer, R., Cabaj, A., Hirschmann, G., & Haider, T. (2008). Disinfection of drinking water by UV irradiation: Basic principles - specific requirements - international implementations. *Ozone: Science & Engineering, 30*(1), 43-48. doi:10.1080/01919510701759181

Spencer, M. J. (2014). *Design considerations for a water treatment system utilizing ultra-violet light emitting diodes.* (Unpublished Master's Thesis). Air Force Institute of Technology

Taghipour, F., & Sozzi, A. (2005). Modeling and design of ultraviolet reactors for disinfection by-product precursor removal. *Desalination, 176*, 71-80. doi:10.1016/j.desal.2004.10.025

Tang, H., Yang, D., Zhang, G. Q., Liang, L., Jia, H., Zhang, Z., & Cai, M. (2012). Multi-physics modeling of LED-based luminaires under temperature and humidity environment. Paper presented at the *Electronic Packaging Technology and High Density Packaging (ICEPT-HDP), 2012 13th International Conference on*, 803-807. doi:10.1109/ICEPT-HDP.2012.6474733

Tran, T. N. (2014). *Comparison of continuous versus pulsed ultraviolet light emitting diode use in water disinfection on bacillus globigii spores.* (Unpublished Master's Thesis). Air Force Institute of Technology

U.S. Environmental Protection Agency (EPA). (2006). *Ultraviolet disinfection guidance manual.* (No. EPA 815-R-06-007). Washington, DC: Office of Water.

UVC LED disinfection. (2013). Green Island, NY: Crystal IS.

UVTOP260 manufacturer's specification sheet. Retrieved February 25, 2014, from http://www.s-et.com/spec-sheets/260nm.pdf

Wolfram mathematica 9. (2014). Retrieved February 16, 2014, from http://www.wolfram.com/mathematica/

Wurtele, M. A., Kolbe, T., Lipsz, M., Kulberg, A., Weyers, M., Kneissl, M., & Jekel, M. (2011). Application of GaN-based ultraviolet-C light emitting diodes - UV LEDs - for water disinfection. *Water Research, 45*, 1481-1489.

Yu, L., Achari, G., & Langford, C. H. (2013). LED-based photocatalytic treatment of pesticides and chlorophenols. *Journal of Environmental Engineering, 139*(9), 1146-1151.

REPORT DOCUMENTATION PAGE

Form Approved
OMB No. 074-0188

PLEASE DO NOT RETURN YOUR FORM TO THE ABOVE ADDRESS.

1. REPORT DATE *(DD-MM-YYYY)*	2. REPORT TYPE	3. DATES COVERED *(From – To)*
27-03-2014	Master's Thesis	Aug 2012 – 27 Mar 2014

4. TITLE AND SUBTITLE

Modeling the effects of Ultraviolet (UV) Light Emitting Diode (LED) use in the Advanced Oxidation Process (AOP)

5a. CONTRACT NUMBER

5b. GRANT NUMBER

5c. PROGRAM ELEMENT NUMBER

6. AUTHOR(S)

Richwine, John P., Capt, USAF

5d. PROJECT NUMBER

13V117

5e. TASK NUMBER

5f. WORK UNIT NUMBER

7. PERFORMING ORGANIZATION NAMES(S) AND ADDRESS(S)

Air Force Institute of Technology
Graduate School of Engineering and Management (AFIT/ENV)
2950 Hobson Way
WPAFB OH 45433-7765

8. PERFORMING ORGANIZATION REPORT NUMBER

AFIT-ENV-14-M-55

9. SPONSORING/MONITORING AGENCY NAME(S) AND ADDRESS(ES)

US Environmental Protection Agency
25 W. Martin Luther King Dr.
Mailstop NG-16
Cincinnati, OH 45268
Matthew Magnuson, (513) 569-7321, magnuson.matthew@epa.gov

10. SPONSOR/MONITOR'S ACRONYM(S)

US EPA

11. SPONSOR/MONITOR'S REPORT NUMBER(S)

12. DISTRIBUTION/AVAILABILITY STATEMENT

DISTRIBUTION STATEMENT A. APPROVED FOR PUBLIC RELEASE; DISTRIBUTION IS UNLIMITED.

13. SUPPLEMENTARY NOTES

14. ABSTRACT

The United States Environmental Protection Agency (EPA) is concerned with both accidental and intentional releases of chemicals into waste streams. Certain chemicals may be detrimental to the effectiveness of municipal wastewater treatment plants. This can lead to reduced capability or costly damage to the plant. An Advanced Oxidation Process (AOP) is one method to pre-treat waste streams. This method uses ultraviolet (UV) energy and hydrogen peroxide to create hydroxyl radicals that can neutralize harmful chemicals. Recent advancements in Ultra Violet Light Emitting Diodes (UV LEDs) are making it possible to use this energy source instead of traditional UV energy sources. This research effort focuses on the modeling and simulation of UV LED energy sources for the purpose of providing the ability to predict the efficiency of different reactor vessel geometries. The model is used to evaluate the irradiance present at any point within a test reactor. When coupled with a suitable AOP production rate equation or pathogen kill rate equation, the model provides insight into tradeoffs when designing a UV reactor suitable for an AOP or pathogen extermination, respectively. Finally, simulated results are compared to measurements collected in actual laboratory experiments.

15. SUBJECT TERMS

UV Energy Propagation, LED Energy Pattern, Modeling, UV Reactor Vessel

16. SECURITY CLASSIFICATION OF:			17. LIMITATION OF ABSTRACT	18. NUMBER OF PAGES	19a. NAME OF RESPONSIBLE PERSON
a. REPORT	b. ABSTRACT	c. THIS PAGE			Dr. Michael R. Grimaila, AFIT/ENV
U	U	U	UU	131	19b. TELEPHONE NUMBER *(Include area code)* (937) 255-3636, x 4800 (michael.grimaila@afit.edu)